UNIVERSITY OF CALIFORNIA
RIVERSIDE

Morphological and Functional Characterization of Intestinal Epithelial Cell Subtypes Regulation by *Ptpn2* in Mice

A Dissertation submitted in partial satisfaction
of the requirements for the degree of

Doctor of Philosophy

in

Biochemistry and Molecular Biology

by

Vinicius Canale

March 2022

Dissertation Committee:
Dr. Declan F. McCole, Chairperson
Dr. Frances M. Sladek
Dr. Ansel Hsiao
Dr. David Lo

The Dissertation of Vinicius Canale is approved:

_____

_____

_____

_____

Committee Chairperson

University of California, Riverside

Acknowledgments

The completion of this work would not have been possible without the tremendous help and support I received throughout my years of graduate school from various people, from family to friends, from colleagues to brothers and sisters, from faculty to undergraduates. This dissertation truly is the fruit of a collaborative work.

First, I would like to thank my current lab members Andy Lei, Pritha Chatterjee, Alina Santos, Salomon Manz, and Dr. Meli'sa Crawford, for all their assistance, discussions, suggestions, collaboration, and for the good and cordial environment created in the lab.

Also, my past lab members, Rosie, Dr. Anica Sayoc-Becerra, Dr. Ali Shawki, Dr. Stephanie King, and Dr. Marianne Spalinger. More than colleagues, you all were exceptional mentors and friends during a crucial moment of my graduate studies. I feel blessed for having had companions like you in the beginning of my journey at the McCole lab. Your work, knowledge, collaborative spirit, and professionalism were inspirational, and I will certainly carry those lessons with me. For all this, I am deeply thankful.

To my mentor and advisor Dr. Declan McCole, first of all, for giving me the opportunity to join his lab and to work in such an exciting project. Thank you for providing me with your guidance, talent, scientific rigor, and challenging me with high scientific standards while offering an environment where I could grow intellectually in the investigative process. Also, your encouragement to showcase my research in major conferences were fundamental for my professional growth.

To my committee members, Dr. Frances Sladek, Dr. David Lo, and Dr. Ansel Hsiao, for your guidance, invaluable expertise, encouragement, and for always challenging me with tough questions. It has been an honor to have researchers of your caliber evaluating my progress.

Thank you to all the graduate students, postdocs, faculty, and staff in the Biomedical Sciences department for welcoming me with opened arms and treating me as one of your own. In particular, I want to thank Dr. Coss for generously permitting usage of her equipment.

The undergraduate students, Sharon Jahng and Timothy Chu, who dedicated some of their time to help me counting cells, staining slides, making gels, and many other tasks in the lab, my sincere thank you.

To Dr. Tuncel from the Graduate division, Dr. Spindler and Dr. Hille from the Biochemistry department, for their unfailing support, understanding, and encouraging words during a very difficult transitional time as a graduate student. I must also thank Julio Sosa and Dawn Loyola who served as my academic advisors in the biochemistry department, for their incredible patience, understanding and diligent assistance, helping me to overcome hurdles, going out of their way to make sure everything was alright.

To Marissa Skari, Johnny Phan, and Leslie Karpinski, remarkable keepers of the mice vivarium. Thank you for your dedication, assistance, and cordiality.

To the staff at IIGB and CFAMM facilities, in special to Dr. David Carter and Matthew Dickson, for their assistance and advice in the acquisition of beautiful confocal and electron microscopy images, bringing to life extraordinary and intricate cell features.

To my parents, sisters, brothers-in-law, nieces and nephews, my grandma, and friends back in Brazil, whom I miss so dearly, thank you for your love, affection, and prayers. Thank you for always bugging me to send more pictures or to call more often. Only God knows how my heart aches longing to be with you again.

To my in-laws and extended family, for the enormous support, encouragement, and prayers. Thank you for listening to my complaints and frustrations, and always putting things into perspective. The ‘Sunday fun days’ and all the family activities certainly were fundamental for my sanity.

To my monkeys, Claire, Levi, Joaquim and Joshua, your spontaneous burst of joy every time I returned home was the greatest motivation of all to keep working hard, while a reminder of the greatest gifts God has granted me.

To my wife, for whom I am most grateful. Thank you for walking this path with me, making it as your own. Thank you for your patience, love, faith, and support throughout this whole journey which does not conclude with this dissertation but begins a new chapter. I look forward to witness with you what God has in store for us. *Cor unum et anima una*.

To CAPES Foundation, Ministry of Education of Brazil, through the program Science without Borders (No. 99999.013456/2013-00 - migrated BEX) and LASPAU for the financial support.

The text of this dissertation, in part, is a reprint of the material as it appears in *Journal of Clinical Investigation - 2021* (Chapters 3 and 4). The co-author Declan F. McCole listed in that publication directed and supervised the research that forms the basis for this dissertation.

To my wife, whose love, dedication, and loyalty are awe-inspiring.

To my children, for their unconditional love, joy, and affection.

To Gaudete Canale, *in memoriam*

"Question the beauty of the earth,
the beauty of the sea,
the beauty of the wide air around you,
the beauty of the sky;
question the order of the stars,
the sun whose brightness lights the day,
the moon whose splendor softens the gloom of night;
question the living creatures that move in the waters,
that roam upon the earth,
that fly through the air;
the spirit that lies hidden,
the matter that is manifest;
the visible things that are ruled,
the invisible that rule them;
question all these.
They will all answer you:
"Behold and see, we are beautiful."
Their beauty is their confession of God.
Who made these beautiful changing things,
if not one who is beautiful and changeth not?"

St. Augustine

ABSTRACT OF THE DISSERTATION

Morphological and Functional Characterization of Intestinal Epithelial Cell Subtypes Regulation by *Ptpn2* in Mice

by

Vinicius Canale

Doctor of Philosophy, Graduate Program in Biochemistry and Molecular Biology
University of California, Riverside, March 2022
Dr. Declan F. McCole, Chairperson

Inflammatory Bowel Diseases (IBDs) are characterized by relapsing chronic inflammation of the gastrointestinal tract that occurs in patients with Ulcerative Colitis (UC) and Crohn's disease (CD). Genome wide association studies have to-date identified 240 independent susceptibility loci associated with IBD. Single nucleotide polymorphisms (SNPs) were identified in the protein tyrosine phosphatase non-receptor type 2 (*PTPN2*) gene locus which decodes T-cell protein tyrosine phosphatase (TCPTP), a negative regulator of diverse intracellular pathways, including several members of the JAK-

STAT signaling. Consequently, *PTPN2* loss of function is unable to repress/regulate inflammatory signals.

Intestinal epithelial homeostasis is maintained by active-cycling and slow cycling stem cells confined within the crypt-based niche, and subsequent differentiation into secretory and absorptive epithelial lineages as cells migrate up the crypt-villus axis. An imbalance in the population of epithelial subtypes can be detrimental for the function of the organ and make it more susceptible to microbial infection. This is demonstrated by studies using IBD patient biopsy and transgenic mice demonstrating that genetic variants, or deletion of IBD-associated genes, can modify IEC subtypes and their functional roles in intestinal homeostasis. Therefore, the goal of this study was to identify whether *Ptpn2*-deficient mice display altered intestinal epithelial cell differentiation and function that could contribute to increased infection susceptibility and onset of IBD. For this, we used two mouse models, one with a constitutive "whole-body" *Ptpn2* deficiency, and another with inducible-tissue specific *Ptpn2* deletion.

Overall, this dissertation shows that the number and function of secretory IECs is negatively affected by whole-body *Ptpn2* loss. Notably, Paneth cells

were almost ablated, with a marked deficit in production of AMPs, contributing to higher susceptibility to microbial infection.

Contents

LIST OF FIGURES

LIST OF TABLES

1. Introduction

1.1. Function and Structure of the Intestinal Epithelium

The elevated complexity of multicellular organisms requires tissue compartmentalization to interface with the external environment while supporting specialized functions internally[1]. To prevent unrestricted exchange of internal and outer material, defined boundaries must be established covering the most external surfaces. The gastrointestinal mucosa is the largest barrier tissue in the human body with a surface area of approximately 300 m^2 in adults, making it the most extensive continuous barrier separating internal organs from the outside luminal environment[2]. It is estimated that 100 trillion (10^{14}) microbes reside in the human gut, with the largest density present in the distal ileum and colon of the intestinal tract, forming an extraordinarily large microbial ecosystem[3]. Furthermore, the gut adaptive immune system imposes a selective pressure on the microbiota, providing an advanced symbiotic relationship with the intestinal flora, efficiently tailoring immune responses to diverse types of microbes, whether to promote mutualism or host defense[4].

The intestinal epithelium is a specialized tissue that forms a selectively permeable barrier, interacting directly with the external environment and the

internal milieu. However, more than just providing a physical separation between two worlds, the intestinal epithelia is a dynamic organ with numerous specialized components responsible for generating ion solute concentration gradients, absorption of nutrients, sampling of bacterial antigens, restricting entry of pathogens and toxins, modulating the microbial intestinal flora by secreting anti-microbial components, and mediating communication with the immune system[5].

The intestinal tract is categorized into segments that indicate their anatomical location, function, and morphological features. For the purpose of this dissertation, it suffices to describe only the major morphological differences between the small and large intestine. The small intestine is the longest segment, and it is primarily involved in the processing and absorption of nutrients. It is connected to the stomach by the duodenum, which is physiologically adapted to withstand the highly acidic chyme, and is the primary site of absorption for fatty acids and water-soluble vitamins[6,7]. The jejunum is the intermediary intestinal segment with similar morphological features, except for not having duodenal Brunner's glands, a branched tubuloacinar gland that secretes products into the luminal space to protect the mucosa from the acidic gastric contents. Additionally, gut

associated lymphoid tissue (GALT), also known as Peyer's patches, begins to appear at the most distal parts of the jejunum and is more prominent in the ileum segment. The distal ileum is the site of absorption of bile salts and vitamin B_{12}, and connecting the small intestine to the large intestine at the ileocecal junction[7]. Finger-like protrusions called villi, also extend out to the lumen of the small intestine, increasing the surface area to maximize nutrient absorption. Each villus is surrounded by a number of tissue invaginations called intestinal crypts (also known as intestinal glands or crypts of Lieberkühn), containing many intestinal secretory cells and the residing intestinal stem cells.

By the time the chyme reaches the large intestine, most nutrients and water have been absorbed by the small intestines. Stool formation occurs as remaining fluids and electrolytes are absorbed. Undigested polysaccharides are metabolized and broken down into short-chain fatty acids (SCFA) by luminal bacteria, releasing acetate, propionate, and butyrate as waste products, which in turn are important energy sources for colonocytes[8]. In the colon, the villi structures are absent while the amount of mucus-secreting goblet cells increases considerably compared to the small intestine. These cells are essential to properly lubricate the lumen of the colon, hinder

bacterial adhesion to the epithelium, and facilitate stool passage. Additionally, the lamina propria of the colon harbors many lymphatic nodules, which are well-defined aggregations of lymphocytes, macrophages, and plasma cells surveilling and sampling bacterial antigens from the luminal space[7].

1.2. The Intestinal Epithelial Barrier

The intestinal epithelium forms a physical and biochemical barrier, impeding commensal and pathogenic microorganisms from easily accessing the intestinal mucosa. This function is accomplished by three layers of protection, each with an exclusive specialization: the intestinal epithelial cell (IEC) layer, the mucus layer, and the underlying immune cells.

1.2.1. *The Intestinal Epithelial Cell Layer*

To protect against harmful agents while selectively allowing transit of vital molecules, junctional complexes are established linking adjacent epithelial cells. These protein-protein interacting networks seal the intercellular space while tightly regulating paracellular passage of water, electrolytes, and macromolecules. Apical junctional complexes are composed of adherens

junctions, and tight junctions, while cellular stability is supported by desmosomes towards the basolateral aspect of adjoining cells. These complexes are formed by transmembrane proteins that interact extracellularly with neighboring cells while connecting intracellularly with adaptor proteins anchored to the actin cytoskeleton[9].

The IECs are at the front line of defense forming the main structural component of the physical barrier between the luminal microenvironment and the host tissue. Pattern recognition receptors (PPR) expressed by IECs enable them to dynamically sense the microbial environment. For example, distinct microbial and viral ligands are recognized by several members of the Toll-like receptor (TLR) family, triggering activation of diverse cellular responses, such as autophagy, glycolysis, enhancing integrity of tight junction complexes, transcription of nuclear factor-κB (NF-κB), heat-shock proteins, and interleukins[10,11]. In fact, studies using mice deficient in TLR2 or Myd88 (myeloid differentiation primary response 88), a critical adaptor protein in the TLR signaling, have shown that bacteria-derived signals contribute to epithelial homeostasis and repair when colitis is induced by dextran sodium sulfate (DSS), showing the homeostatic role of microbial recognition by IECs[12]. Furthermore, IEC-specific deletion of downstream

TLR signaling in mice, including members of the NF-κB pathway, such as IκB, IKK, NEMO (NF-κB essential modulator), results in spontaneous colitis[13,14].

Another mechanism by which IECs modulate innate immune responses, is through nucleotide-binding oligomerization domain proteins (NOD). NODs function as cytosolic receptors for invading bacteria, enabling rapid induction of host defenses following infection. NOD1 detects D-glutamyl-meso-diaminopimelic acid (iE-DAP), a dipeptide found in Gram-negative bacteria and also in select groups of Gram-positive bacteria. Conversely, NOD2 detects muramyl dipeptide (MDP) that is ubiquitously present in bacterial peptidoglycan, and thus plays a critical role in intestinal homeostasis[15]. In fact, loss-of-function mutations in the *NOD2* gene locus confers the greatest genetic risk for development of Crohn's disease[16–18]. Activation of NOD proteins trigger innate inflammatory signaling pathways, resulting in transcriptional activation of the pro-inflammatory cytokines tumor necrosis factor (TNF), interleukin-6 (IL-6), CC-chemokine ligand 2 (CCL2), neutrophil chemoattractant CXC-chemokine ligand 8 (CXCL8), CXCL2, and various antimicrobial factors. Moreover, NOD2 stimulation induces autophagy and adaptive immune responses[19,20].

In sum, IECs possess multiple regulatory mechanisms to ensure intestinal homeostasis by controlling transit across the epithelial barrier, to sense and rapidly respond to harmful agents, and to orchestrate defensive mechanisms together with the innate and adaptive immune systems.

1.2.2. *The Mucus Layer*

To prevent bacterial adherence to the epithelial cell lining and facilitate stool transit, the intestinal barrier relies on an extra layer of protection, the mucus layer, which coats the entire intestinal tract. The mucus layer is composed of several large heavily *O*-glycosylated glycoproteins (mucin) that assemble into homo-oligomers. In fact, the numerous *O*-glycan acceptor sites may result in a molecule with up to 80% carbohydrate by mass[21]. The major gel-forming mucin, MUC2, is secreted by goblet cells and forms the structural backbone of the mucus layer in the gut. MUC2 *O*-linked glycan modifications bind water thereby forming extended, stiff, and voluminous rod mucin domains with a central protein core, resulting in multiple potential ligands for microbial adhesins that can be utilized by some commensals in the outer mucus layer[22,23]. Moreover, several mucus-associated proteins have been identified although they do not yet have a well-defined role[22].

There are two types of mucin proteins: membrane-bound and gel-forming. Enterocytes express important transmembrane mucin proteins that cover the apical cell membrane. These protective mucins reach further out into the lumen than any other membrane-associated protein, generating an attached glycan-rich diffusion barrier, and are an intrinsic part of the cell glycocalyx[24].

The mucus of the small intestine is single-layered and relatively porous, which is important for efficient nutritional uptake while limiting the number of bacteria that reaches the epithelium[25,26]. In contrast, the large intestine has two layers, with the inner layer firmly attached to the epithelium in a dense, well-organized structure, approximately 50μm thick, that is almost impenetrable to bacteria. This slow-diffusing mucus layer is then converted into a less dense and detached mucus layer by proteases in the outer region, generating a secondary mucus layer usually 100μm thick. Furthermore, the impenetrability of the mucus is assisted by an arsenal of antimicrobial peptides (AMPs) including α-defensins, lysozyme, cathlecidins, secretory phospholipase A2, lectins, and sIgAs) secreted by IECs. These create an antibacterial gradient from the IEC layer out toward the lumen that prevents direct bacterial interaction with the epithelium[22].

Once secreted, the compact mucin proteins expand up to 1,000-fold into well-organized large nets, forming pore sizes of around 0.5 μm, sufficiently small to hinder bacterial penetration[27]. Furthermore, it has been shown that *O*-glycosylation patterns have a regional distribution, thus forming microenvironments of commensal bacteria that can adhere to the glycans and use them as a nutritional source[28,29]. Thus, the mucus layer is a fundamental component of the intestinal epithelial barrier. In fact, investigations using *Muc2*-KO mice have shown that the absence of an integral mucus layer leads to development of spontaneous colitis and colorectal cancer[30–33].

1.2.3. *The Underlying Immune Cells*

Beneath the IEC layer, the lamina propria is made up of stromal cells (myofibroblasts), B cells (IgA-producing plasma cells), T cells, macrophages, dendritic cells, and innate lymphoid cells. IECs generate several immunoregulatory factors that are fundamental for creating immune tolerance, limiting steady-state inflammation, and modulating innate and adaptive immune cell responses (Figure 1).

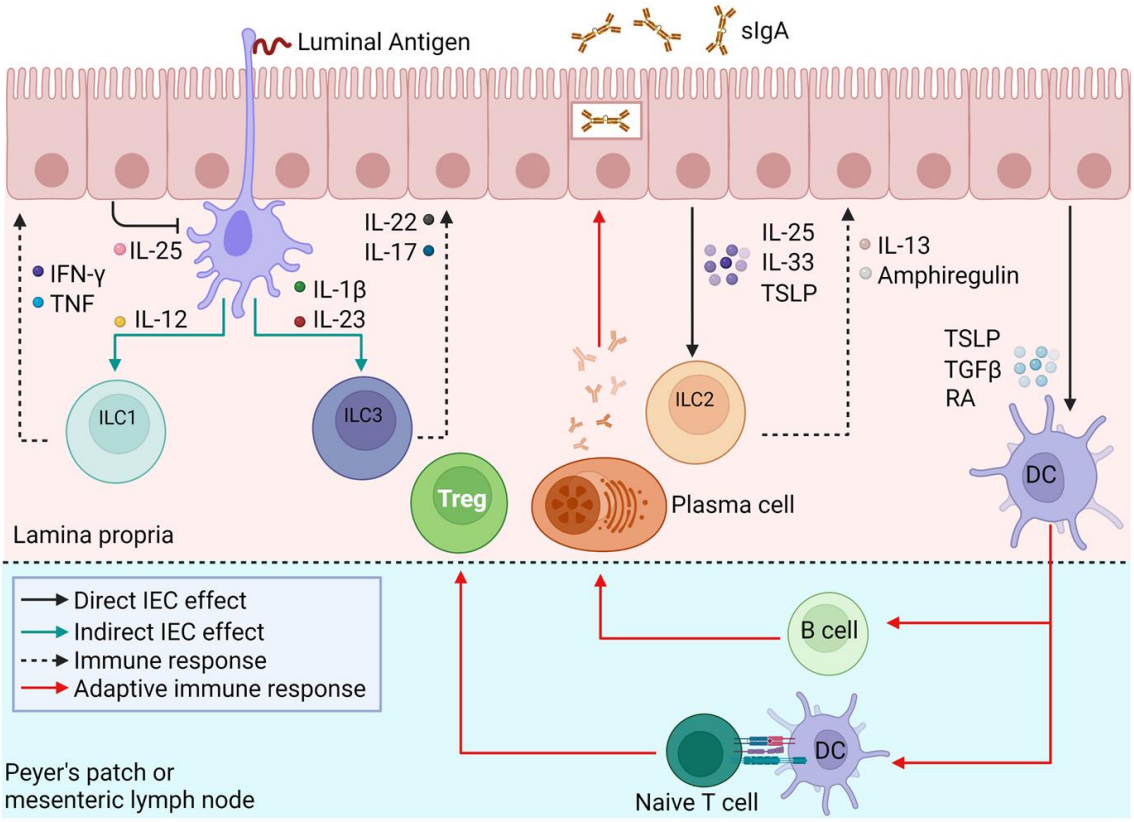

Figure 1. Diagram depicting the extensive communication between IECs and the immune system, regulating innate and adapted responses. IEC-derived cytokines interleukin-25 (IL-25) and thymic stromal lymphopoietin (TSLP) elicit the expansion and differentiation of basophil progenitors and multipotent progenitor type 2 (type 2 MPP) cells, respectively. IL-25, IL-33 and TSLP stimulate group 2 innate lymphoid cells (ILC2s), whereas IL-25 suppresses innate lymphoid cell subset 1 (ILC1) and ILC3 function by limiting macrophage production of pro-inflammatory cytokines IL-1β, IL-12 and IL-23. IECs condition dendritic cells (DCs) and macrophages towards a tolerogenic phenotype through the production of TSLP, transforming growth factor-β (TGF-β) and retinoic acid (RA). DCs promote the differentiation of naive $CD4^+$ T cells into regulatory T (TReg) cells and the maturation of B cells into IgA-secreting plasma cells. Mucosal cell-derived DCs also imprint a gut-homing phenotype on primed B cells and T cells through the production of RA. IFN-γ, interferon-γ; sIgA, secretory IgA; TCR, T cell receptor; TLA, thymus leukemia antigen; TNF, tumor necrosis factor. Adapted from Peterson; Intestinal epithelial cells: Regulators of barrier function and immune homeostasis[34].

IEC-derived thymic stromal lymphopoietin (TSLP), transforming growth factor-β (TGF-β), and retinoic acid (RA) are produced in response to commensal bacteria-derived signals, promoting the development of dendritic cells (DC) and macrophages with tolerogenic properties, including production of IL-10 and RA[34]. Intestine-resident macrophages lie in close interaction with IECs, where they function as phagocytes against bacteria that cross the epithelial barrier, modulating intestinal homeostasis and tissue regeneration[35]. Macrophage-epithelial interaction are also critically involved in regulating epithelial permeability to maintain gut homeostasis[36].

In contrast, DCs migrate to peripheral organs, such as Peyer's patches, isolated lymphoid follicles, and mesenteric lymph nodes, where they mediate regulatory and effector T cell responses[37]. Several subsets of DCs have been described, and the balance of regulatory and effector responses is influenced by the contribution of functionally distinct DC subsets as well as their modulation by environmental cues[38]. Moreover, they modulate the expression of tight junction proteins in IECs allowing the formation of transepithelial dendrites reaching to the lumen for antigen sampling[34]. Interestingly, the extension of these transepithelial dendrites is initiated by TLR signaling in IECs instead of myeloid cells, showing extensive

communication and modulation between the intestinal epithelial cell layer and the underlying immune cells[39].

Furthermore, the epithelium interacts with innate lymphoid cells (ILC) and intraepithelial lymphocytes (IEL), also known as tissue-resident T cells. ILCs lack properties of adaptive lymphocytes and are regulated, at least in part, by epithelial cell-derived immunoregulatory signals. ILC subtypes and their functions have not been fully characterized, but they can be categorized in three groups according to their primary cytokine production: Group 1 includes ILC subset 1 (ILC1) and natural killer cells (NK), characterized by production of IFN-γ and TNF-α in response to IL-12 and/or IL-15; Group 2 includes ILCs subset 2 (ILC2) which is activated by epithelial-derived cytokines IL-25, IL-33, and TSLP, which in turn produce the T_H2 cell-associated cytokines IL-15, and IL-13. Finally, group 3 includes ILC3s and lymphoid tissue inducer (LTi), responsible for T_H17 and T_H22 cell-associated cytokines IL-17A and IL-22 in response to IL-23[34,40,41]. Conversely, effector T cells can be primed by intestine-derived antigen-presenting cells (APC) in secondary lymphoid tissues. Then, after circulating through the body, they settle in the intestine with intimate contact with the IEC layer maintaining homeostasis at the intestinal barrier[42]. IELs essentially

comprise antigen-primed T cells expressing the γδ and αβ receptors, which distinguishes them from conventional T cells, and maintain tolerance to innocuous antigens from the diet or from commensals[43].

Lastly, the stimulation of naïve B cells towards mature IgA-secreting plasma cells is dependent on exposure to antigen presentation by DCs; however, this process is conditioned by IEC-derived signals, such as nitric oxide (NO), IL-10, retinoic acid and TGF-β signaling. Furthermore, IECs induce proliferation-inducing ligand (APRIL) and B-cell activating factor (BAFF) production by DCs through TSLP signaling, thus amplifying the effect on B cell stimulation[44–46]. Therefore, the IEC layer plays a central role in modulating adaptive and innate immune responses through numerous mechanisms to maintain intestinal homeostasis.

1.3. Differentiation and Function of Intestinal Epithelial Cell Subtypes

As described above, the intestinal epithelium is a remarkable multitasking tissue. To accomplish such a wide variety of functions, the epithelium encompasses several specialized IEC subtypes strategically located in the crypt-villus axis. However, the integrity of the epithelial barrier is

challenged by a high rate of cell turnover, necessary to replenish cell loss due to shedding, being completely renewed every 4-5 days[47]. Moreover, challenges from bacteria and harmful agents present in the lumen might accelerate this process, while failure accelerate epithelial renewal in response to injury could cause barrier defects[48]. The continuous turnover of IECs is enabled by rapidly proliferating intestinal stem cells (ISC) at the crypt base that generate transit-amplifying cells, the precursors for all IEC subtypes.

Regulation of the intestinal cell population is accomplished by an exquisite proliferation-to-differentiation axis which maintains a homeostatic balance. Cues from adjacent epithelium and underlying stromal cells instruct the stem progenitor cells to remain quiescent, proliferate, differentiate or activate a rapid response to epithelial injury[49].

Wnt signaling is critical for maintaining the crypt cell populations in a proliferative state. In the canonical pathway, Wnt proteins act in an autocrine or paracrine fashion, inducing heterodimeric complex formation of Frizzled and low-density lipoprotein receptor-related protein 5/6 (LRP5/6). Dimerization of these receptors activates a transduction cascade involving inhibition of the β-catenin complex degradation. Stabilized β-catenin then

translocates to the nucleus to associate with the lymphoid enhancer factor (LEF) and T-cell factor (TCF) family of transcription factors to activate Wnt target genes crucial for stem cell identity[50,51]. However, Wnt signaling must be tightly orchestrated with Notch signaling to balance the proliferation/differentiation ratio in the crypt-villus axis (Figure 2).

The Notch signaling pathway plays a key role in specifying IEC fate by modulating proliferation, inhibiting differentiation, and controlling the balance between secretory and absorptive cells[52,53]. Upon activation, the Notch receptor induces expression of the hairy and enhancer of split 1 gene (*Hes1*), which in turn represses transcription factors that promote cell differentiation, including *Atoh1*, a secretory cell differentiation factor[50]. This signaling pathway depends on direct interaction between two cells, a ligand-presenting cell, and a receptor-expressing cell. Intestinal stem cells depend on active Notch signaling to maintain their identity, however secretory lineage commitment requires Notch silencing. Interestingly, cells committed to the secretory lineage produce the Notch ligands DLL1 and DLL4 themselves, thus individually promoting Notch activity in six to eight neighboring cells to differentiate into absorptive cells. By doing so, a fixed ratio of secretory/absorptive cells can be achieved by lateral inhibition[50,54].

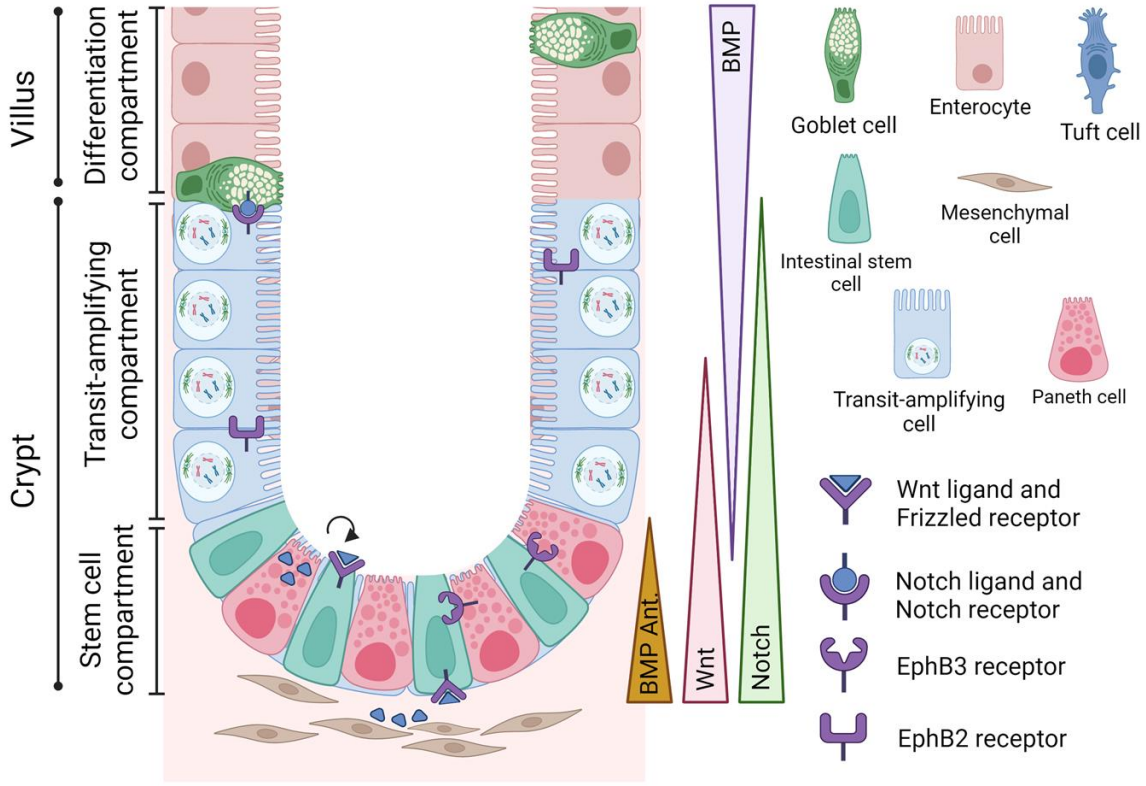

Figure 2. Regulatory signaling pathways within small intestinal crypts. Paneth cells and mesenchymal cells secrete Wnt ligands that interact with Frizzled receptors expressed by intestinal stem cells. Secretory precursors of the transit-amplifying compartment secret Notch ligands, which bind to Notch receptors expressed by absorptive precursors, promoting lateral inhibition to secretory cell lineage of neighboring cells. Notch signaling activates *Hes1*, a bHLH transcription factor that inhibits *Atoh1* and directs developments of an absorptive progenitor. Interaction between Ephrin B ligands and EphB receptors direct cell compartmentalization and migratory behavior within the crypt. Both Paneth cells and stem cells express Ephb3, but only stem cells express Ephrin B ligands, thereby restricting both cell types to the crypt base. A gradient of EphrinB1/B2 ligands exists within the crypt, thereby restricting upward migration of transit-amplifying cells and ensuring that they are localized near their respective niches. (TA)= transit-amplifying; (BMP Ant.)= BMP antagonists (chordin, gremlin, noggin). Adapted from Sailaja et al (2016); Scoville et al. (2008); Martini et al. (2017)[48,56,57].

Furthermore, there are defined boundaries of IEC compartments in the crypt-villus axis of the small intestine, such as the intestinal stem cell zone and the transit-amplifying cell compartment, which are determined by β-catenin/TCF (transcription factor) signaling, regulating the expression of B-type ephrin receptors, EphB2 and EphB3. Ephrin receptors are membrane bound and require direct cell-cell interaction for activation. In the gut, they function by restricting cell intermingling and allocating specific IEC populations within epithelial boundaries in an intimately coupled cell migration process and in a spatially organized manner[55].

Bone morphogenetic proteins (BMP), inhibitors of proliferation in the gut, are mainly produced by mesenchymal cells at the top of the villi, whereas the stromal cells surrounding the crypt secrete BMP inhibitors such as noggin, chordins, and gremlins[50]. Thus, a BMP gradient signaling is established along the crypt-villus axis, with elevated activity in the villus and correspondingly less activity within the crypt. Conversely, a WNT gradient signaling is inversely proportional to BMP gradient, providing a proliferative stimulus, being highest at the crypt base and lowest at villus zone (Figure 2)[57,58]. Altogether, this shows the extraordinary organization of the intestinal mucosa with a finely tuned communication between epithelial

cells with the supportive stromal cells, creating microenvironments that modulate epithelium renewal while promoting differentiation of all IECs.

1.3.1. *Intestinal Stem Cells*

Intestinal epithelial homeostasis is maintained by active-cycling and slow-cycling ISCs. Actively cycling crypt base columnar ISCs reside at the crypt base intercalated between Paneth cells. Quiescent, or slow cycling, ISCs are normally found around the +4 regions of the crypt, right above the Paneth cells. The progeny of ISCs, known as transit-amplifying (TA) cells, gradually move upwards along the crypt-villus axis as new cells emerge from the bottom of the crypt while committing to the absorptive or secretory cell lineages, although this process has not been fully elucidated[49]. Leucine-rich repeat-containing G-protein coupled receptor 5 (LGR5), also known as G-protein coupled receptor 49 (GPR49), was the first marker of actively cycling ISCs identified using lineage tracing studies[59]. The main function of $Lgr5^{+}$ ISCs is to give rise to all mature IECs while replenishing themselves through self-renewal. On the other hand, quiescent ISC comprise a reserve stem cell population that is induced following injury. Lineage tracing studies

have shown that *Lrig1*$^{+}$ and *Bmi1*$^{+}$ ISCs have augmented activity upon intestinal injury following γ-radiation[51].

ISCs are maintained by their surrounding niche for self-renewal and proliferation under homeostatic conditions. The ISC niche comprises distinct neighboring cells and various components that form the extracellular matrix surrounding the crypt base, such as myofibroblasts, endothelial cells, immune cells, neural cells, smooth muscle cells, and the intermingled Paneth cells (Figure 2). The latter is an important source of stem cell niche factors, such as Wnt3, Notch ligands, and EGF that are required for ISC function, although Paneth cell ablation does not affect ISC homeostasis, suggesting redundant sources of Wnt ligands, possibly from the stromal microenvironment[60,61]. Additionally, stromal-derived R-spondin is a potent Wnt agonist that potentiates Wnt signaling in the presence of Wnt ligands via Lgr5-dependent mechanism, which plays a critical role in controlling the size of the Lgr5^{+} ISC pool[61]. In fact, stromal-free organoid culture is dependent on the presence of R-spondin, indicating the importance of this factor in ISC identity[62].

1.3.2. *Paneth Cells*

Paneth cells are highly specialized secretory IECs responsible for releasing several antimicrobial peptides (AMPs) that modulate the gut microbiome. These cells are easily distinguished from other IECs due to their large cytosolic granules packed with AMPs, which is noticeable under conventional microscopy. In contrast to other IECs, Paneth cells migrate downwards in the crypt axis when they are first committed to this secretory lineage, reaching the stem cell zone and dwelling among the ISCs where they release important stem cell factors as described previously. In addition, Paneth cells have a longer life span, of approximately 30 days. Moreover, they have the capability of undergoing dedifferentiation to repopulate the stem cell zone when γ-radiation injury depletes $Lgr5^+$ ISCs, although other differentiated IECs have the same capability depending on the injury model[63–65].

As mentioned earlier, under homeostatic conditions, Paneth cells are present only in the small intestine. However, a subset of patients with inflammatory bowel disease (IBD) display metaplastic Paneth cells in colonic segments, which seems to be associated with the severity of the inflammatory condition and intestinal cancer[66–68].

Of the secreted AMPs, α-defensins, also known as cryptdins, are major contributors to the modulation of the microbiota. These proteins are small peptides (~4 kDa) with disulfide bridges between cysteine residues that are important for their antimicrobial activity[69]. In mice, α-defensins require proteolytic activation from inactive pro-α-isoforms to active cryptdins by matrix metalloproteinase-7, also known as matrilysin, which is expressed and secreted by Paneth cells themselves. Conversely, it has been demonstrated that humans α-defensin 5 (HD5) and α-defensin 6 (HD6) are cleaved into their active isoform by luminal trypsin[70,71].

1.3.3. *Goblet Cells*

Goblet cells are abundantly present in several mucosal surfaces. In the intestinal tract, they appear in increasing numbers from the proximal small intestine to the distal colon. In the small intestine they are found at higher numbers in the crypt compared to the villi, where they become more interspersed by enterocytes[24]. Though goblet cells perform multiple tasks to maintain intestinal homeostasis, they are largely responsible for mucin protein secretion, forming the key structural backbone of the mucus layer that creates a physical barrier between the epithelial surface and the luminal

contents. Maturation of secretory cells into the goblet cell lineage is controlled, at least in part, by the transcription factor SAM pointed domain-containing Ets transcription factor (*Spdef),* and including several genes that are critical for goblet cell maturation, such as *Klf4*, *Foxa1*, *Foxa2*, and *Cdh1*[72–76].

Goblet cells display a goblet-like shape with the nucleus displaced to the basal region of the cell, whereas the cytoplasm is filled by compactly packed mucin granules near the apical surface. It is believed that goblet cells secrete mucin proteins at a constant basal rate, however T_H2-mediated IL-4, IL-5, IL-9, and IL-13 induce goblet cell hyperplasia and hypersecretion[24]. Moreover, mucus secretion is induced by microbial ligands, inflammasome activation, acetylcholine, histamine, and prostaglandins[77–79].

Besides mucus secretion, goblet cells can also release important peptides involved in intestinal immunity, such as Resistin-like molecule-β, (RELM-β), trefoil factor 3 (TFF3)[80], and IL-8, showing direct involvement in mucosal inflammation[81]. Moreover, goblet cells can form goblet cell-associated antigen passages, known as GAPs, to deliver luminal substances to antigen-presenting cells (APCs), an important adaptive immune response mechanism supporting steady state antigen tolerance[82,83].

1.3.4. *Tuft Cells*

Tuft cells, also known as brush cells, are characterized by the presence of a unique tubulovesicular system and an apical bundle of microfilaments connected to a tuft, with approximately 120-140 microvilli per cell projecting into the luminal space that can be visualized only by electron microscopy. They are a rare IEC subtype, representing only 0.4% of all IECs in the mouse intestinal epithelium. Morphologically, they have a pear-like shape, a wide base, and a narrow microvillous apex[84]. They were first described in the rat airway, but since then tuft cells have been characterized in most epithelial tissues, including the proximal respiratory tract, gastrointestinal tract, pancreato-biliary system, taste buds, and thymus. These organ-specific tuft cells perform quite distinct functions, albeit gene expression of these cells across tissues revealed a uniform gene expression profile even though tuft cell subtypes could also be present in the same organ[85,86].

Similar to other IEC subtypes, tuft cells are derived of $Lgr5^+$ cells. The hypothesis that tuft cells differentiate from an early secretory precursor cell has been the subject of debate with divergent findings[84]. Nevertheless, the transcription factor Pou domain class 2 transcription factor 3 (Pou2f3) has

been identified as the master regulator of tuft cell differentiation. Biological markers have also been identified, with the doublecortin-like kinase 1 (Dclk1), and the transient receptor potential cation channel subfamily M member 5 (Trpm5) recognized as specific markers for this cell lineage[80,87].

Much of intestinal tuft cell function remains obscure, though some investigations have shown that these cells are dynamically regulated and central to type 2 immune circuit involving ILC2 and crypt epithelial progenitors. They are an important source of IL-25 (also known as IL-17E), leukotrienes, prostaglandin D_2 (PGD_2), and acetylcholine[88]. Luminal succinate appears to be a potent activator of small intestinal tuft cells, triggering the IL-25-dependent activation of stromal ILC2s to release IL-13, promoting expansion of goblet and tuft cells, inducing mucus secretion and smooth muscle hypercontractility, a response known as “weep and sweep” that aid in worm expulsion[87,89].

Tuft cells are an important constitutive player of the normal intestinal tract, modulating immune responses and activation of other IEC subtypes during helminth infection. A role for bacterial or viral infection has been suggested as well, although as yet, there is no substantial evidence of this role.

1.3.5. *Enteroendocrine Cells*

Enteroendocrine cells represent nearly 1% of all IECs in the gut, however there are at least 7 different subtypes in the intestinal tract alone, each one associated with production of a primary hormone. Their main role is to function as sensory cells, sampling for luminal nutrients and microbial metabolites, releasing peptide hormones that modulate digestive functions.

Precursor secretory cells depend on transient expression of Neurogenin3 (*Neurog3*) followed by a number of overlapping transcription factors, including Neurogenic differentiation 1 (*Neurod1*), for the development of intestinal enteroendocrine cells. Then, spatiotemporal expression of transcription factors *Pdx1*, *Cdx2*, *Gata4, 5,* and *6*, *Hnf1a*, *Hnf1b* and *Cdp*, determine which enteroendocrine subset will develop[90].

Table 1 summarizes the enteroendocrine cell subtypes found throughout the intestinal tract with the associated peptide hormone of each subtype, although other signaling components can be secreted by more than one subtype, such as leptin, serotonin and chromogranin A, the latter being a pan-marker of enteroendocrine cells[90].

The secreted peptides can execute endocrine and paracrine functions, including signaling to vagal afferent and enteric neurons, thus

enteroendocrine cells are essential components of a complex network of signaling circuits, linking the gut with the rest of the body[91]. Furthermore, reports from mice lacking *Neurog3* gene, resulting in ablation of all enteroendocrine cell subtypes, showed impaired lipid absorption, reduced weight gain, growth retardation, and high lethality, demonstrating the essential role played by enteroendocrine cells in gut and nutritional homeostasis[92].

Enteroendocrine cell subtype	Associated hormone	Location	Physiological Function
D cells	Somatostatin	Small intestine	Acidity and insulin
Enterochromaffin cells	Histamine	Large intestine	Appetite and motility
I cells	Cholecystokinin (CCK)	Small intestine	Appetite, motility, bile acid, and enzyme release
K cells	Gastric inhibitory polypeptide (GIP)	Small intestine	Insulin
S cells	Secretin	Small intestine	Acidity
M cells*	Motilin	Small intestine	Motility
L cells	Glucagon-like peptide-1 (GLP-1) GLP-2, and Peptide YY (PYY)	Large intestine	Appetite, insulin, and motility
N cells	Neurotensin	Small intestine	Motility

Table 1. Location, function, and associated hormones by enteroendocrine cell subtypes. (*) Not to be confused with microfold 'M' cells, a specialized epithelial cell specific to the luminal surface of Peyer's patches.

1.3.6. *Enterocytes and Colonocytes*

Enterocytes, the absorptive IEC lineage present in the small intestine, and the colonocytes, its counterpart in the large intestine, are the most abundant IEC subtype of the intestinal tract. Enterocytes and colonocytes do not represent a homogeneous IEC subtype lineage, having functional and metabolic differences according to their location in the intestinal tract. Additionally, single cell RNA sequencing (scRNA-seq) survey, using small intestinal epithelial cells, revealed that enterocytes could be categorized into 7 different clusters according to their transcriptomic profile[80].

The enterocytes have a clear role in digestion, responsible for uptake of ions, water, sugar, amino acids, lipids, vitamins, and reabsorption of unconjugated bile salts. However, it has become evident that enterocytes have an active role in the induction of immunological tolerance toward dietary and microbial antigens, cooperating with mucosa-associated lymphoid tissue (MALT) to achieve a non-reactivity state[93].

Regarding enteric immune defenses, enterocytes participate directly in the transport of sIgA across the epithelial barrier. Following their production by plasma cells in the lamina propria, dimeric IgA complexes interact with the polymeric immunoglobulin receptor (pIgR), expressed on the basolateral

membrane of enterocytes, then actively transcytosed into the intestinal lumen[34,94]. Additionally, enterocytes can be stimulated by inflammatory cytokines to express antimicrobial peptides, such as β-defensins, and members of the regenerating family member 3 (REG3) of intestinal C-type lectin proteins, such as hepatocarcinoma-intestine-pancreas/pancreatic-associate protein (HIP/PAP), that contribute to the modulation of the gut microbiota[95,96].

Colonocytes exhibit regional adaptations to reflect a different environment, but also different functions compared to small intestinal enterocytes. For example, as glucose is scarce in the lumen of the large intestine, colonocytes have specialized mechanisms to obtain energy primarily from short-chain fatty acids, such as butyrate, which in turn is a by-product of dietary fibers metabolized by colonic bacteria. In fact, the production of these short-chain fatty acids is essential to ensure a healthy colon[97]. Thus, dietary style and shifts in the colonic microbial community can be detrimental to the host by depriving colonocytes of their primary energy source.

1.3.7. *Microfold Cells*

Microfold cells, or M-cells, are specialized epithelial cells found covering the most apical region of Peyer's patches, a follicle-associated epithelium (FAE), appendix, and in non-enteric MALT sites. At the apical surface, M-cells display short and poorly organized microvilli, having instead the characteristic 'microfolds', which assist them in surveilling the lumen for bacterial antigens by cancelling the electrostatic repulsion generated by the microvilli, distinguishing the M-cells morphologically and enzymatically from other IEC subtypes[98]. Additionally, at the basolateral surface, M-cells have an invagination "pocket", that functions as a docking site for lymphocytes and APCs, contributing to an efficient communication between M-cells and immune cells[99]. Therefore, the main function of M-cells is trans-epithelial transport of luminal components, via endocytosis, across the epithelial barrier, and their delivery to underlying immune cells[99]. Development of M-cells is independent of *Hes1*/*Atoh1* differentiation factors, instead relying on activation of receptor activator of NF-κB ligand (RANKL) followed by induction of transcription factor Spi-B[100]. Moreover, TNF-α signaling can act in synergy with RANKL, augmenting differentiation of M-cells during intestinal inflammation[100,101].

1.4. Inflammatory Bowel Diseases

Inflammatory Bowel Diseases (IBD) are pathologies characterized by relapsing chronic inflammation of the gastrointestinal tract. The symptoms commonly present are diarrhea, abdominal cramping, anemia, weight loss, and fatigue. Due to the nature of the disease, it considerably affects productivity, social functioning, and the quality of life of patients, requiring therapy, hospitalization, and occasionally surgery[102]. Ulcerative Colitis (UC) and Crohn's Disease (CD) are the two main entities affecting patients with IBD and although CD and UC share similarities, they have quite distinct pathophysiological characteristics. UC affects the colonic mucosa by causing erosions or microulcerations visible through endoscopic imaging[103]. Conversely, patients with CD may have sparse areas of inflammation, the most common being the distal ileum, but flares could happen in any region of the gastrointestinal tract. Different from UC, the inflammation process in CD affects all the layers of the intestinal wall[104]. Both entities share high incidence of dysplasia, placing IBD patients at an increased risk of developing colorectal cancer[103,105].

Many factors have been suggested to be involved with IBD development, such as genetics, environmental factors, diet, appendectomy, smoking,

stress, sleeping patterns, and physical activity[102]. The current paradigm is that these factors do not act in isolation, but rather in synergy. Mounting evidence indicates that interaction between genetic predisposition, external factors, and the intestinal microbiota are the three triggering factors for impaired intestinal barrier function and IBD onset. Consequently, luminal bacteria and/or antigens translocate across the intestinal epithelial layer into the lamina propria, triggering immune cell activation and cytokine production. In normal subjects, the inflammatory process leads to inactivation and destruction of exogenous components, barrier function reestablishment, and inflammatory process resolution. However, susceptible subjects are unable to resolve inflammation or eliminate invading microorganisms, leading to development of a chronic inflammatory state[106].

Normally, IEC subtypes are functionally altered in IBD although such impairments are dependent on IBD entity (Crohn's disease vs. ulcerative colitis), genetic susceptibility and site of disease activity, generally affecting Paneth cells number and function in Crohn's disease ileitis, whereas reduced numbers of goblet cells and a defective mucus layer are present in ulcerative colitis[107–112]. Moreover, UC patients with active disease display a thinner, deficient, variable mucus layer, immature goblet cells, and an altered MUC2

glycosylation profile that is not observable in patients in remission[110,111]. As a result, bacteria can be visualized dwelling in the normally impenetrable inner mucus layer of these patients[113]. Taken together, the functionally altered Paneth and goblet cells compromises innate immune mechanisms, impairing the host-microbiome relationship, which could result in increased susceptibility to infection.

1.5. Gut Microbiota, Dysbiosis and IBD

The gut microbiota consists of bacteria, viruses, archaea, and eukaryotic microbes. Commensal bacteria and pathobionts, defined as opportunistic bacteria that under favorable conditions can expand and drive development of clinical disease, are resident members of the gastrointestinal tract. Nevertheless, whether changes in the intestinal flora precede disease onset is still under investigation.

It is a daunting task to define what a balanced intestinal microbial community is, as the resident microbial flora is highly diverse, differs between individuals, and shifts with changes in the diet[97,114]. Moreover, gut microbiota composition varies by region of the gastrointestinal tract, developmental period, while many other factors have been shown to play a

role (i.e. genetics, metabolism, immunity, environment, and even host birth and delivery conditions)[21,115]. Yet, gut dysbiosis has been associated with many diseases, including obesity, chronic inflammatory conditions, cardiovascular disease, and neurodegenerative disorders[116]. In this context, dysbiosis is defined as an imbalance of the gut microbiota, with changes at their functional composition and metabolic activities[117].

It is believed that a 'normal' microbiota contributes to a healthy gut, by digesting certain nutrients that cannot be processed by the host and modulating the intestinal barrier by promoting tolerogenic immune responses. As an example, *Akkermansia muciniphila*, a human intestinal mucin-degrading bacteria, has been shown to induce mucin secretion, promote intestinal homeostasis and is inversely associated with intestinal inflammation[118]. Other identified human beneficial bacteria include: *Peptostreptococcus russellii*, *Faecalibacterium prausnitzii*, *Lactobacillus rhamnosus* Gorbach-Goldin, and *Bacteroides fragilis*[118].

Conversely, evaluation of fecal contents and mucosal bacterial isolations from patients with IBD, have reported alterations of the microbial community and expansion of pathobionts, showing depletion of certain commensals, notably members of the *Firmicutes* and *Bacteroidetes* phyla,

with increasing concentrations of anaerobes, including *Clostridium perfringens*, virulent strains of *Escherichia coli*, *Bacteroides* species, and others[117,118]. Although many investigations report corroborating data on the composition of IBD-associated microbial communities, they failed to identify individual species that are grossly enriched in a manner suggestive of an active etiologic agent. Furthermore, neither ulcerative colitis (UC) nor Crohn's disease (CD) is characterized by a uniform stereotypical microbiota[119].

Nevertheless, some CD and UC patients show increased prevalence of adherent-invasive *Escherichia coli* (AIEC)[120]. AIEC are distinct from other *E. coli* strains because they show nonclassic virulence factors of adherence and invasion, such as a type III secretion system, allowing replication of AIEC within IECs and macrophages that potentially further exacerbate barrier dysfunction and contribute to IBD pathogenesis[121,122].

1.6. *PTPN2* Variants and Their Contribution to IBD

Genome wide association studies have identified 240 independent single nucleotide polymorphisms (SNPs) associated with IBD[123]. Many of these genes are involved in activation and modulation of immune responses

(innate and adaptive), maintenance of epithelial barrier, autophagy, bacterial sensing, and production of antimicrobial factors, thereby emphasizing the complexity and heterogeneity of IBD pathophysiology[124,125]. Of interest, SNPs on the chromosome 18 locus (18p11) containing the protein tyrosine phosphatase non-receptor type 2 (*PTPN2*) gene, were found to be in association with IBD (CD and UC), type 1 diabetes mellitus, rheumatoid arthritis, and celiac disease[124,126–128]. Three SNPs have been identified within intronic regions of the *PTPN2* gene locus to be associated with elevated risk of IBD among different ethnic groups: rs2542151, rs1893217, and rs7234029[129–132], rendering the gene product enzymatically non-functional[130]. In fact, *PTPN2* activity (expression and protein levels) was found elevated in IECs of patients with active Crohn's disease, suggesting that *PTPN2* plays a significant role during intestinal inflammation[135]. However, the mechanism by which intronic SNPs in the *PTPN2* locus result in phosphatase loss-of-function remains to be elucidated[136].

Studies *in vitro* have shown that stimulation by IFN-γ induces *PTPN2* expression, suggesting a negative feedback response whereby IFN-γ induces expression of an inhibitor of its own signaling cascade[137,138]. With respect to intestinal function, we and others have shown, *in vitro* and *in vivo*, that

Ptpn2-loss increases intestinal barrier permeability[135,139], changes the composition of tight junction proteins[140], impairs IEC-macrophage communication[36], promotes differentiation of macrophages into an inflammatory phenotype subtype[141], and alters the intestinal microbiota to allow the expansion of an IBD-associated AIEC pathobiont[142]. Thus, accumulating evidence shows that *PTPN2* plays a critical role in intestinal homeostasis, whereby *PTPN2* loss affects primarily three aspects of intestinal function: (a) disrupting the intestinal barrier by increasing intestinal permeability along with remodeling of tight junction protein complexes; (b) generating a chronically inflamed intestinal mucosa, and (c) by altering the gut microbiome allowing expansion of pathobionts. Moreover, evidence also suggests that these aspects could be interconnected, in which the disruption of one, could promote the disruption of the other.

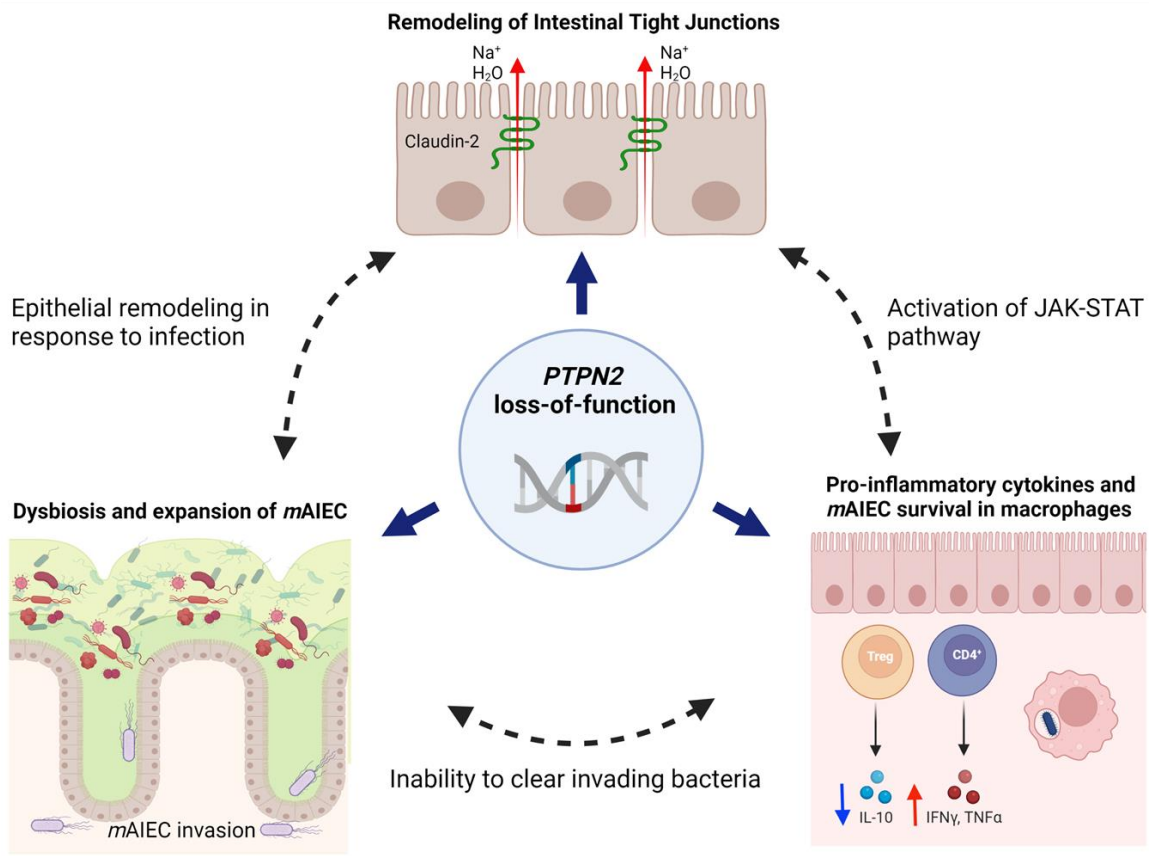

Figure 3. Diagram depicting *PTPN2* contributions to IBD. *PTPN2* loss-of-function has been shown to remodel intestinal epithelial tight junctions by increasing expression and localization of the "pore-forming" claudin-2 into the apical-lateral membrane, creating a more permissible epithelial barrier to paracellular passage of water, cations, and macromolecules[143]. In addition, *PTPN2* loss has been shown to increase abundance of pro-inflammatory cytokines, both in the serum and in the intestinal mucosa, which in turn contributes to remodeling of the tight junction proteins mediated by JAK-STAT activation in IECs. Moreover, constitutive *Ptpn2* loss, and specific-*Ptpn2* deletion in macrophages negatively affects macrophage ability to clear invading mouse AIEC (*m*AIEC)[144]. Furthermore, *Ptpn2* deletion has been shown to restrict expansion of pathobiont *m*AIEC (purple rod-shaped bacteria) while decreasing the abundance of symbionts (faded blue bacteria). Collectively, evidence from several studies report how *Ptpn2* activity is essential for modulating gut bacteria, controlling expression of tight junction proteins, and by attenuating inflammatory responses.

1.7. The *Ptpn2* Gene Product, T-Cell Protein Tyrosine Phosphatase, and its Substrates

T-cell protein tyrosine phosphatase (TCPTP) is the *PTPN2* gene product. It is ubiquitously expressed and functions as a negative regulator of diverse intracellular pathways[145]. It can bind to its substrates both in the cytosol and in the nucleus, due to two different isoforms expressed in human cells, where the cytosolic isoform, TC48, has an extended C-terminal domain that masks the nuclear localization sequence[146,147]. However, the shorter nuclear isoform, TC45, can translocate to the cytosol upon activation and perform its enzymatic function[148]. Of note, only the TC45 isoform of TCPTP protein has been detected in the mouse[149].

Among the TCPTP substrates are: Insulin Receptor (IR), Epidermal growth Factor Receptor (EGFR), Colony Stimulating Factor 1 Receptor (CSF1R), Platelet-Derived Growth Factor Receptor (PDGFR), Signal Transducer and activator of Transcription (STATs) 1, 3, and 6, Src family kinases and the Janus Kinases JAK1 and JAK3[150–158]. These substrates exemplify how broad and complex the activity of TCPTP is, hence an inactive form of this protein can negatively impact several cellular pathways/responses.

1.8. Study Proposal

Given the numerous findings regarding impaired function of the intestinal epithelial barrier in *Ptpn2*-deficient mice, it seems unlikely that the additive effects of a highly inflamed intestinal mucosa, together with structural changes between adjacent IEC, and the shift in the microbial communities present in these mice, would not be accompanied by functional changes in specific IEC subtypes.

Therefore, the hypothesis of this study is that *Ptpn2* plays a vital role in restricting intestinal inflammation that otherwise can functionally alter intestinal epithelial cell populations, compromising the integrity of the intestinal epithelial barrier and their interaction with the gut microbiota, thereby increasing susceptibility to microbial infection. Supporting this hypothesis, it has been reported that patients with CD and UC display functionally altered Paneth and goblet cells, as described previously[159,160]. Moreover, investigations using IBD-associated gene deletion mouse models, have shown that specific IEC subtypes are more susceptible to dysfunction and/or ablation, particularly Paneth cells, leading to dysbiosis and higher susceptibility to colitis[161,162].

To test this hypothesis, we utilized here both constitutive whole-body, and novel inducible tissue-specific, *Ptpn2*-deficient mouse models to investigate the function and morphology of IEC subtypes of the intestinal tract.

2. Methods

2.1. Animal models and colony maintenance

Mice colonies were held in a specific-pathogen free (SPF) facility with free access to food (PicoLab® Rodent Diet 20 5053, St. Louis, MO, USA) and water under 12 light/12 dark hour cycle with controlled temperature and humidity. Housing density was limited to 5 mice per cage. Adult mice were bred in a pair scheme and pups were weaned at 21 days of life. All animal experiments were performed according to, and approved by, the Institutional Animal Care and Use Committee (IACUC) at University of California, Riverside (UCR) under protocol #A20190032E.

2.1.1. *Constitutive Ptpn2-deficient mice*

BALB/c mice with constitutive (whole-body) *Ptpn2* deficiency were provided by Michel Tremblay, McGill University[163]. Briefly, to inactivate the *Ptpn2* gene, a targeting vector was constructed that contained the genomic sequences flanking a neo resistance sequence. After proper homologous recombination, approximately 9kb of genomic sequence was eliminated, including 1.5 exons encoding amino acids 64-121 from the *Ptpn2* locus, rendering the gene product enzymatically nonfunctional. Adult

heterozygous mice were bred yielding *Ptpn2*-wild type (WT), -heterozygous (HET) and -knockout (KO) mice. Tissues were harvested when mice reached 21 days old as whole-body homozygotic *Ptpn2* deficient mice succumb between four and five weeks of age due to systemic inflammation[163,164].

2.1.2. *Mice with inducible Ptpn2-KO in intestinal epithelial cells*

Inducible tissue specific *Ptpn2*-KO mice were generated by Dr. Lars Eckmann and Elaine Hanson at the University of California San Diego. Briefly, a mouse line where the critical exon 3 within the *Ptpn2* locus is flanked by loxP sites ($Ptpn2^{tm1a(EUCOMM)Wtsi/Wtsi}$), were obtained from the Wellcome Trust. These mice were crossed with a transgenic mouse line expressing the Cre recombinase enzyme that carry a tamoxifen-induced *ERT2* gene under the Villin-1 promoter [B6.Cg-Tg(Vil-cre/ERT2)23Syr/J][143,165]. Recombinase activity was induced by tamoxifen administration intraperitoneally (50mg/kg body weight) for five consecutive days in 6-10 weeks old mice. Tissues were harvested >30 days after final dose of tamoxifen to minimize any potential residual effect from estrogen receptor activation[165].

2.2. Sacrifice and sample collection

Mice were anesthetized with 4% isoflurane (Piramal, NDC 66794-017-25) and kept under anesthesia during blood collection. Incision was performed on the abdomen to expose the inferior vena cava. Following blood collection, mice were sacrificed by cervical dislocation. Distal ileum, cecum, proximal and distal colon were excised. Small tissue samples from each intestinal segment were collected according to optimized protocols for further examination as described below.

2.3. Tissue fixation, microscopy, and image acquisition

Intestinal segments from ileum, cecum, proximal and distal colon were excised and fixed in 4% paraformaldehyde overnight at 4°C. Tissues were then rinsed with ice-cold phosphate buffered saline (PBS) (3x) and dehydrated with increasing concentrations of ethanol washes using Shandon Excelsior ES Tissue Processor (Thermo Fisher Scientific - Kalamazoo, MI, USA). Paraffin embedding was performed using Histoplast LP (Richard-Allan Scientific - Kalamazoo, MI, USA) in a Tissue-Tek station set (Miles Scientific - Naperville IL, USA). Intestinal cross-sections (5 μm thick) were obtained using a rotary microtome (RM2235, Leica – Nussloch, Germany).

Paraffin sections were warmed up in a water bath (42°C) to prevent wrinkles, placed on a charged slide (Fisher Scientific – Pittsburg, PA, USA) and dried overnight in an oven at 37°C. Slides were stored in the dark at room temperature until utilized for conventional staining techniques and immunohistochemistry/immunofluorescence.

2.3.1. *H&E staining*

Slides were deparaffinized in xylene (2x) for 5 minutes, rehydrated in serial decreasing ethanol baths (100, 95, 80, and 70%) for 3 minutes, then placed in tap water. Slides were stained with hematoxylin (30 seconds; RICCA – 3530-16, Arlington, TX), and eosin Y (1 minute; Sigma-Aldrich HT110132, St. Louis, MO) with tap water rinses following each stain. Next, slides were dehydrated with increasing concentrations of ethanol (95%, 100%), cleared with xylene for 1 minute and mounted with a coverslip using Permount® medium (FISHER SP15-500, Fair Lawn, NJ). Slides were visualized and images acquired with a Leica microscope model DM5500B coupled with DFC450C camera (Leica – Nussloch, Germany).

2.3.2. *PAS staining*

To visualize the presence of goblet cells in the intestinal segments, mucopolysaccharide filled-cells were stained using the Periodic Acid-Schiff (PAS) kit (Sigma, Procedure No. 395) following the manufacturer's protocol. Briefly, after deparaffinization, slides were immersed in Periodic acid solution for 5 minutes in a glass coupling jar. Slides were rinsed in three changes of distilled water and then immersed in Schiff's reagent for 15 minutes. Slides were washed in running tap water for 5 minutes and counterstained with Hematoxylin solution, Gill No.3 for 90 seconds. Slides were washed in running tap water again, dehydrated and cleaned like described before and mounted with coverslip and Permount®. This staining procedure results in mucin proteins stained in magenta, whereas cell nuclei are stained in blue.

2.3.3. *Morphometric analysis and cell counting*

Only well-oriented intestinal structures (i.e., crypt and villi) with bottom-to-top axis visibility were used in the analysis. The straight-line tool from FIJI software was calibrated using the scale bar from the image being measured. A straight line was drawn to measure crypt depth, villus length and crypt

width. All measurements from each parameter were averaged out to represent the mean of an individual mouse. A minimum of 4 measurements *per* parameter was set as a cutoff to provide a more accurate representation of the mouse. For cell counting, total number of IECs *per* crypt was counted using the Cell Counter tool on FIJI software. For Paneth cell counting, Paneth cells were discriminated from other intestinal epithelial cells by the presence of large cytosolic granules at the crypt base. The same quantification was performed discriminating Paneth cells from other IECs by the presence of lysozyme staining. The ratio of Paneth cells/total IECs *per* crypt was then calculated and averaged to represent a single mouse. Similarly, PAS-stained images were used to count goblet cells *per* crypt by calculating the same PAS^+ cells/total IECs ratio. In the ileum, goblet cells were counted by half-villus structures.

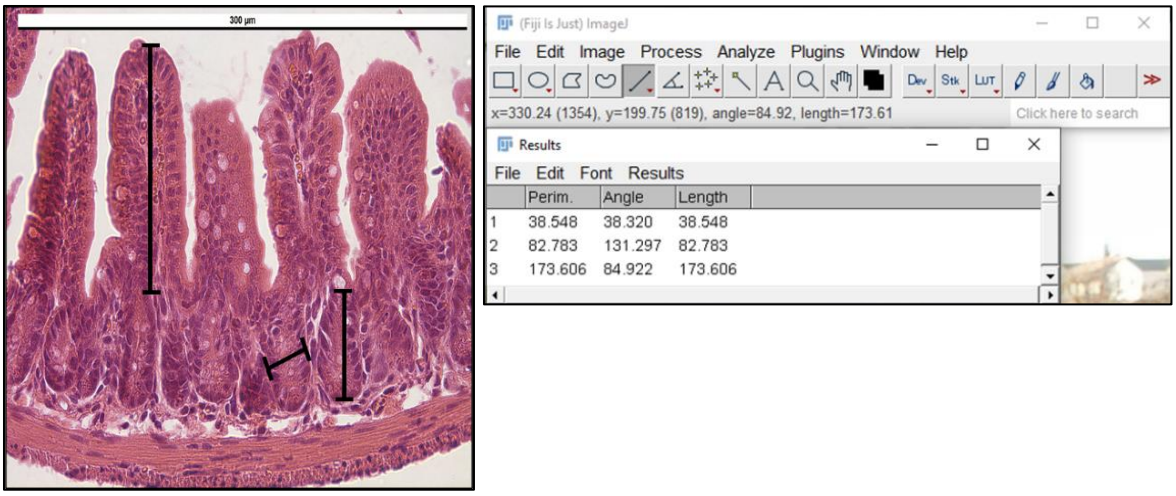

Figure 4. Measuring intestinal morphological parameters with ImageJ.

2.3.4. *In situ protein localization by immunohistochemistry and immunofluorescence*

Slides were deparaffinized and rehydrated as previously described in section 2.3.1. To expose the tissue epitopes for antibody binding, heat-induced antigen retrieval was performed for 20 minutes at ~96°C, with appropriate antigen retrieval buffer depending on the primary antibody/epitope. Selection of appropriate antigen retrieval buffer followed antibody datasheet instructions or optimization in the laboratory. The primary antibodies, concentration, antigen retrieval buffer and secondary antibody are shown in Table 2. After antigen retrieval, intestinal sections were encircled with hydrophobic PAP PEN (Research Products International Corp. Cat. No.

195505), endogenous peroxide was quenched with 3% hydrogen peroxide in PBS for 10 minutes (for immunohistochemistry using peroxidase reaction only). Non-specific antigens were blocked with blocking buffer (2% normal donkey serum, 1% bovine serum albumin, 0.1% Triton-X, 0.05% Tween-20 and 0.05% sodium azide in PBS) for 30 minutes at room temperature. Primary antibodies were incubated for 1 hour at RT in PBS with 5% normal donkey serum (NDS). A biotin-conjugated secondary antibody against the primary species was used to tag the protein of interest (Jackson ImmunoResearch, Cat. No. 711.065.152, West Grove, PA). Then, a horseradish peroxidase (HRP), or fluorophore-streptavidin conjugated molecule, was used for labeling the protein conjugate (Jackson ImmunoResearch, Cat. No. 016.030.084, West Grove, PA). For immunohistochemistry, HRP signal was developed by 3,3'-diaminobenzidine (DAB; Cell Signaling Technology #8059 Beverly MA, USA) incubation according to manufacturer's protocol. Incubation time was optimized for each target. Sections were counterstained with hematoxylin and mounted with Permount®. For immunofluorescence, Prolong® Gold with DAPI was applied to the slides according to manufacturer's guidelines (Cat. No. P36936; Life Technologies, Carlsbad, CA). Confocal images were

acquired on an inverted Zeiss 880 in the microscopy core in the IIGB microscopy core facility located in Keen Hall at UCR. Cryptdin-1 (Defa1) monoclonal antibody was generated and kindly provided by Tokiyoshi Ayabe and André Ouellette, and stained as previously described[166].

Table 2. List of immunohistochemistry reagents

Antibody	Company	Cat. No.	Antigen Retrieval Buffer	Primary Concentration
Lysozyme	Abcam	ab108508	Na-Citrate pH 6	1:3000
Ki-67	Abcam	ab16667	Na-Citrate pH 6	1:400
UEA1-649 DyLight	Vector Labs	DL-1068	Na-Citrate pH 6	1:500
Tunel	Millipore	S7110	Proteinase K	Data sheet
E-cadherin	R&D Systems	AF748	Na-Citrate pH 6	1:200
pSTAT3	Cell Signaling	9145	Tris-EDTA pH 9	1:50
TCPTP	Cell Signaling	58935	Na-Citrate pH 6	1:400
Defa1	Provided by Andre Ouellette	N/A	Tris-EDTA pH 9	1:500
Claudin-2	Abcam	Ab53032	Na-Citrate pH 6	1:400
CEACAM-6	Abcam	Ab78029	Na-Citrate pH 6	1:200
CEACAM-1	Cell Signaling	14771	Na-Citrate pH 6	1:50

2.3.5. *Analysis of the mucus layer*

To preserve and visualize the colonic mucus layer, distal colon segments containing fecal pellets were excised (cut around the fecal pellets) and

placed in a 1.5mL tube with methacarn fixative [modified Carnoy fixative with 60% methanol (v/v), 30% chloroform (v/v), and 10% glacial acetic acid (v/v)], to preserve the mucus layer as described previously by Malin Johansson and Gunnar Hansson[167]. Tissues were fixed in methacarn for >7 days at room temperature and washed twice with methanol (30 mins/wash), absolute ethanol (20 minutes/wash) and xylene (15 minutes/wash). Finally, tissues were embedded into paraffin blocks and sectioned (5μm). The sections were stained with PAS as previously described.

2.3.6. *TUNEL staining - ApopTag*

To localize apoptotic cells *in situ*, we performed a terminal deoxynucleotide transferase mediated dUTP-digoxigenin nick-end labeling (TUNEL) stain (ApopTag®, Millipore S71110, Billetica, MA, USA). This methodology labels apoptotic cells by detecting DNA strand breaks enzymatically and labeling the free 3'-OH termini with modified nucleotides. The enzyme responsible for this reaction is terminal deoxynucleotidyl transferase (TdT). The incorporated nucleotides form an oligomer composed of digoxigenin-nucleotide which is detected by an anti-digoxigenin antibody conjugated with fluorescein. In brief, slides were deparaffinized, rehydrated and DNA-

binding proteins were digested enzymatically by 20μg/mL proteinase K (Cat. No. 21627, Millipore, Temecula, CA) for 15 minutes at room temperature and assayed according to manufacturer's protocol. Positive control slides were pretreated with DNase buffer (30mM Trizma base, pH 7.2, 4mM $MgCl_2$, 0.1mM DTT) at room temperature for 5 minutes, then incubated with DNase I in 10,000 U/mL DNase buffer for 10 minutes at room temperature. For the negative control slide, the incubation step with TdT enzyme was done with buffer alone. Cell nuclei were counterstained with DAPI, mounted and visualized using confocal microscopy.

2.3.7. *Transmission electron microscopy*

Ileal sections were excised, cut open longitudinally, and fixed in 1.25% glutaraldehyde and 4% paraformaldehyde in 0.1M cacodylate buffer for 5-6 hours at room temperature. The fixative was then removed, and samples were rinsed in 0.1M cacodylate buffer. Samples were further processed at UCR's Facility for Advanced Microscopy and Microanalysis (CFAMM) according to a protocol published by Satoh et al[168]. Briefly, samples embedded and plasticized in Spurr's resin then sectioned into 80nm, gold-colored sections with a surface area of about 0.25mm^2. Images were

acquired using a Tecnai T12 transmission electron microscope (FEI, Hillsboro, OR). The bottom of the intestinal crypts were evaluated for morphology, presence/absence of dense core vesicles and the endoplasmic reticulum, of Paneth cells. Linear adjustments (brightness and contrast) were performed in original images in its entirety using FIJI software to enhance visibility of cell organelles.

2.4. Isolation of intestinal epithelial cells

Intestinal segments were cut open longitudinally and immersed in 500μL of Cell Recovery Solution (Corning #354253; Bedford, MA) for 2 hours on ice. Tissues were then shaken with forceps to release the intestinal crypts/villi into the solution. Samples were centrifuged at 1.5 x g for 10 minutes at 4°C. The supernatant was aspirated and IECs were washed with ice-cold PBS (x2). The solution with IECs was then split: 70% of IEC suspension was centrifuged and cells lysed using RIPA buffer (150mM NaCl, 5mM EDTA, 50Mm Tris, 1% NP-40, 0.5% sodium-deoxycholate, and 0.1% SDS) supplemented with protease inhibitor cocktail (Roche, Mannheim, Germany), 2mM sodium fluoride, 1mM PMSF, 2mM sodium orthovanadate, and phosphatase inhibitor cocktails 2 and 3 (Millipore Sigma, P5726 and

P0044 respectively, Israel) and stored at -80°C. The remaining 30% was centrifuged and stored in 200µL of RNAlater™ solution (Invitrogen #AM7020, Lithuania) was added to the pelleted cells, according to manufacturer's guidelines, and stored in -80°C.

To assess the purity of isolated IECs, we evaluated the abundance of epithelial cell markers (EpCAM), immune cell marker (CD45) and fibroblast/mesenchymal cell marker (α-SMA) by western blot as shown in Figure 5.

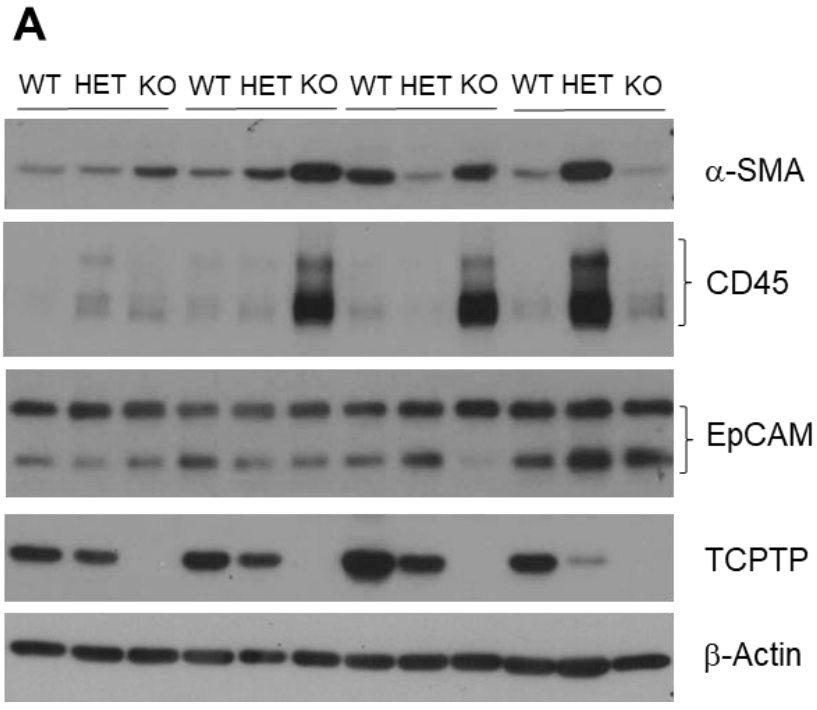

Figure 5. Assessment of isolated IEC sample purity. **(A)** Western blot of ileal IECs probing for α-smooth muscle actin (α-SMA) to assess presence of mesenchymal cells; CD45 to assess presence of leukocytes; and EpCAM to assess abundance of epithelial cells.

2.5. RNA extraction, cDNA synthesis and gene expression analysis

Total RNA was isolated using the RNeasy Mini Kit (Cat. No. 74106 - Qiagen, Venlo, NL), according to manufacturer's instructions. Briefly, samples were washed with PBS to remove RNAlater™. 10μL of β-Mercaptoethanol was added to each 1000μL of RLT lysis buffer to prevent RNA degradation. Cells were lysed using sterile needle (22G) and syringe and RNA was isolated according to manufacturer's guidelines. Total RNA concentration was quantified by measuring the absorbance at 260 nm and 280 nm using NanoDrop 2000c spectrophotometer (Thermo Scientific - Wilmington, DE, USA). Complementary DNA (cDNA) synthesis was performed using the qScript® cDNA SuperMix (Cat. No. 95048 Quantabio - Beverly, MA, USA) in a Bio-Rad thermocycler (C1000 Touch, Singapore) following the manufacturer's instructions (incubation at 25°C for 5 mins followed by 42°C for 30 mins, 85°C for 5 minutes and ramped down to 4°C). The cDNA was stored at -20°C total RNA was stored at -80°C.

2.5.1. *Nanostring analysis*

Total RNA was extracted as described above. Estimation of total RNA was determined by Qubit 2.0 Fluorometer (ThermoFisher Scientific) and sample purity by NanoDrop™ 2000c spectrophotometer by measuring the 230/260 and 260/280 ratios. Samples were diluted to 10 ng/μL with RNAse-free water. Hybridization reaction was performed following manufacturer's guidelines using 50 ng of total RNA from each sample. In short, gene expression of IECs from ileum, cecum, and distal colon was investigated using the PanCancer Pathways Panel and the AutoImmune Profiling Panel, totaling more than 1,500 targets. Gene expression of liver samples using whole tissue lysates was performed using the AutoImmune Profiling Panel. Samples were hybridized with reporter and capture probes for 18 hours at 65°C. Reaction was ramped down to 4°C, 12 μL of RNAse-free water added to each sample and immediately pipetted into a cartridge and processed by nCounter® SPRINT Profiler (Nanostring® Technologies, Seattle, WA, USA). Data sets were normalized by nSolver™ Analysis Software 4.0 for each panel separately then combined using multiRLF function and advanced analysis tools. The α-value was set at 0.05 and false discovery rate (FDR) calculated by the Benjamini-Yekutieli method setting a cutoff at 10%

(Q=0.1) for multiple-comparisons testing. The datasets generated from nanostring analysis were submitted to Gene Expression Omnibus (GEO) repository. GEO is a public functional genomics data repository supporting MIAME-compliant data submissions[169,170]. Access to datasets will be made publicly available on August 02, 2022, or when manuscript referring the data is published. Accession numbers are listed in Table 3.

Table 3. GEO repository accession numbers from Nanostring experiments

Accession Number	Description
GSE181923	Super series record provides access to all data
GSE181531	Targeted transcriptome analysis of isolated intestinal epithelial cells from mice with constitutive Ptpn2-deficiency [Ileum]
GSE181531	Targeted transcriptome analysis of isolated intestinal epithelial cells from of mice with constitutive Ptpn2-deficiency [Cecum]
GSE181916	Targeted transcriptome analysis of isolated intestinal epithelial cells from mice with constitutive Ptpn2-deficiency [Distal Colon]

2.5.2. *Primer design and validation*

Primers were designed using the Primer-BLAST tool from NCBI website. The RefSEQ numbers of targets of interest were entered in the PCR template field. In addition, primers were designed to align over an exon-exon junction span to prevent alignment with residual genomic DNA. Search mode selected was ‘automatic’ and the database was *mus musculus* species (taxid:

10090) Refseq mRNA. The Primer-BLAST tool then returned 10 different pairs of primer sequences. Primer selection was based on the following parameters: PCR product size (amplicon) ranging between 70 and 300 nucleotides; primer length ranging between 18 and 23 nucleotides, GC content ranging between 45% and 60%; and the lowest scores of self-complementarity and self-3' complementarity. Selected primer sequences were purchased from IDT (Integrated DNA Technologies, San Diego, CA). Upon receipt, lyophilized oligos were resuspended to a total of 100μM concentration in TE buffer (IDT Cat. No. 11-05-01-13) and stored at -20°C.

Table 4. Primers and conditions used for RT-qPCR

Gene	Primer Sequence	GC %	Length	Tm	Amplicon	RefSEQ
Ascl2	F: TCTTGGGGCTTAAGGGCTGA R: GTCAAGGTGTGCTTCCATGC	55 55	20 20	59°	192	NM_008554.3
Reg3b	F: GAATATACCCTCCGCACGCA R: TCTTTTGGCAGGCCAGTTCT	55 50	20 20	60°	119	NM_011036.1
Reg3g	F: TGCAAGGTGAAGTTGCCAAG R: GGTTCATAGCCCAGTGTCGG	50 60	20 20	60°	274	NM_011260.2
Tbp (HK)	F: CCTTGTACCCTTCACCAATGAC R: ACAGCCAAGATTCACGGTAGA	50 47	22 21	61°	119	NM_013684.3

Primers were validated and optimized empirically. First, a thermal gradient optimization was done to find out what is the most efficient annealing temperature for a specific set of primers in the conditions used. The

annealing temperature with the lowest Ct value was selected as optimal. Then, a melting curve analysis was performed to confirm amplification of a single target (specificity) and primer-dimer formation (Figure 6A-B). Finally, PCR products were separated in a 2% agarose gel electrophoresis to confirm presence of a single amplicon (Figure 6C).

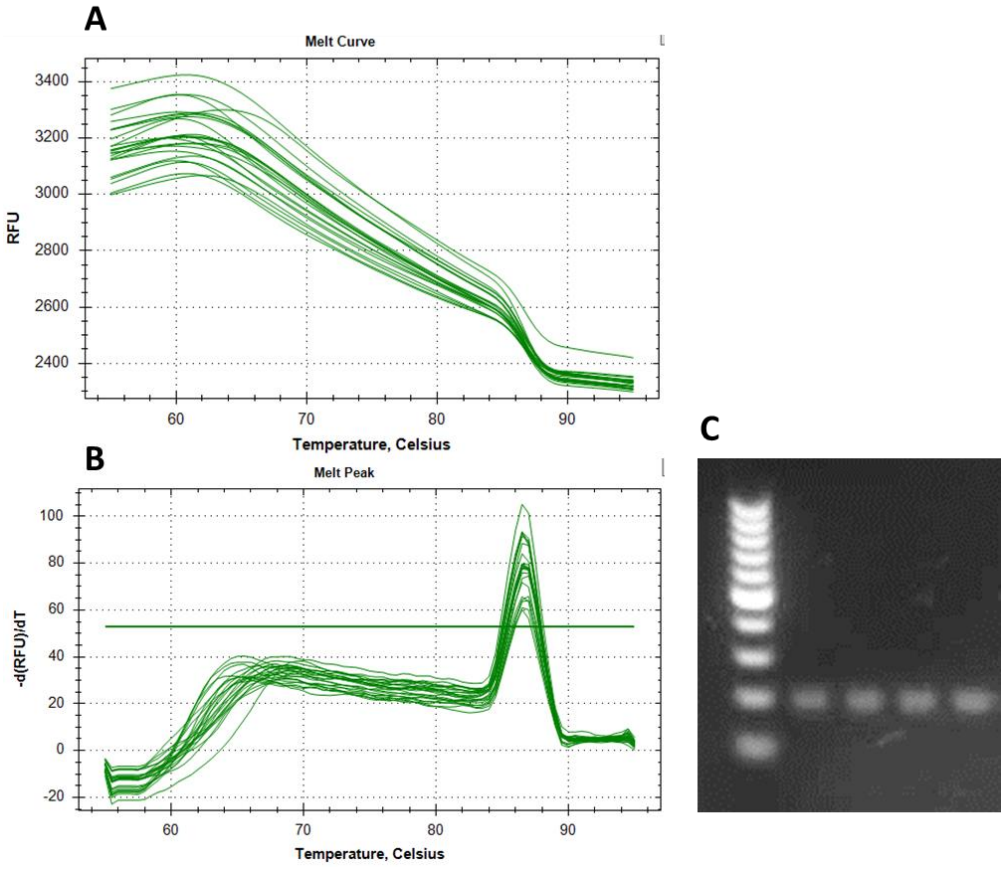

Figure 6. Validation of RT-qPCR primers through **(A)** melt curve, **(B)** melt peak, and **(C)** gel electrophoresis.

2.5.3. *RT-qPCR*

Real-time PCR was performed using iQ SYBR Green Supermix (Bio-Rad, Hercules, CA) on a C1000 Thermal cycler equipped with a CFX96 Real-Time PCR system using BioRad CFX Manager 3.1 Software following manufacturer's protocol. Each PCR target was assayed in triplicate. *Tbp* was used as a reference gene. All primers were designed using NCBI Primer-BLAST and specificity and optimal annealing temperatures were tested empirically. The real-time quantitative PCR contained an initial enzyme activation step (3 min, 95°C), followed by 45 cycles consisting of denaturing (95°C, 10 seconds), annealing (53°- 60°C, 10 seconds) and extension (72°C, 10 seconds) steps. The primers and conditions used in the RT-qPCR experiments are listed in Table 2. Results were analyzed by the ΔΔCT method and graphs display geometric mean ± SD of geometric mean in a $\log_{10}$ scale.

2.6. Detection of protein levels by immunoblotting

Frozen IEC samples in RIPA buffer were thawed on ice and lysed using a sonicator (QSONICA Model Q125, Newtown CT, USA) with the following settings: 30% amplitude for a total time of 40 seconds with 10 seconds

intervals. Lysates were centrifuged at 13,000 RPM for 10 minutes at 4°C and the supernatant transferred to new microcentrifuge tubes. Total amount of protein was estimated by Pierce™ BCA colorimetric assay (Cat. No. 23225 - Thermo Scientific – Rockford, IL, USA) according to manufacturer's guidelines. Protein quantification was estimated by measuring the sample absorbance in plastic cuvettes at 562nm in a NanoDrop™ 2000c (Thermo, Wilmington, DE, USA) spectrophotometer, and plotted against a standard curve with known protein concentrations. 20μg of protein per sample was prepared for gel electrophoresis under reducing conditions using 4X Laemmli loading buffer (Cat. No. 1610747 BioRad, Hercules, CA, USA). Samples were heated to 95°C for 5 mins and stored at -20°C. Samples were loaded on polyacrylamide gels and after separation by gel-electrophoresis transferred onto Immobilon-P Polyvinylidene Fluoride (PVDF) membranes (Immobilon-P Millipore Cat. No. IPVH00010, Temecula, CA) in a wet transfer system (Mini-PROTEAN® Tetra System, BioRad). Non-specific epitopes were blocked with 5% non-fat milk in Tris-buffered saline with 0.1% Tween-20 added (TBST) for 1 hour at RT.

Table 5. List of antibodies used for immunoblotting.

Antibody	Company	Cat. No.
Lysozyme	Abcam	ab108508
β-Actin	SIGMA	A 5316
TCPTP	Cell Signaling	58935
Caspase3	Cell Signaling	14220
Cleaved Caspase 3	Cell Signaling	9664
CHOP	Cell Signaling	2895
PARP	Cell Signaling	9542
Bip	Cell Signaling	3117
Xbp-1s	Cell Signaling	40435
α-SMA	SIGMA	A 2547
CD45	Cell Signaling	72787
EpCAM	Cell Signaling	42515
Mist1	Santa Cruz	sc-80984
Reg3-γ	Abcam	ab198216
eIF2-α	Cell Signaling	5324
p-eIF2-α	Cell Signaling	3398
Olfm4	Cell Signaling	39141
STAT1	Cell Signaling	14994
p-STAT1	Cell Signaling	9167
STAT3	Cell Signaling	9139
p-STAT3	Cell Signaling	9145
Beclin-1	Cell Signaling	3495
LC3B	Cell Signaling	2775
Atg3	Cell Signaling	3415
Atg5	Cell Signaling	12994
Atg7	Cell Signaling	8558
Atg12	Cell Signaling	4180
Atg16l1	Cell Signaling	8089

Membranes were incubated overnight with primary antibody at 4°C in 5% non-fat milk or bovine serum albumin (Cat. No. A9418 SIGMA, USA) washed (x4) with TBST, and incubated with HRP-conjugated secondary antibody anti-primary species for 1 hour at RT in TBST with 3% non-fat milk. Membranes were washed again with TBST (x4), and immunoreactive proteins were detected using SuperSignal™ West Pico PLUS chemiluminescence detection kit (Cat. No. 34580 Thermo Fisher Scientific). Membranes were then exposed to X-ray films (Labscientific Inc., Highlands, NJ) at various times in a dark room and developed immediately after. Densitometry of protein blots was measured using the gel tool on FIJI software.

2.7. Flow cytometry

For flow cytometry of immune cells, lamina propria immune cells were isolated as described[171]. For analysis of myeloid immune cells, the cells were washed in PBS, incubated with FcR blocking antibody (Miltenyi Biotec, Bergisch Gladbach, Germany) for 10 minutes and stained with anti-CD45-Pacific Blue, anti-CD3-BV650, anti-NK1.1-BV650, anti-B220-BV650, anti-CD11b-BV605, anti-CD11c-PECy7, anti-Ly6C-PerCPCy5.5, anti-F4/80-

APC, anti-CD64-PE, anti-MHC-II-AF700 (all from BioLegend) for 15-30 minutes. ZOMBI-NIR live dead stain (BioLegend, San Diego, CA) was used for discrimination between live and dead cells. For cytokine staining, the cells were incubated with Ionomycin and PMA in the presence of Brefeldin A for 3.5 hours prior to surface staining with anti-CD25-AlexaFluor700, Anti-CD3-PerCPCy5.5 anti-CD4-BV510, anti-CD8-BV570 for 15 minutes. Cells were then fixed with the FoxP3 Staining kit (eBioscience) according to the manufacturer's instruction, stained with anti-FoxP3-Pacific Blue, anti-IFN-γ-PECy7, anti-IL-17-APC, anti-TNFα-BV650, anti-IL-22-PE for 30 min, washed in PermWash buffer (eBioscience) and samples acquired on an LSRII cytometer (BD, Franklin Lakes, NJ), and analyzed using FlowJo (Tree Star, Inc. Ashland, OR). The gating strategy is demonstrated in Figure 7.

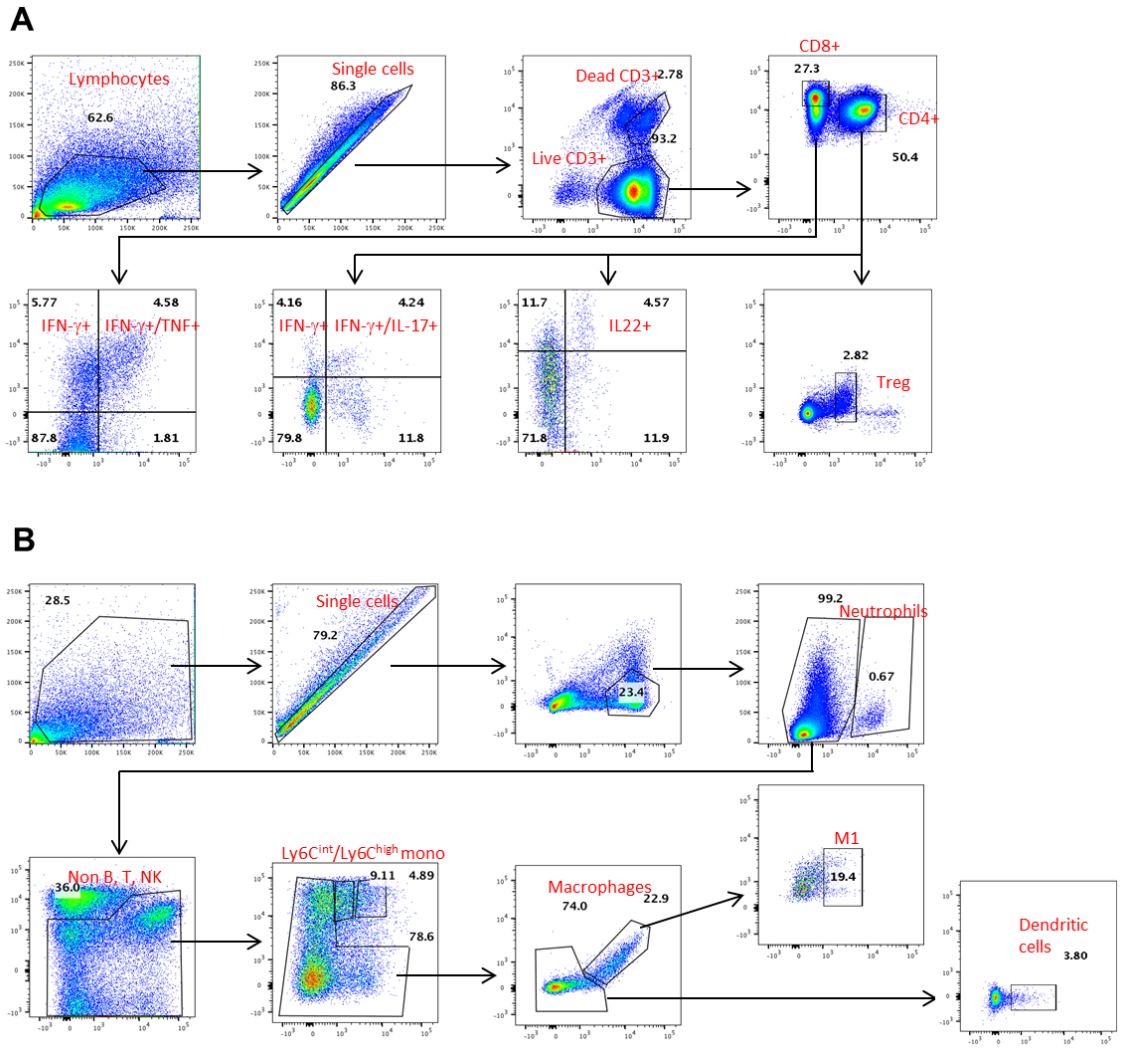

Figure 7. Flow cytometry gating strategy for **(A)** T-cells; and **(B)** myeloid cells.

2.8. Human samples

Human samples were obtained from IBD patients attending the IBD Center at Cedars-Sinai Medical Center after informed consent. The collection of intestinal biopsies, DNA preparation and genotyping were approved by the Cedars-Sinai Medical Center Institutional Review Board (3358). Tissue samples were reviewed by pathologists and active inflammation had been excluded. Diagnoses of IBD were made using standard clinical, endoscopic, radiological, and histological criteria. Genotyping and quality control for the rs1893217 SNP was performed as previously described utilizing the Immunochip™ (Illumina, San Diego, USA) platform[172]. Formalin-fixed paraffin embedded human colon and ileal tissues were sectioned at 5μm and processed for immunohistochemistry as described above.

Table 6. IBD-genotyped patients characteristics

Variant	Diagnosis	Region	Sex	Age
AA/TT	CD	Colon	F	47
AA/TT	CD	Colon	M	22
AA/TT	CD	Colon	F	43
AA/TT	CD	Colon	F	73
AA/TT	CD	Colon	F	32
GA/CT	CD	Colon	F	24
GA/CT	CD	Colon	M	74
GA/CT	CD	Colon	F	16
GA/CT	CD	Colon	F	47
GA/CT	CD	Colon	F	45
GG/CC	CD	Colon	F	70
AA/TT	CD	Ileum	M	34
AA/TT	CD	Ileum	F	47
AA/TT	CD	Ileum	M	22
AA/TT	CD	Ileum	F	43
AA/TT	CD	Ileum	F	73
AA/TT	CD	Ileum	F	32
GG/CC	CD	Ileum	F	24
GG/CC	CD	Ileum	F	46
GG/CC	CD	Ileum	M	25
GG/CC	CD	Ileum	F	36
GG/CC	CD	Ileum	M	28
GG/CC	CD	Ileum	F	38
GG/CC	CD	Ileum	M	41

2.9. Diagram design and software

Figures 1, 2, 3, 37, and 50 were constructed using BioRender online software based on scientific findings. The original articles in which the figures were based are cited in the figure legend and publication information can be found in the references section.

2.10. Statistical analysis

Datasets were tested for two parameters: normality (Shapiro-Wilk test) and variance homogeneity (Brown-Forsythe test; F test) using GraphPad Prism 9.0.0. software. Statistical and post-hoc tests were chosen according to these parameters and are indicated on figure legends. Two-tailed student t-test was applied when comparing two groups and ordinary one-way ANOVA for comparison of three experimental groups. Critical significance level was set at α=0.05. Data are expressed as mean, SD for *n* independent observations per group unless stated otherwise. Outliers were identified using the ROUT method with Q set at 1% and excluded when appropriate.

3. Validation, Characterization, and Assessment of Structural Components of the Intestinal Epithelial Barrier in Mouse Models, with Constitutive, and Tissue Specific, *Ptpn2* Deletion

3.1. Introduction

Evidence from *in vitro* studies show that *PTPN2* loss has dramatic consequences not only for immune cells but also for intestinal epithelial cells and maintenance of the intestinal barrier. Scharl et al. demonstrated that treating T84 epithelial cells with IFN-γ significantly increased TCPTP transcription, protein levels and enzyme activity, resulting in decreased levels of phosphorylated STAT1 and 3 in the cytosol[135]. Additionally, cells knocked-down for *PTPN2* and challenged with IFN-γ had increased levels of phosphorylated STAT1 and 3 that contributed to barrier dysfunction, assessed by increased permeability to macromolecules and reduced trans-epithelial resistance (TER) across polarized monolayers[135]. These findings are clinically relevant since analysis of biopsies from IBD patients with active disease revealed upregulation of *PTPN2* expression[135].

A mouse model with constitutive *Ptpn2*-deficiency was originally developed by Michel Tremblay's group, in which the *Ptpn2* gene product was inactivated by inserting a neomycin resistance gene replacing nearly 9 kb of the genomic sequence, including 1.5 exons encoding amino acids 64-121, rendering the gene product enzymatically nonfunctional[163]. While *Ptpn2*-KO mice appear normal at birth, within two weeks they begin to show reduced body weight, decreased mobility with hunched posture, and diarrhea followed by death between 3 and 5 weeks of age. *Ptpn2*-KO mice also display splenomegaly, defects in lymphopoiesis and erythropoiesis with elevated levels of circulating IFN-γ[163,164,173]. Conversely, heterozygous mice do not display physiological abnormalities nor overt inflammatory phenotype, however they show increased susceptibility to DSS-induced colitis[174]. The whole-body *Ptpn2* deficient mouse model, together with tissue-specific *Ptpn2* deletion in IECs, has enabled important discoveries in understanding how loss-of-function *Ptpn2* mutations could contribute to the pathogenesis of chronic inflammatory diseases and cancer[175–179].

While several studies have focused on the implications of *Ptpn2* deletion upon modulation of the intestinal barrier and immune cell responses, data regarding intestinal morphology, differentiation and function of individual

IEC subtypes is scarce. Moreover, since functions of different specific IEC subtypes encompass tissue regeneration, production of AMPs, surveillance of the luminal environment, and generation of the mucus layer, an imbalance in one of these populations could be detrimental to intestinal homeostasis, ultimately contributing to higher susceptibility to infection and chronic inflammation. Therefore, we aimed to further characterize and validate the constitutive and tissue-specific mouse models carrying *Ptpn2* deficiency, evaluate intestinal tissue morphology, and probe for markers that could indicate alterations in the recognition and/or handling of bacteria by IECs, while corroborating findings in the animal setting with samples from genotyped-IBD patients.

3.2. Methods

For this study, we utilized histology, immunohistochemistry and western blotting of isolated intestinal epithelial cells that were described in detail in the methods chapter. The experiments and data shown in this chapter were partially or fully included in articles recently published by our group.

3.3. Results

3.3.1. *Characterization and Validation of TCPTP Expression and Intestinal Morphology in Whole-Body Ptpn2-KO Mice*

Our group described for the first time the consequences of whole-body *Ptpn2* loss-of-function regarding intestinal architecture, morphology, and intestinal barrier function[143]. Figure 8 shows that *Ptpn2*-KO mice display reduced body weight, splenomegaly when normalized to body weight, and shortening of the colon when they reach 21 days old, corroborating the findings of You-Ten et al, in our own setting[163]. Moreover, we also observed that KO mice begin to show signs of hunched posture, lethargy, closed eyelids and diarrhea around day 14 post-birth (data not shown).

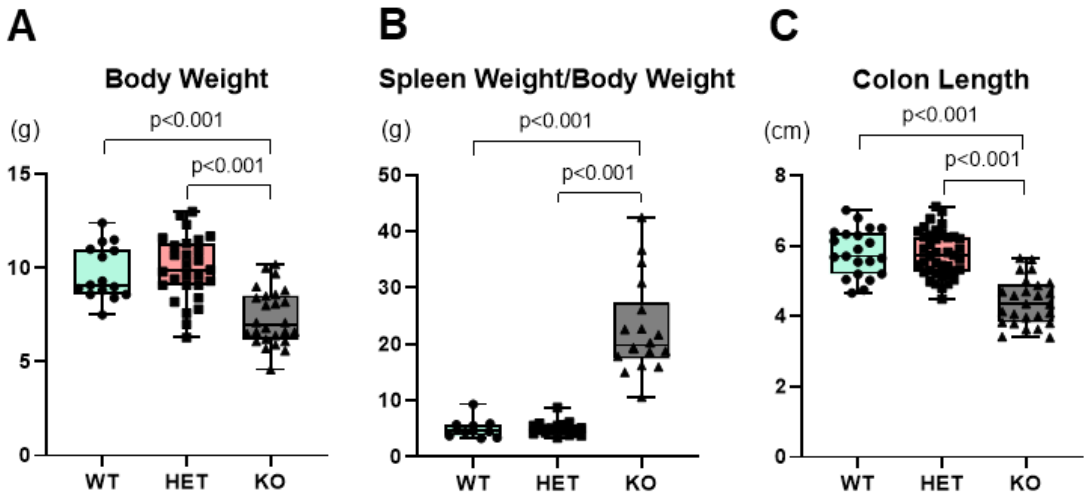

Figure 8. Phenotype of whole-body *Ptpn2*-WT, -HET and -KO mice. **(A)** Body weight, **(B)** spleen weight normalized to body weight, **(C)** and colon length of 21 days old whole-body KO mice. One-way ANOVA and Tukey's post-hoc test.

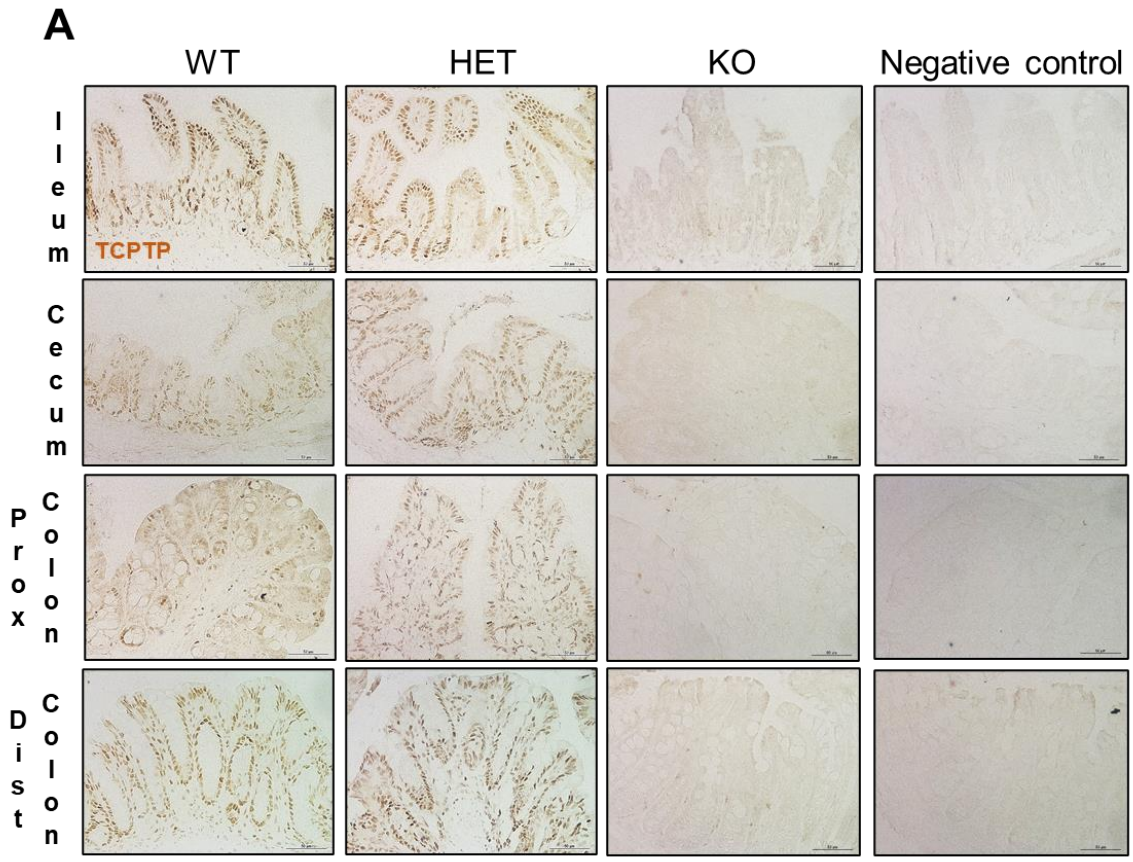

Figure 9. Validation of whole-body *Ptpn2*-KO mice through immunohistochemistry. **(A)** Representative immunohistochemistry staining for TCPTP in intestinal segments (n=4).

To confirm that intestinal tissues from *Ptpn2*-KO mice do not express *Ptpn2*, we performed IHC staining for the gene product, TCPTP. As expected, KO mice exhibited loss of TCPTP expression in the ileum, cecum, proximal and distal colon (Figure 9A). Concomitantly, staining for phosphorylated-STAT3, the active form of a TCPTP substrate, was enhanced in ileal IECs of KO mice (Figure 10A). Additionally, western blotting for p-STAT1 and p-

STAT3 showed that abundance of these proteins were elevated in isolated IECs of *Ptpn2*-KO mice (Figure 11A), confirming that lack of constitutive TCPTP results in activation of the JAK-STAT pathway in IECs, as shown here and in previous studies[143].

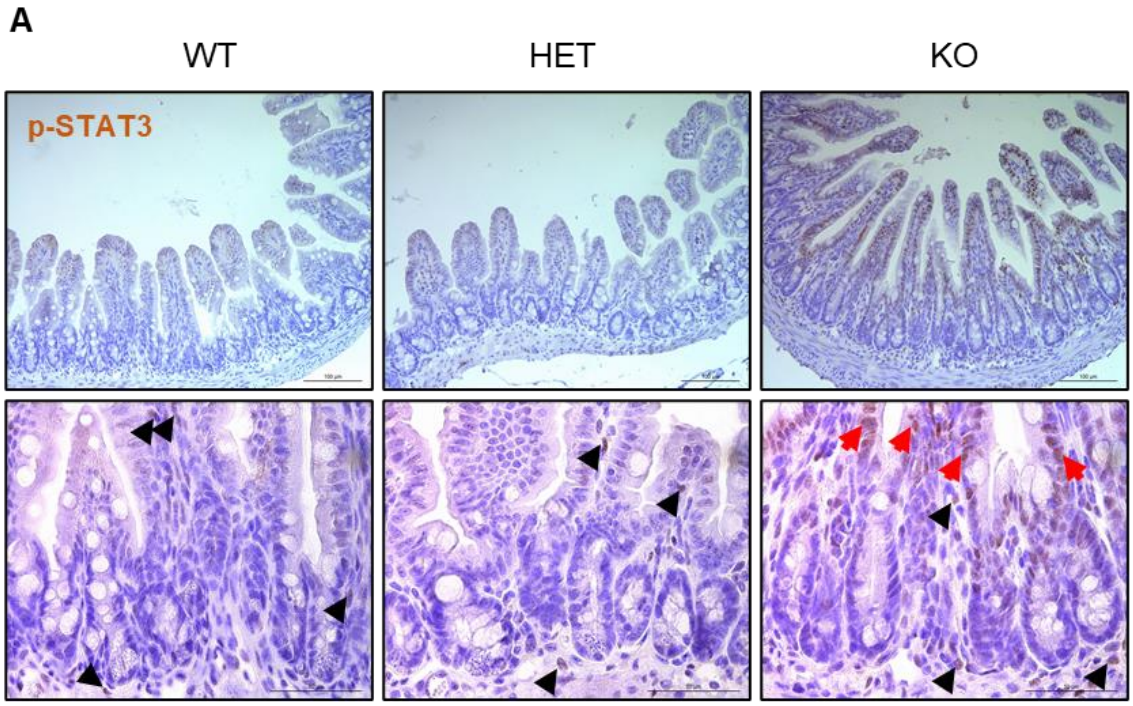

Figure 10. Whole-body *Ptpn2*-KO mice showed elevated staining for p-STAT3 in ileal IECs. **(A)** Immunohistochemistry for phosphorylated-STAT3, showing increased staining in ileal IECs of *Ptpn2*-KO mice (n=3).

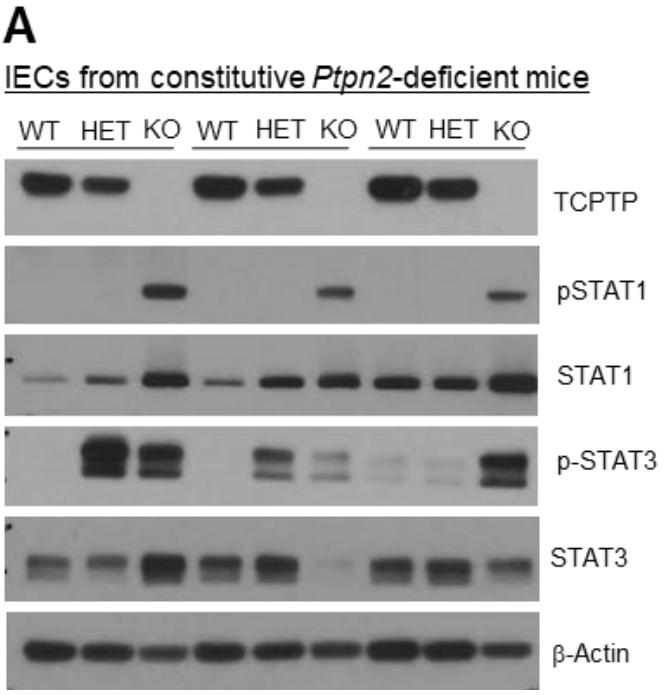

Figure 11. Constitutive *Ptpn2* loss results in elevated levels of phosphorylated STAT1 and STAT3 in isolated ileal IECs. **(A)** Western blot of ileal IECs showing absence of TCPTP and increased abundance of TCPTP substrates STAT1 and STAT3 in their total and phosphorylated isoforms. WT=5, HET=5, KO=5.

Next, we analyzed the intestinal mucosa architecture and morphology. Histological analysis (H&E staining) revealed an intact epithelium with no gross alterations in small and large intestine of KO and HET mice compared with WT (Figure 12A). However, increased ileal villus length, crypt depth and width in the cecum and proximal colon were observed in KO mice (Figure 13A-I), suggesting dynamic changes in IEC activity (i.e. cell proliferation, crypt fusion, crypt fission)[180,181].

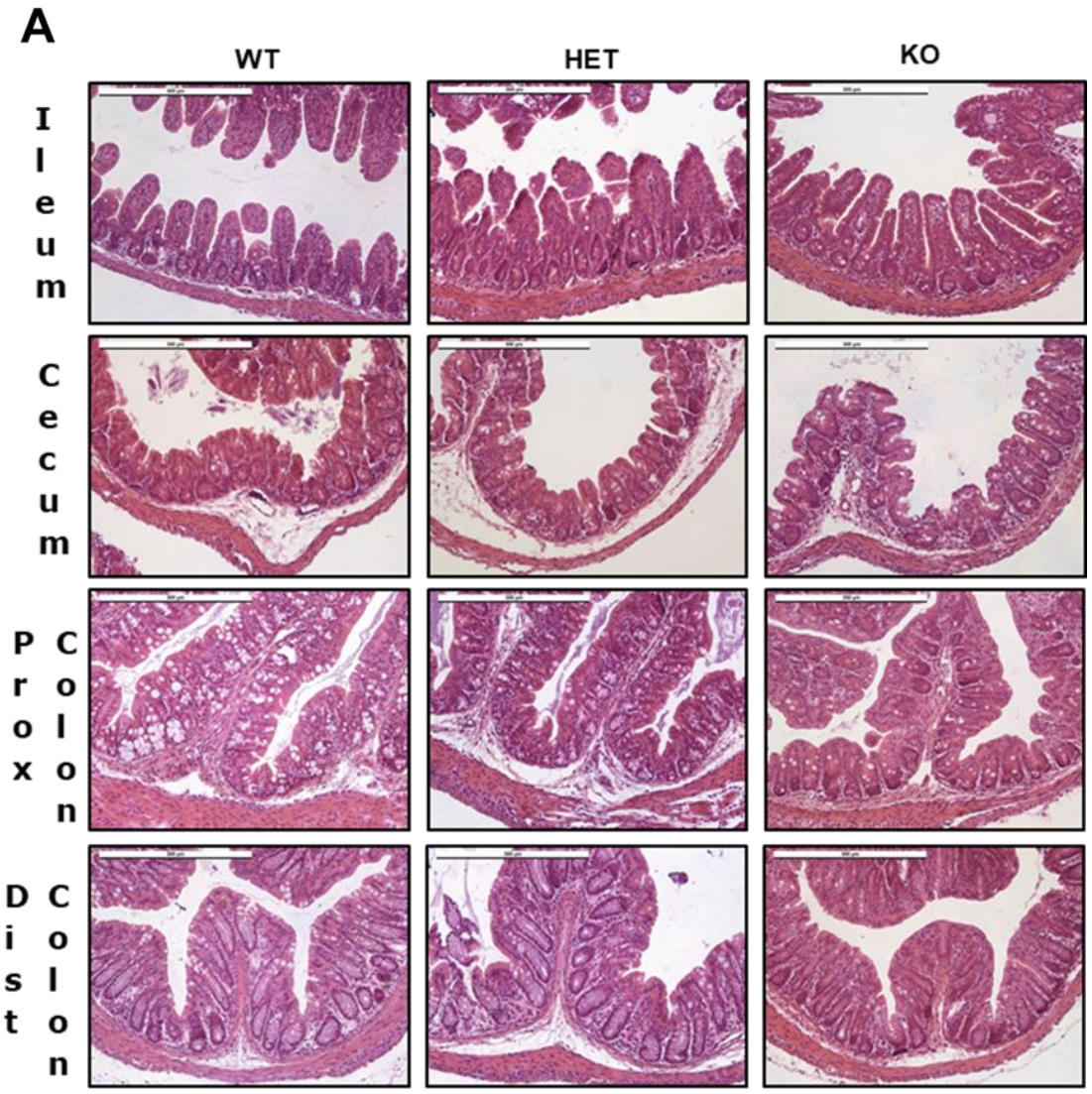

Figure 12. Morphological analysis of the intestinal mucosa architecture. **(A)** H&E staining of ileum, cecum, proximal and distal colon of WT, HET, and KO mice.

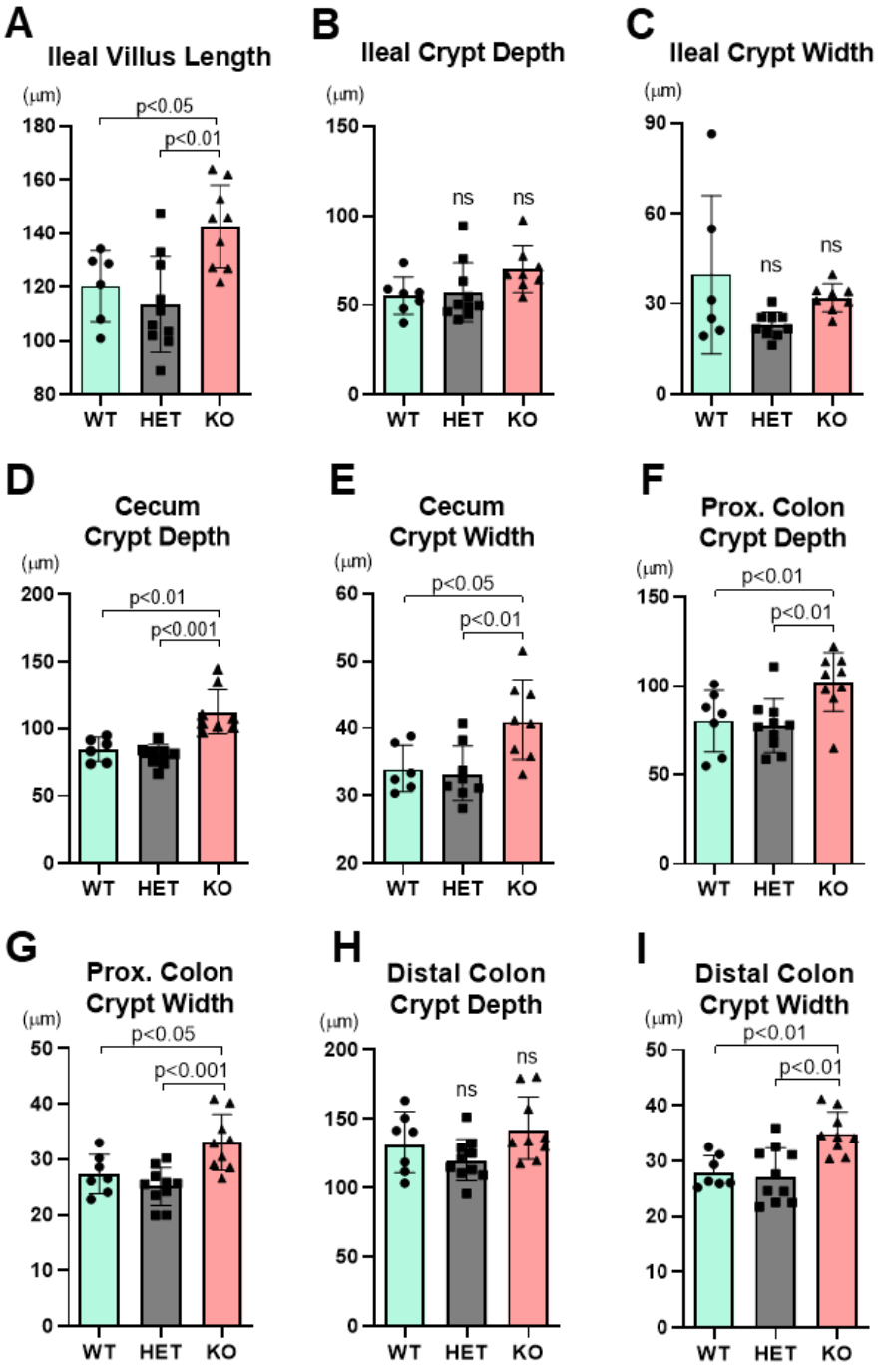

Figure 13. Morphometric analysis of intestinal structures. Panels **A** through **I** show morphometric analysis of intestinal structures from ileum, cecum, proximal and distal colon of WT, HET, and KO mice. Columns show mean ± SD. One-way ANOVA and Tukey's post-hoc test.

3.3.2. *Characterization and Validation of TCPTP Expression and Intestinal Morphology in Tissue-Specific Ptpn2 Deletion*

To evaluate the importance of *Ptpn2* gene in IECs without the additional effects of a hyperactive immune system, we generated a tamoxifen-inducible *Ptpn2*$^{\Delta IEC}$ mouse as described previously[143]. Here we show the validation of this new mouse line, to ensure that *Ptpn2* deletion occurs only in the IECs. Furthermore, we show that cre recombinase activity does not take place spontaneously, as demonstrated by mice administered vehicle alone vs. tamoxifen (Figure 14A).

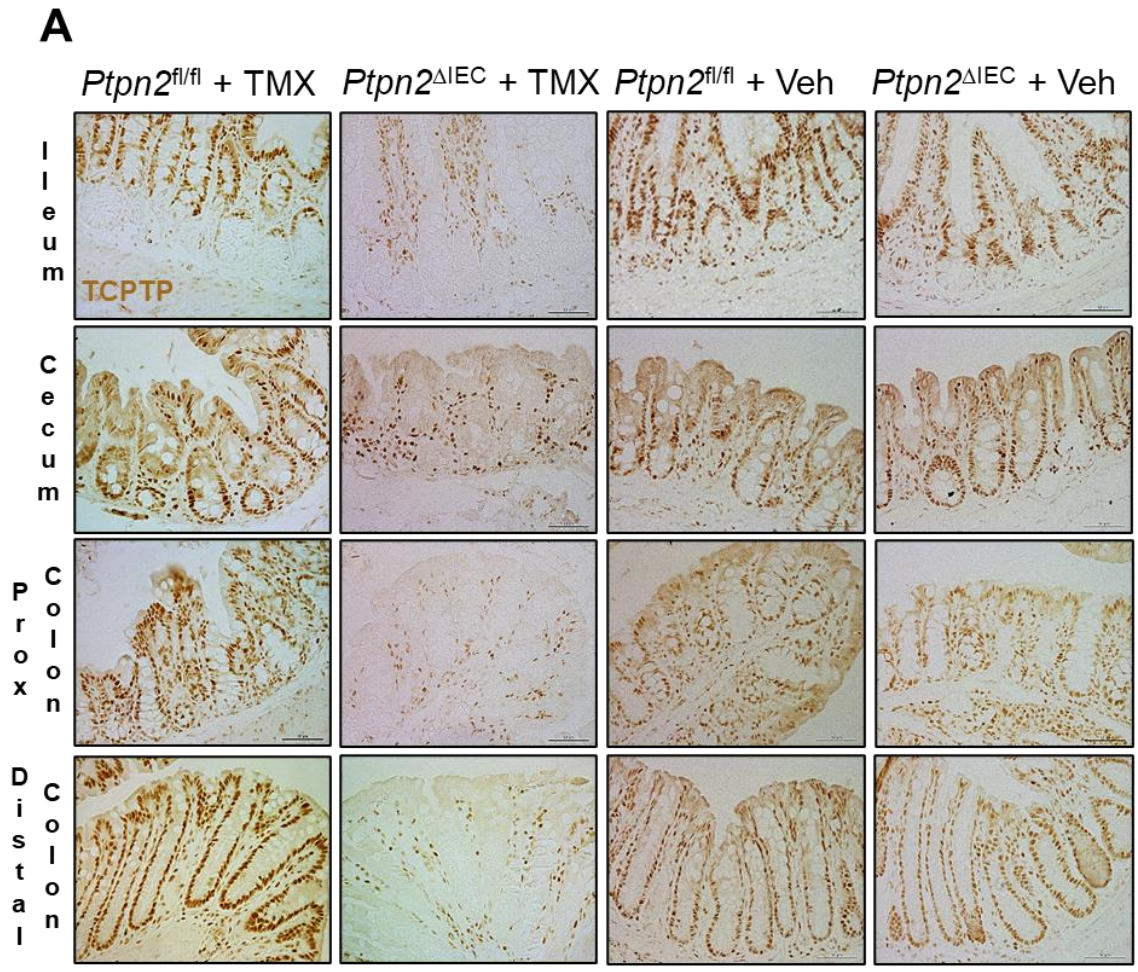

Figure 14. Validation of the tamoxifen-inducible IEC-specific *Ptpn2* deletion mouse model. **(A)** Immunohistochemistry staining for TCPTP in ileum, cecum, proximal and distal colon, shows that TCPTP was unaffected in *Ptpn2*$^{\Delta IEC}$ treated with vehicle and floxed mice (*Ptpn2*$^{fl/fl}$) treated with tamoxifen or vehicle.

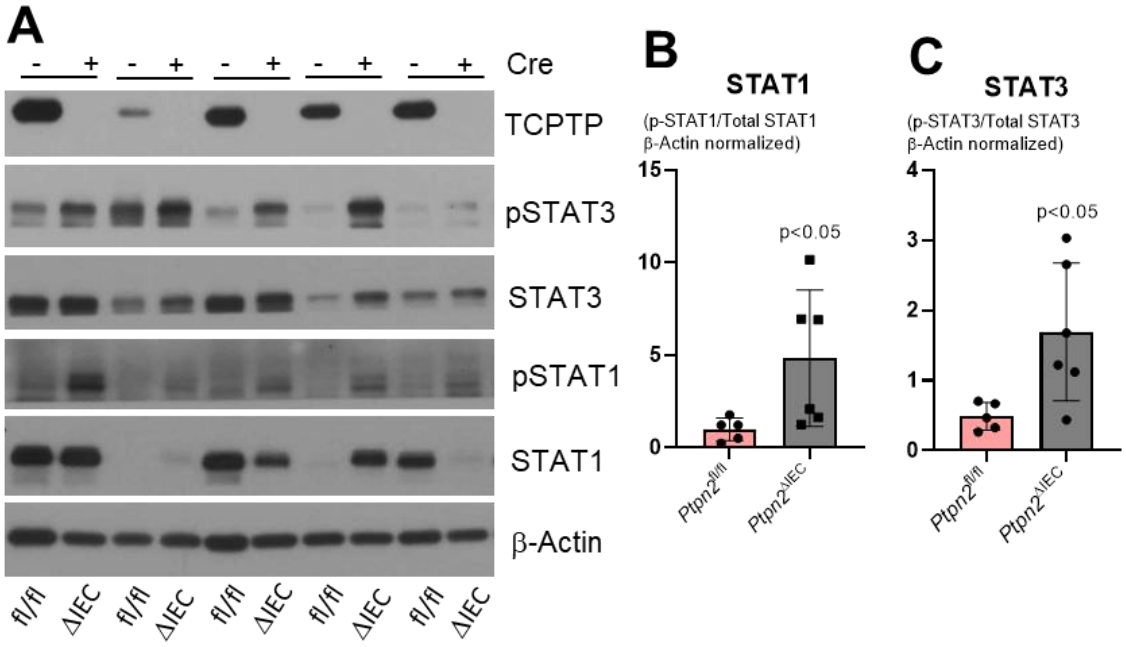

Figure 15. Deletion of *Ptpn2* in intestinal epithelial cells showed elevated levels of phosphorylated STAT1 and STAT3 in isolated ileal IECs. **(A)** Western blot of epithelial cells isolated from ileum of *Ptpn2*$^{fl/fl}$ and *Ptpn2*$^{\Delta IEC}$ probing for TCPTP, total STAT1, STAT3 and β-Actin levels, as well as phosphorylation of STAT1 (Y701) and STAT3 (Y705). **(B)** Densitometry analysis of STAT1 phosphorylation relative to total STAT1 and **(C)** STAT3 phosphorylation relative to total STAT3, all normalized to β-Actin. Columns show mean ± SD. Two-tailed student's t-test.

Furthermore, we confirmed that isolated ileal IECs lacked TCPTP by Western blot, whereas TCPTP substrates, STAT1 and STAT3, had elevated levels of the active phosphorylated isoform when normalized to the total abundance of those proteins in comparison with *Ptpn2*$^{fl/fl}$ controls (Figures 15A-C).

3.3.3. *Genotyped IBD Samples of Subjects with PTPN2 Variant Show Enhanced Staining for the Pore-forming Claudin-2 Tight Junction Protein in the Colon and Small Bowel*

Increased intestinal permeability is a hallmark of IBD pathogenesis that contributes to intestinal fluid loss, while also permitting translocation of microbes and microbial products from the luminal space into the intestinal mucosa, leading to immune cell activation and cytokine production[182,183].

Our group has reported that *PTPN2* loss-of-function compromises the homeostatic balance of the intestinal epithelial barrier properties *in vitro* and *in vivo*, by decreasing TER and by allowing passage of molecules with increased molecular weight. In fact, loss of epithelial TCPTP was sufficient to increase expression of claudin-2, a cation-pore forming tight junction protein[135,140,143,184]. The "pore pathway" is permissive to increased paracellular flux of electrolytes (i.e., Na^+) and water into the intestinal lumen, promoting diarrhea, perhaps in an attempt to flush the intestinal lumen free of exogenous and potentially pathogenic agents[185–187]. These observations confirm epithelial TCPTP as a key regulator of barrier function and suggest a mechanism by which *PTPN2* loss-of-function mutations contribute to chronic inflammatory diseases, such as IBD.

Here, we demonstrate the physiological relevance of increased claudin-2 expression in *Ptpn2*-HET and -KO mice by corroborating previous data from animal models with data obtained from colonic tissues of CD patients harboring the loss-of-function IBD-associated SNP rs1893217 in the *PTPN2* locus (Table 6). Patients homozygous (GG/CC) or heterozygous (GA/CT) for this SNP displayed increased claudin-2 localization in colonic (Figure 16A) and ileal epithelium (Figure 17A) compared with patients with WT *PTPN2* alleles (AA/TT).

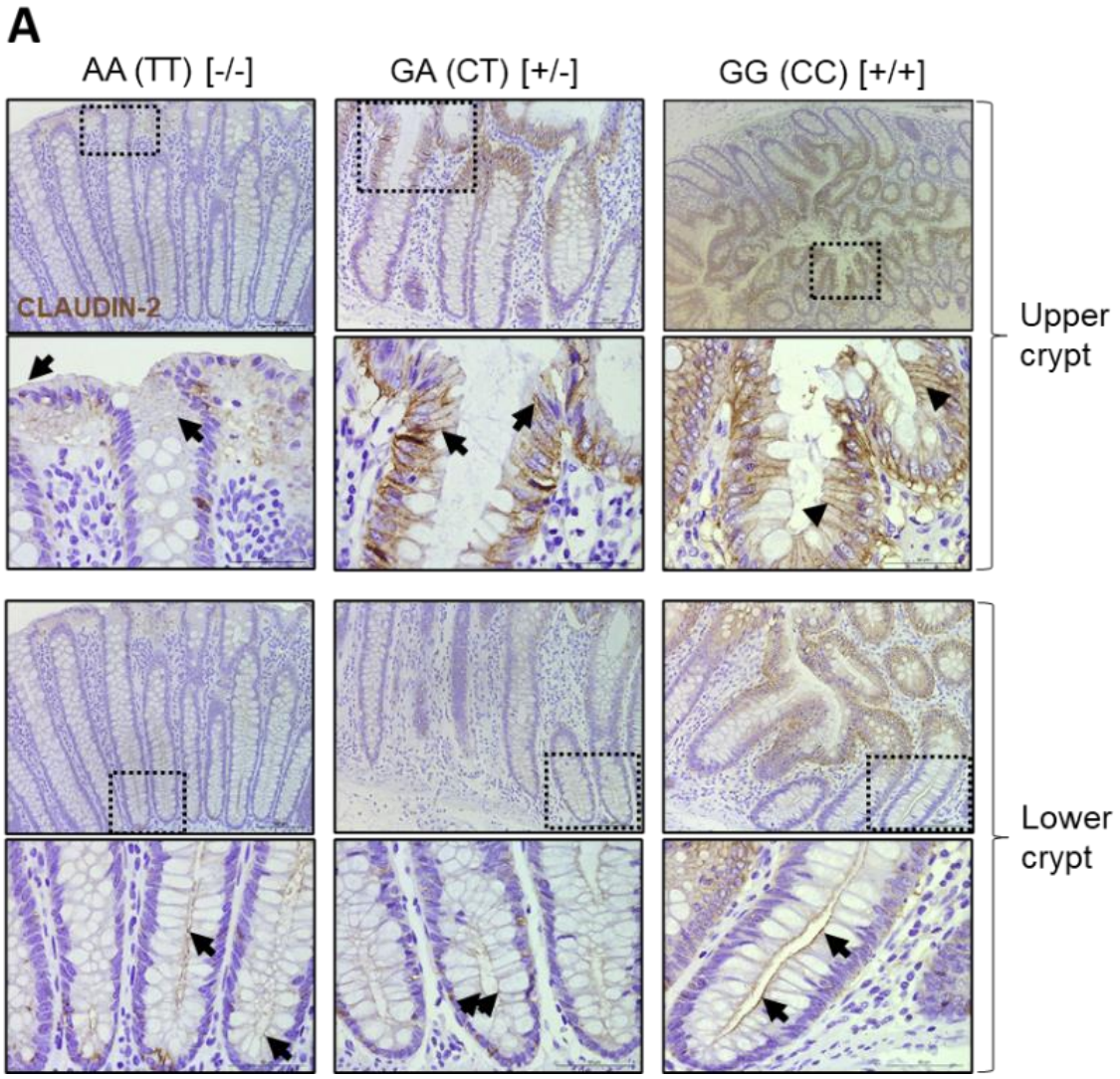

Figure 16. *PTPN2* loss-of-function increases colonic epithelial membrane localization of Claudin-2 in *PTPN2*-genotyped CD patients. **(A)** Claudin-2 staining in colonic tissue from CD patients with WT *PTPN2* who tested negative for the rs1893217 loss-of-function mutation (AA/TT[–/–]; n = 5), 1 copy of the rs1893217 mutation (GA/CT[+/–]; n = 5), or 2 copies of the mutation (GG/CC[+/+]; n = 1). Arrows indicate membrane localization of claudin-2.

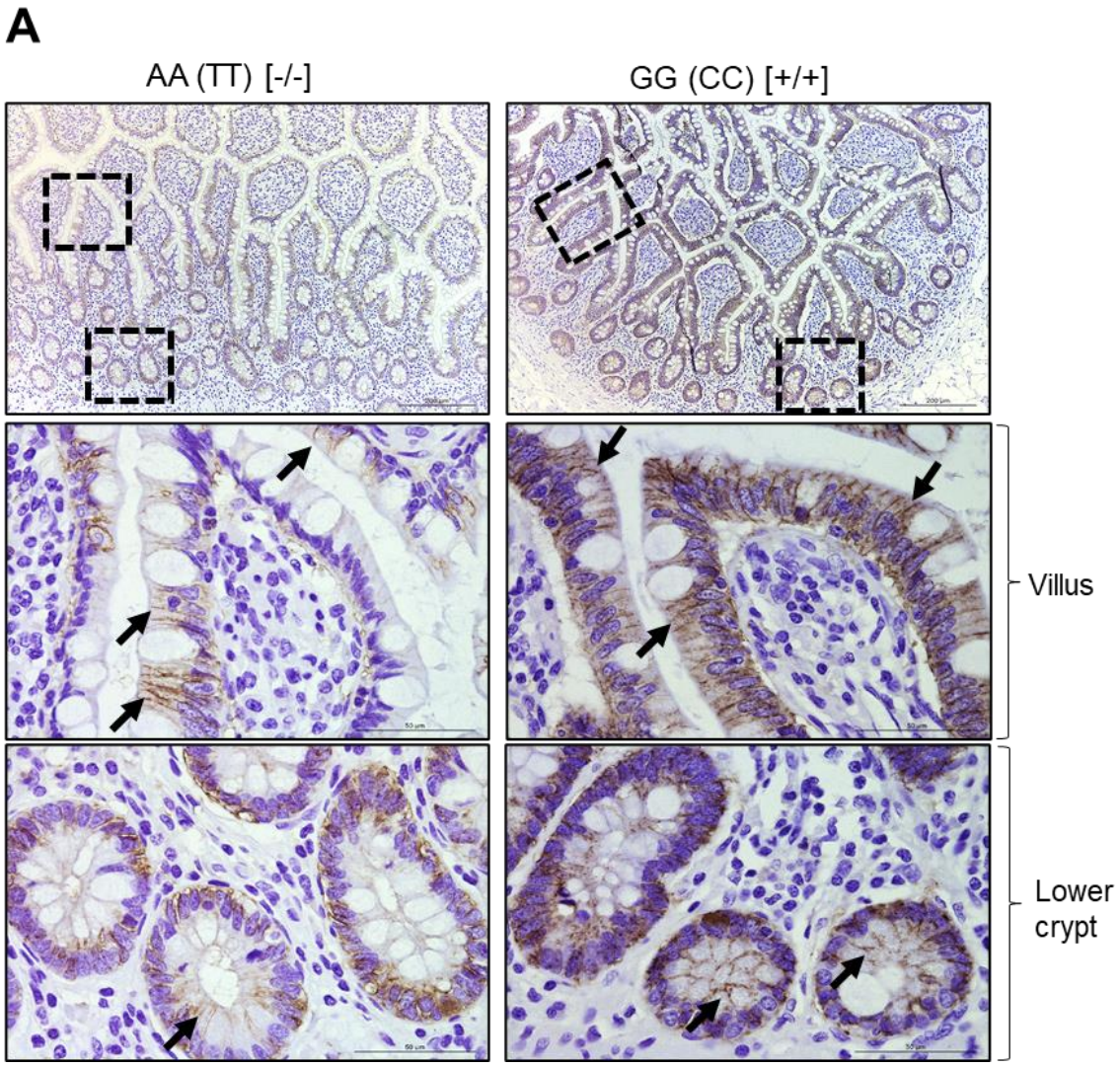

Figure 17. (A) *PTPN2* loss-of-function increases epithelial membrane localization of Claudin-2 staining in ileum from CD patients with WT *PTPN2* rs1893217 SNP null (AA/TT[–/–]; n = 6) — or who tested homozygous for the *PTPN2* loss-of-function variant (GG/CC[+/+]; n = 6). Arrows indicate membrane localization of claudin-2.

3.3.4. *Constitutive Ptpn2-deficiency in Mice, or the Presence of the PTPN2-variant in Human Intestine, Increases Staining Intensity and Internalization of E. coli Receptors CEACAM-1 and CEACAM-6 Respectively*

In a previous study from our group, we identified that constitutive *Ptpn2* loss contributes to altered gut microbiome population dynamics, with expansion of a murine adherent-invasive *E. coli* (*m*AIEC) strain. Interestingly, *m*AIEC showed similar capabilities of adherence and invasion of IECs, compared to the human isolated AIEC, LF82[142]. Additionally, *m*AIEC administration into microbiome-reconstituted germ-free mice resulted in intestinal inflammation, confirm it has characteristics of a pathobiont. Moreover, *m*AIEC increased DSS-induced colitis severity and prevented recovery in mice without genetic deficiency. However, the mechanisms AIEC exploits to adhere to, and invade, host cells remain to be fully determined.

Nevertheless, AIEC strains do not represent an exclusive IBD-associated microorganism as their presence was also detected in ileal and colonic regions of healthy subjects, suggesting an abnormal expression and/or tissue tropism of a specific host receptor that can be recognized by bacteria in a genetically predisposed host gut[120]. AIEC adhesion requires type 1 pili

expression on the bacterial surface to initiate the engulfing process by IECs via mannose-containing receptors[122]. It has been reported that the expression of carcinoembryonic antigen-related cell adhesion molecule 6 (CEACAM6) is upregulated in IBD patients, and this acts as a receptor for adherent-invasive *E. coli*[188]. CEACAM6 is not expressed in mice. Therefore, we investigated whether staining for CEACAM1, a murine CEACAM protein homologous to the human CEACAM6, had altered localization and/or intensity that could be linked to *m*AIEC activity. Moreover, to validate the potential clinical relevance of mechanism, we tested whether patients expressing a *PTPN2* variant show altered localization patterns for CEACAM6.

In an initial screen for CEACAM1, we observed increased protein levels in IECs from ileum and cecum of *Ptpn2*-KO mice compared with WT and HET mice (data not shown/not published). Figure 18 shows CEACAM1 staining in intestinal segments of whole-body WT, HET and KO mice. Noticeably, staining in the cecum indicated a higher intensity of cytosolic CEACAM-1 (red arrows) compared with cecal staining in WT and HET mice.

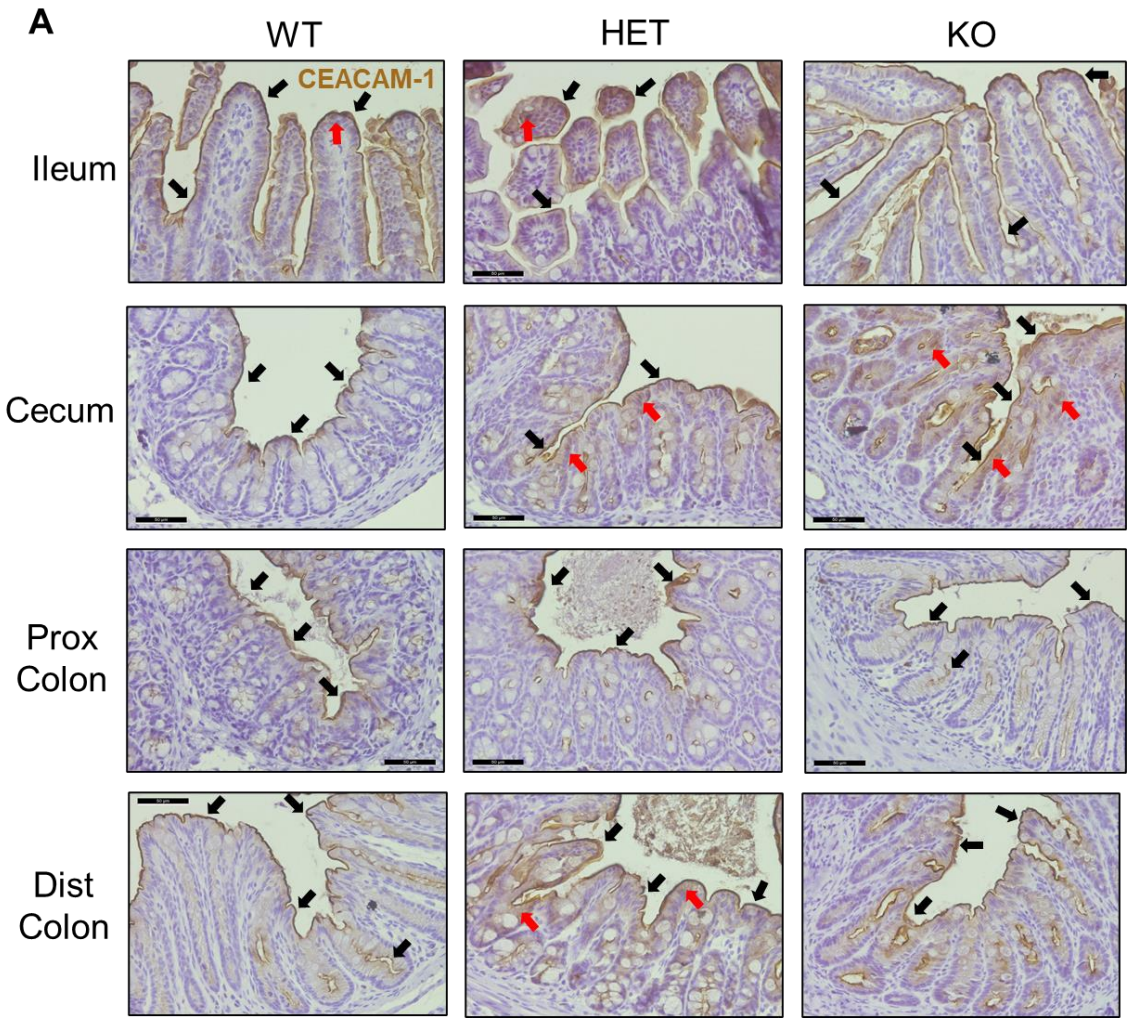

Figure 18. (A) CEACAM1 staining in ileum, cecum, proximal and distal colon of *Ptpn2* WT, HET and KO mice (n=2-3). Black arrows indicate apical membrane CEACAM1, whereas red arrows indicate cytosolic CEACAM1.

Conversely, CEACAM6 has been validated as a human AIEC binding protein[188]. Although it has been reported that CEACAM6 is generally upregulated in IBD patients, we wanted to confirm whether IBD patients carrying a *PTPN2* variant would display a similar phenotype.

A preliminary study revealed increased CEACAM6 mRNA expression and protein levels in *PTPN2*-KD HT-29 cells compared with controls (data not shown/not published). Next, we stained samples from patients with rs1893217 SNP, revealing that CEACAM6 staining was much more prominent in the apical membrane and in the cytosol of certain areas of the large intestine in a patient homozygous for risk allele (Figure 19). Conversely, the small bowel did not show any alteration in the pattern or intensity of CEACAM6 staining (Figure 20).

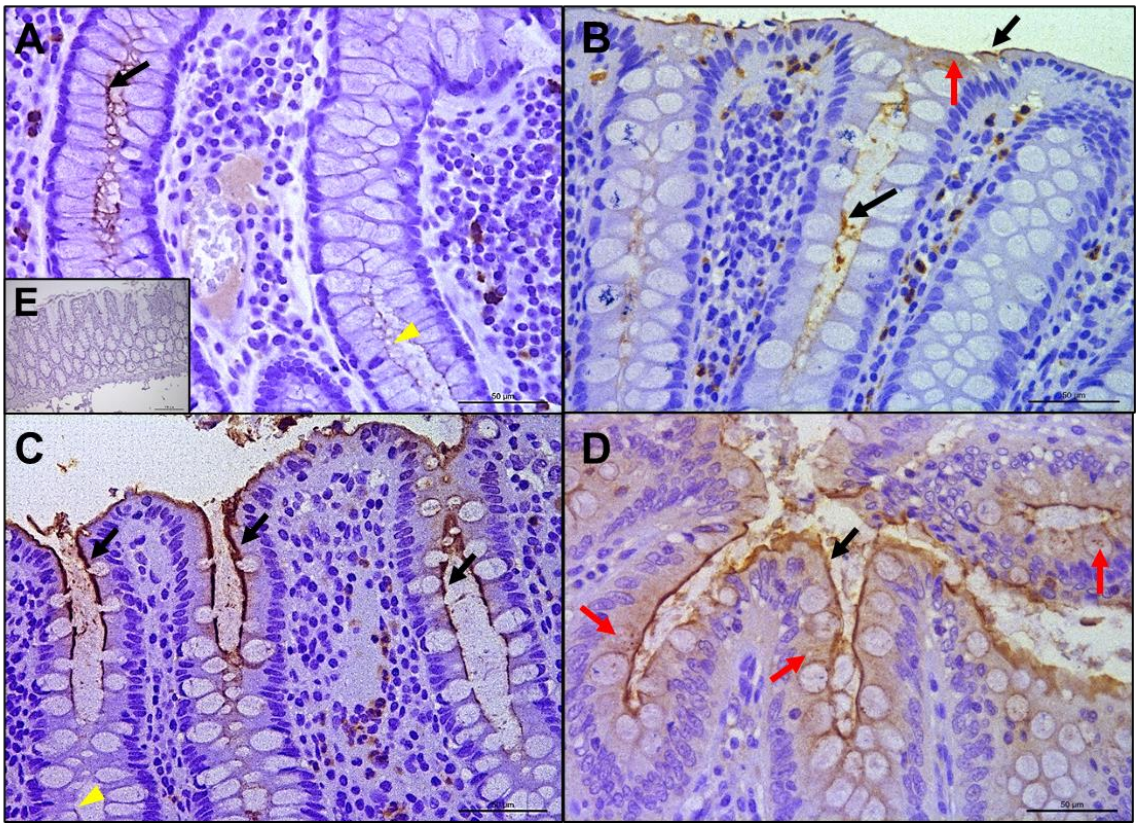

Figure 19. Large Intestine CEACAM6 staining in human biopsies of IBD-genotyped patients. **(A)** Human adenocarcinoma used as control; **(B)** Crohn's with *PTPN2* TT allele (wildtype); **(C)** Crohn's with *PTPN2* CT allele (heterozygous); **(D)** Crohn's with *PTPN2* homozygous for risk allele CC; **(E)** Negative control; Black arrows indicate apical membrane staining; red arrows indicate internalized localization; yellow arrows indicate apical membranes without CEACAM6 detection.

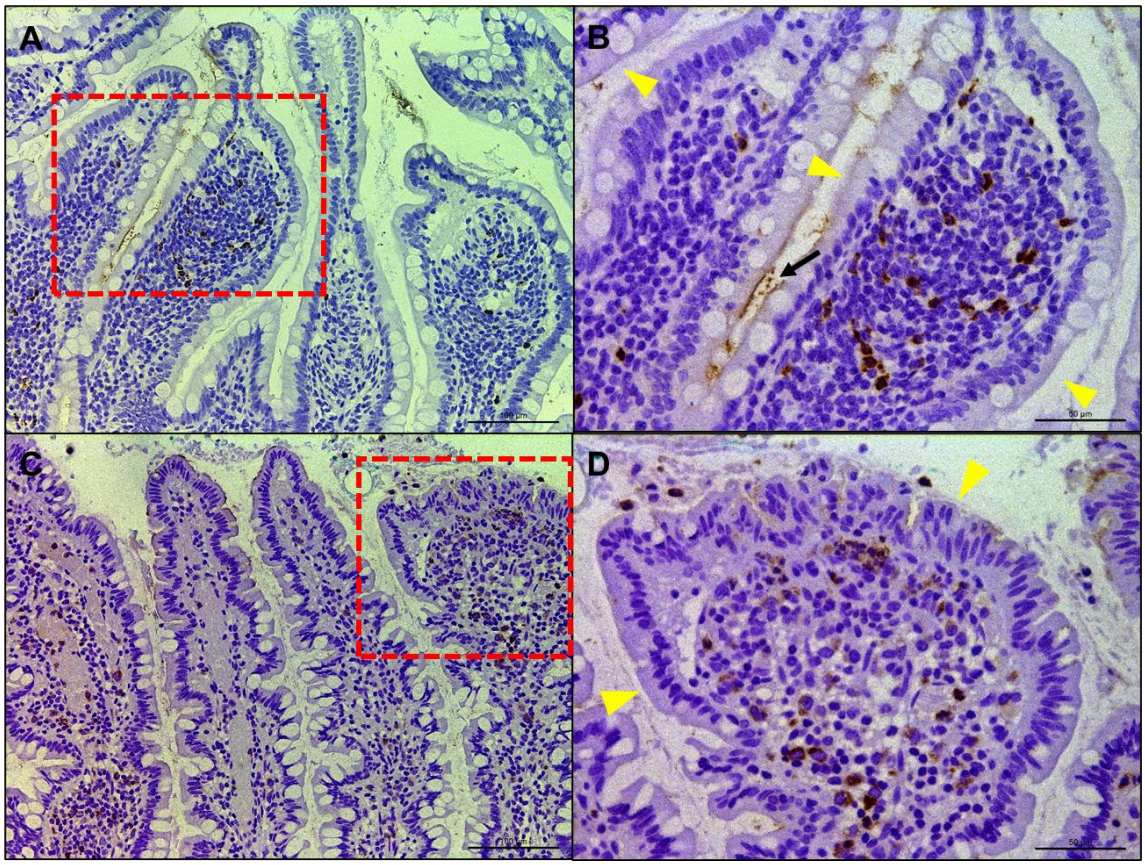

Figure 20. Small Bowel CEACAM6 staining in human biopsies of IBD-genotyped patients. **(A)** Crohn´s with *PTPN2* TT allelle (wildtype); **(B)** Higher magnification (40x) of the red squared area in image A; **(C)** Crohn´s with *PTPN2* homozygous for risk allele CC; **(D)** Higher magnification (40x) from the red squared area in image C; Black arrows indicate positive staining for CEACAM-6 at the apical membrane; Yellow arrowheads indicate apical membrane negative for CEACAM-6 staining. Red arrows indicate CEACAM-6 internalized in the cytosol.

3.4. Discussion

Here, we show data highlighting the breadth of investigations I have contributed to that explore the multi-functional contributions of *Ptpn2* to intestinal homeostasis. In depth characterization and validation of mouse models, coupled with the complementary use of intestinal tissues from genotyped humans subjects with IBD, show how *PTPN2* loss-of-function contributes to disease onset[143]. While the data presented here were generated in projects that do not form the primary research focus of this thesis, they are relevant since they help paint the larger picture of how *PTPN2* regulates multiple aspects of the intestinal environment. Moreover, the data presented in this chapter have contributed to manuscripts that are either published or in preparation, on which I am a co-author[142,143].

One of the hallmark disturbances in intestinal homeostasis that contributes to IBD pathogenesis is increased permeability. Increased epithelial expression of the cation pore-forming claudin-2 is commonly present in IBD patients, facilitating fluid loss consistent with IBD-associated diarrhea[189], but can also have protective roles against pathogen infection[190]. As mentioned before, our group has shown that TCPTP protects the intestinal epithelial barrier by restricting cytokine-induced tight junction remodeling and increased

permeability to macromolecules using *in vitro* approaches, linking experimental findings to a clinically relevant genetic deficiency[133,135,184,191,192]. This study brings our knowledge one step further, by confirming that findings from IBD patients carrying a specific *PTPN2* loss-of-function variant corroborate our previous *in vitro* and *in vivo* findings. This opens new possibilities for a more targeted therapeutic approach to improve intestinal epithelial barrier function, such as administration of JAK-STAT inhibitors that could rescue the normal organization of intestinal tight junction proteins and re-establish intestinal homeostasis[139,193].

With respect to intestinal receptors that could function as sites for bacterial interaction, our preliminary data show that *PTPN2* loss increases expression of both, CEACAM6 and CEACAM1, in humans and mice, respectively. Therefore, it is reasonable to hypothesize that these two proteins could play a role in AIEC adherence and invasion in our *PTPN2*-deficient mouse models. However, it is unclear why CEACAM1 cytosolic staining was enhanced in *Ptpn2*-KO mice. We speculate that this feature could be driven by the host itself, in an attempt to prevent bacterial adherence, or bacteria driven as internalization would facilitate bacteria invasion. Thus,

mechanistic investigations are necessary to answer these and several other questions, such as: can *m*AIEC directly interact with CEACAM1 in mice, using it as a binding site similar to LF82 and CEACAM6 in IBD patients? Do bacteria play any role in upregulating expression and/or glycosylation patterns of CEACAM1/CEACAM6? Does specific deletion of *Ptpn2* in IECs result in dysregulation of CEACAM1 expression? Are there inhibitors/antagonists that could disrupt bacterial/receptor interaction to prevent adherence and invasion even in a genetically susceptible host? Finally, is the expansion of *m*AIEC in mice induced by *PTPN2* loss or a result of systemic inflammation?

In summary, the data presented here suggest that, apart from the contribution to broader investigations, constitutive *Ptpn2* loss-of-function impairs intestinal barrier function and the handling of the gut microbiome by IECs. However, the mechanisms involved that lead to gut dysbiosis and expansion of a pathobiont are still unknown. Furthermore, although recent studies demonstrated that *Ptpn2* deletion modulates the intestinal barrier and immune cell responses, data regarding differentiation and function of individual IEC subtypes are scarce. Since the functions of different specific IEC subtypes encompass tissue regeneration, production of AMPs,

surveillance of the luminal environment, and generation of the mucus layer, an imbalance in one of these populations could be detrimental to intestinal homeostasis which could lead to higher susceptibility to infection. Thus, the role(s) of *Ptpn2* in regulating epithelial subtypes will be the focus of Chapters 4 & 5.

4. *Ptpn2* is a Critical Regulator of Ileal Paneth Cell Viability and Function in Mice

4.1. Introduction

The intestinal epithelial barrier comprises three layers of protection: the mucus layer, intestinal epithelial cell (IEC) lining and immune cells in the lamina propria. A healthy IEC layer is essential to restrict entry of pathogens and toxins. Specialized and highly differentiated IECs subtypes are strategically located along the crypt-villus axis of the small intestinal mucosa. Among them, Paneth cells are normally present only in the small intestines, dwelling at the crypt base intermingled with intestinal stem cells, and are critically involved in innate immune responses. Paneth cells secrete several AMPs such as α-defensins (cryptdins in mice), lysozyme, and phospholipase A2 group IIA (sPLA2). Additionally, Paneth cells are an important source of stem cell niche factors, such as WNT3, Notch ligands, and EGF which are required for intestinal stem cell function[60]. Moreover, dysfunction of Paneth cells may play a role in intestinal inflammation[109]. For example, a subset of CD patients display reduced expression of AMPs and

defective Paneth cells, suggesting that loss of critical Paneth cells functions alters the host-bacterial interaction in ways that increase the risk of chronic inflammation[107,194,195].

IEC subtypes are functionally altered in IBD although such impairments are dependent on IBD manifestation (CD *vs*. UC), genetic susceptibility and site of disease activity[107]. In CD ileitis, Paneth cell number and function are affected whereas reduced numbers of goblet cells and a defective mucus layer have been reported in UC[160,194–196]. Furthermore, studies examining IBD patient biopsies and transgenic mice show that genetic variants or deletion of IBD-associated genes can functionally impair IEC subtypes, thereby increasing susceptibility to intestinal infections and promoting dysbiosis[197–200].

Here, we show for the first time that constitutive *Ptpn2*-deficiency alters the expression of ileal IEC markers in mice. Notably, the number of Paneth cells was dramatically reduced in *Ptpn2*-KO mice, negatively affecting the production of AMPs that directly modulates the intestinal microbiota. These findings, indicate a new mechanism by which *Ptpn2*-loss-of-function might increase susceptibility to infection and contribute to intestinal dysbiosis and disease onset.

4.2. Methods

For this study, we utilized several imaging techniques, such as histology, immunohistochemistry and transmission electron microscopy for localization of proteins of interest and visualization of cell organelles. Isolated ileal intestinal epithelial cells were used for western blot and gene expression analysis. Flow cytometry was performed using ileal mucosa as described in detail in the methods chapter. The experiments and data shown in this chapter are included in a manuscript that is currently under revision at a peer-reviewed journal.

4.3. Results

4.3.1. *Whole-body Ptpn2-deficient Mice Display Epithelial Structural Changes and Unique Gene Expression in Ileal Isolated IECs*

Our group has recently shown that whole-body *Ptpn2*-KO mice display increased crypt depth in the cecum and proximal colon, although no other gross alteration was present in the intestinal epithelium (Figure 12A)[143]. However, ileal villus length was increased in *Ptpn2*-KO mice when compared with *Ptpn2*-WT and *Ptpn2*-HET mice (Figure 13A), whereas ileal crypt depth and width were not affected (Figures 13B-C). Increased villus length in the *Ptpn2*-KO mice was accompanied by increased numbers of proliferating cells detected by Ki-67 immunofluorescence (Figures 21A-B).

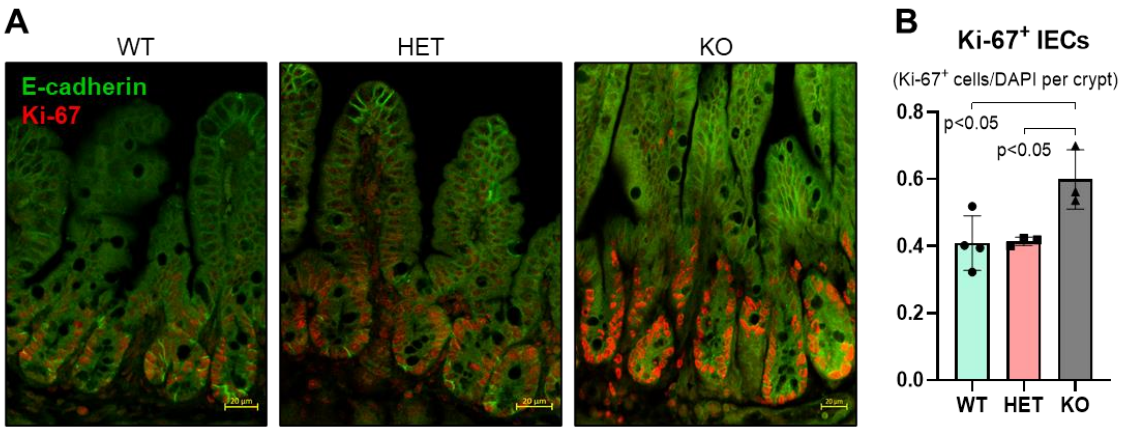

Figure 21. *Ptpn2*-KO mice displayed higher numbers of proliferating ileal IECs. **(A)** Immunofluorescence imaging of ileal sections staining for proliferation marker Ki-67 (red) and IEC marker E-cadherin (green). **(B)** Quantification of Ki-67$^+$ IECs indicates that numbers of proliferating IECs were increased in KO mice. WT=4, HET=3, KO=3. Columns show mean ± SD. One-way ANOVA and Tukey post-hoc test.

Next, to investigate whether constitutive *Ptpn2* deletion also affects IEC subtypes and their function, we performed partial transcriptomic analysis of isolated IECs from *Ptpn2*-WT, HET and KO mice. Gene expression analysis was performed using Nanostring® technology. Results of two separate panels with a predefined set of targets, 'AutoImmune Profiling' and 'PanCancer Pathways' were combined, with the addition of 60 customized targets comprising IEC markers, function and differentiation factors, host-bacteria interaction, autophagy, immune response and iron transport, totaling >1500 targets (GEO database - accession number GSE181531). Principal component analysis (PCA) showed unique gene expression patterns in *Ptpn2*-KO IECs, that clustered separately from IECs of WT or HET mice (Figure 22A, red ellipse), indicating that genotype corresponds to 76% of the gene expression variance. Furthermore, the same analysis revealed that at least one set of littermates clustered together when data points were compared by this parameter, indicating that co-housing contributes to gene expression variance (Figure 22A, green ellipse). When adjusted for the littermate effect, we found 97 genes were markedly dysregulated (False Discovery Rate (FDR) <0.1) out of 1398 targets with detectable levels (GEO database - accession number GSE181531). A heatmap of pathway scores

summarizes the overall effect of constitutive *Ptpn2* deletion on cellular pathways in each sample (Figure 22B). Figure 22C lists all genes associated with IEC markers and differentiation factors found to be altered in *Ptpn2*-KO relative to WT mouse ileum. Notably, the Paneth cell-associated AMP genes *Defa6*, *Lyz1* and *Pla2g2a* were downregulated (blue) in KO IECs, suggesting that the function of Paneth cells could be impaired by constitutive *Ptpn2*-deficiency. Figure 23 shows the differential expression of genes associated with IEC differentiation (Figure 23A), and differential expression of genes associated with IEC markers and function (Figure 23B).

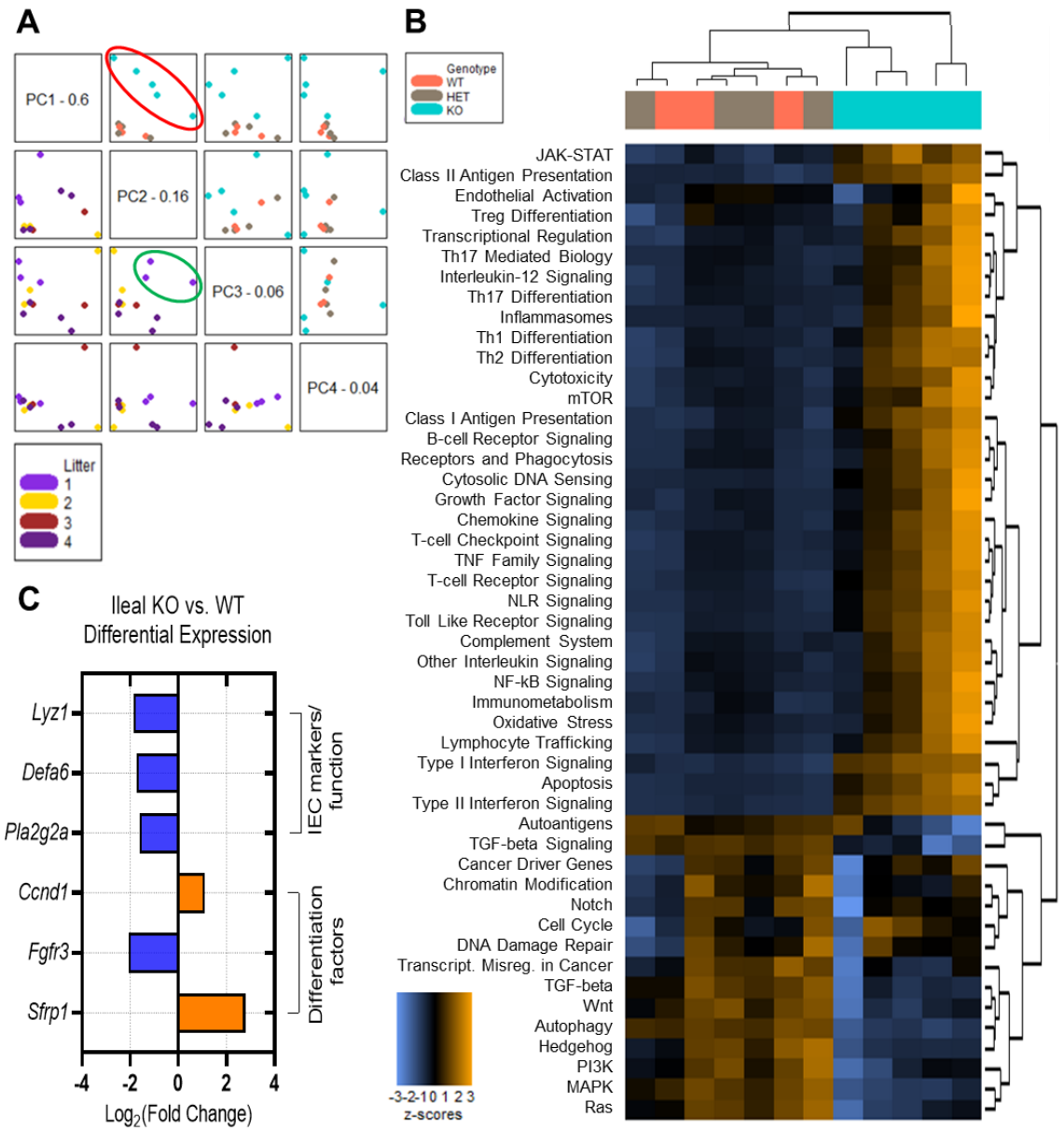
A
PC1 - 0.6
PC2 - 0.16
PC3 - 0.06
PC4 - 0.04
Litter
1
2
3
4
B
Genotype
WT
HET
KO
JAK-STAT
Class II Antigen Presentation
Endothelial Activation
Treg Differentiation
Transcriptional Regulation
Th17 Mediated Biology
Interleukin-12 Signaling
Th17 Differentiation
Inflammasomes
Th1 Differentiation
Th2 Differentiation
Cytotoxicity
mTOR
Class I Antigen Presentation
B-cell Receptor Signaling
Receptors and Phagocytosis
Cytosolic DNA Sensing
Growth Factor Signaling
Chemokine Signaling
T-cell Checkpoint Signaling
TNF Family Signaling
T-cell Receptor Signaling
NLR Signaling
Toll Like Receptor Signaling
Complement System
Other Interleukin Signaling
NF-kB Signaling
Immunometabolism
Oxidative Stress
Lymphocyte Trafficking
Type I Interferon Signaling
Apoptosis
Type II Interferon Signaling
Autoantigens
TGF-beta Signaling
Cancer Driver Genes
Chromatin Modification
Notch
Cell Cycle
DNA Damage Repair
Transcript. Misreg. in Cancer
TGF-beta
Wnt
Autophagy
Hedgehog
PI3K
MAPK
Ras
-3-2-10 1 2 3
z-scores
C
Ileal KO vs. WT
Differential Expression
Lyz1
Defa6
Pla2g2a
Ccnd1
Fgfr3
Sfrp1
IEC markers/ function
Differentiation factors
-4
-2
0
2
4
Log2(Fold Change)

Figure 22. Partial transcriptome analysis of isolated ileal IECs by Nanostring®. Data consolidated from two different panels: 'AutoImmune Profiling' and 'PanCancer Pathways' with the addition of 60 custom targets. **(A)** Principal Component Analysis (PCA) is a statistical method that transforms large data sets with multiple variables into a linear set of principal components retaining most of the information from the large set. Component 1 (PC1) captures the highest level of variance, PC2 the next highest, PC3 next, and so on. The resulting image plots each PC vs. another twice and colors the points by the selected covariate helping to identify clusters in the data associated with a covariate. The boxes on the diagonal each contain a PC name and value representing the variance percentage; all plots in the same row will have this PC on their y-axis and all plots in the same column will have this PC on their x-axis. The upper quadrants, above the diagonal line, were color-coded with the genotype of each sample indicating that gene expression of *Ptpn2*-KO mice is unique. The red ellipse indicates how data points from KO mice cluster apart from WT and HET mice. Lower quadrants were color-coded with littermates, indicating that littermates number 1 clustered together as indicated by the green ellipse. Data was normalized by littermates (co-housed mice) as a covariate. **(B)** Heatmap of pathway scores is a high-level overview of how the cellular pathway scores change across samples. Orange indicates high scores; blue indicates low scores. Scores are displayed in the same scale by Z-transformation. Each column represents an individual sample. **(C)** KO vs. WT differential expression of ileal intestinal epithelial markers, differentiation factors and function. WT=3, HET=4, KO=5. All targets had p-value <0.05 and FDR <0.1.

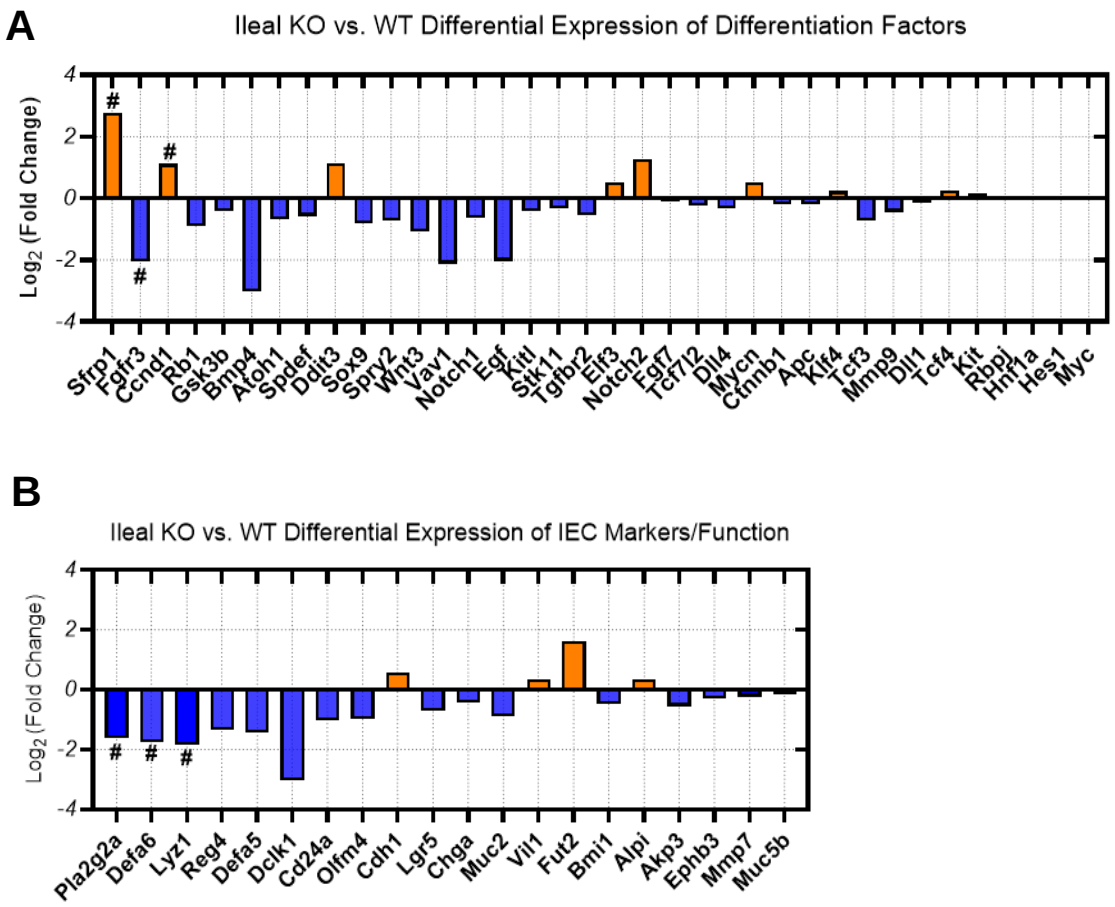

Figure 23. Log_2 fold change of genes associated with IEC markers and function. **(A)** Differential expression of IEC differentiation factors (KO vs. WT); **(B)** Differential expression of IEC markers/function (KO vs. WT). # Indicates targets statistically significant (α <0.05; FDR <0.1).

4.3.2. *Whole-body Ptpn2 Deletion Depletes Paneth Cells and AMP Production*

Given the established importance of Paneth cells in shaping host-microbial interactions in the gut, we investigated whether whole-body *Ptpn2*-deficiency compromises Paneth cells function in mice[195,201]. Counting of Paneth cells on H&E sections (Figure 12A), distinguished from other IECs by the presence of characteristic large cytosolic granules, showed that their number was decreased in *Ptpn2*-KO mice (Figure 24A). In parallel, immunohistochemistry (IHC) staining showed a marked reduction of Paneth cells-associated lysozyme in the ileal mucosa of *Ptpn2*-KO mice (Figures 24B-C), a finding that was confirmed by Western blot analysis of isolated ileal IECs (Figures 24D-E). Moreover, immunofluorescence staining of another Paneth cell-specific AMP, Defensin alpha 1 (*Defa1*; cryptdin-1 in mice), showed a dramatic reduction of Defa1-positive Paneth cells in *Ptpn2*-KO mice in comparison with WT and HET mice (Figures 24F-G).

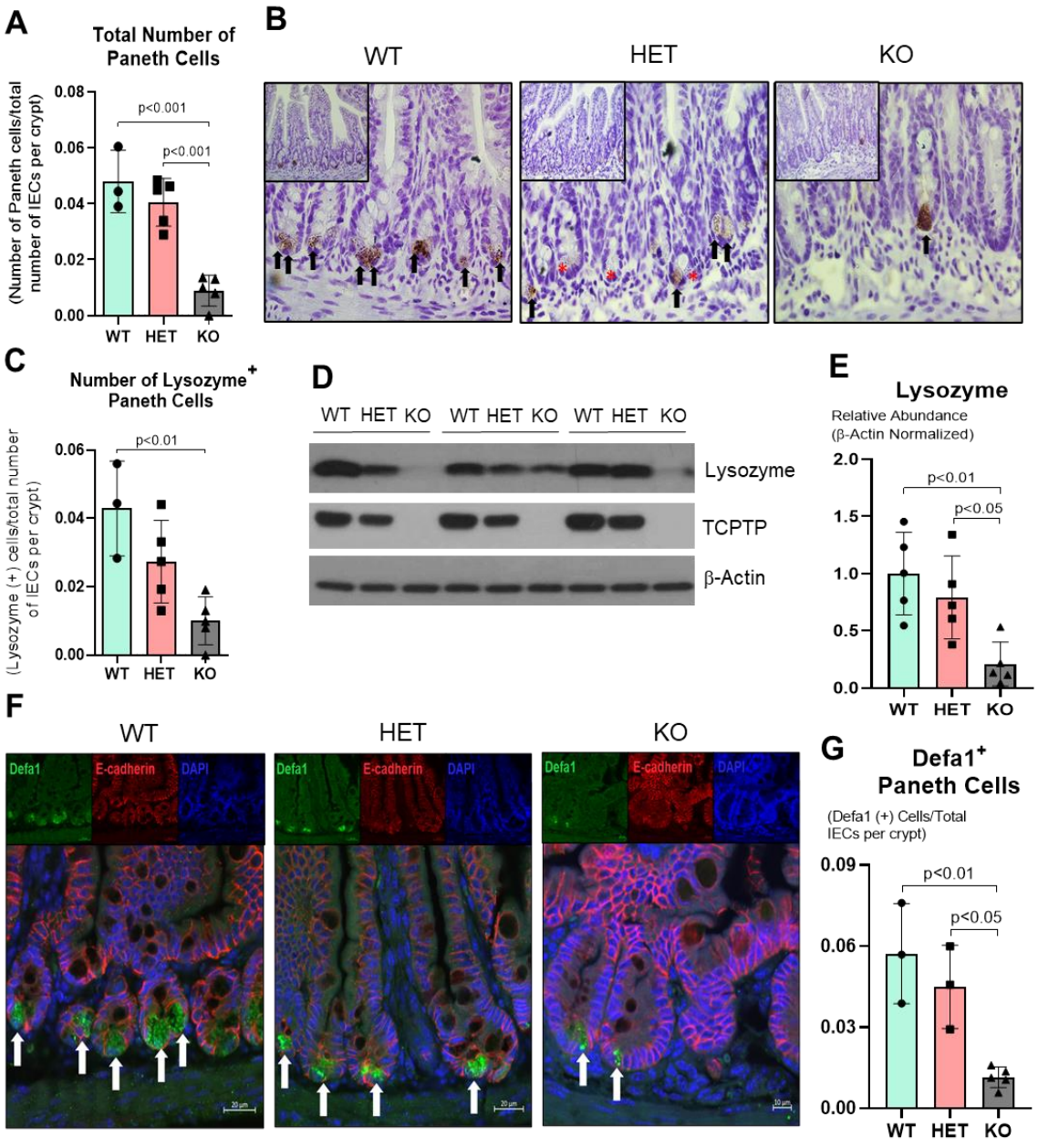
A
Total Number of Paneth Cells
(Number of Paneth cells/total number of IECs per crypt)
0.08
0.06
0.04
0.02
0.00
p<0.001
p<0.001
WT HET KO
B
WT
HET
KO
C
Number of Lysozyme+ Paneth Cells
(Lysozyme (+) cells/total number of IECs per crypt)
0.06
0.04
0.02
0.00
p<0.01
WT HET KO
D
WT HET KO WT HET KO WT HET KO
Lysozyme
TCPTP
β-Actin
E
Lysozyme
Relative Abundance (β-Actin Normalized)
2.0
1.5
1.0
0.5
0.0
p<0.01
p<0.05
WT HET KO
F
WT
HET
KO
Defa1
E-cadherin
DAPI
G
Defa1+ Paneth Cells
(Defa1 (+) Cells/Total IECs per crypt)
0.09
0.06
0.03
0.00
p<0.01
p<0.05
WT HET KO

Figure 24. Number of Paneth cells and expression of AMPs are reduced in *Ptpn2*-KO mice. **(A)** Counting of Paneth cells by calculating the ratio of the total number of Paneth cells by the total number of IECs per crypt. Columns show mean ± SD. One-way ANOVA and Tukey post-hoc test. **(B)** Ileal Paneth cells were stained for antimicrobial peptide lysozyme through IHC. Black arrows indicate Paneth cells positively stained for lysozyme whereas red star indicates Paneth cells without lysozyme staining (characterized by large cytosolic granules at the crypt base). WT=3, HET=5, KO=5. **(C)** Ratio of the number of Paneth cells positively stained for lysozyme by total number of IECs per crypt. **(D)** Western blot of ileal IECs probing for lysozyme. **(E)** Densitometry of lysozyme protein levels in ileal IECs. WT=5, HET=5, KO=5. **(F)** Immunofluorescence of ileal sections staining for Defa1 (green), a Paneth cell-specific AMP; E-cadherin (red), a marker of IECs; and DAPI (blue) a marker of cell nuclei. White arrows indicate Paneth cells positive for Defa1 staining. **(G)** Counting and ratio of Defa1 positive cells over total number of IECs per crypt. WT=3, HET=3, KO=5.

To further confirm that *Ptpn2*-KO mice lack Paneth cells, I used transmission electron microscopy (TEM) to assess the presence/absence of dense core vesicles, a cytoplasmic structure present in Paneth cells responsible for packing and storing AMPs. *Ptpn2*-KO mice displayed fewer Paneth cells at the crypt base (Figure 25A; delineated by blue dashed lines) and these were associated with fewer DCVs (yellow arrows). Satoh et al. reported that large cytoplasmic vacuoles were formed when DCVs released their contents into the luminal space after Paneth cell stimulation[202]. However, we did not observe cytoplasmic vacuole formation in any of the constitutive *Ptpn2* mouse genotypes (WT, HET, KO) (Figure 25A). Although *Ptpn2*-HET mice had normal numbers of Paneth cells, it is notable that some of the Paneth cells in HET mice had a low density halo surrounding the DCVs, indicated by red arrows, a feature that has been suggested to be associated with increased expression of the mucin protein MUC2 in Paneth cells (Figure 25A)[168,203].

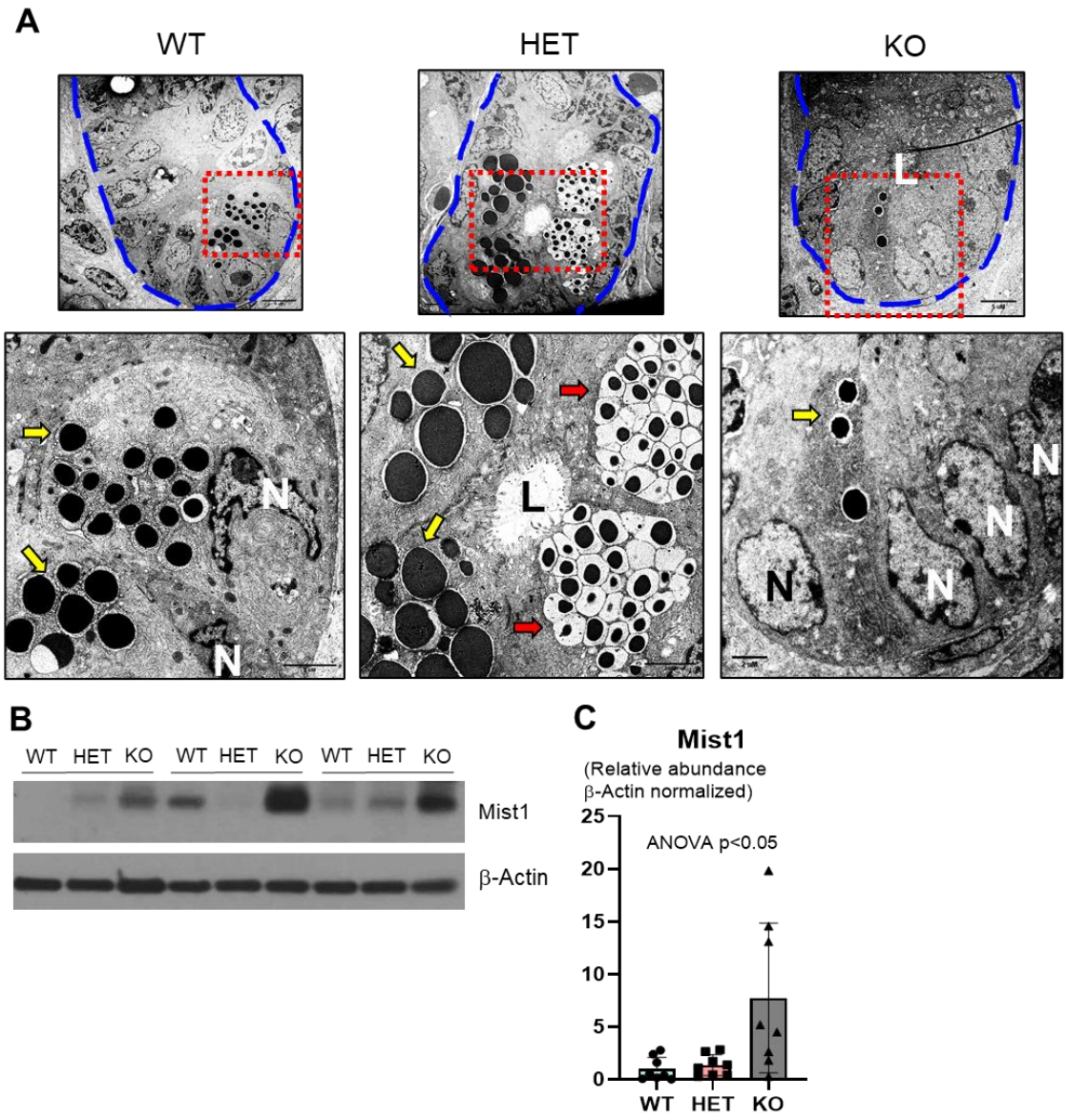

Figure 25. TEM images show that number of Paneth cells and dense core vesicles are indeed reduced. **(A)** TEM images of the ileal crypt base (delineated by dashed blue lines). Higher magnification images were captured from red dashed lines displaying Paneth cells and their dense core vesicles (DCVs indicated by yellow arrows). Note the absence of DCVs in the KO mice whereas HET mice display Paneth cell vesicles with large translucid halos around DCVs (red arrows); N = nucleus; L = luminal space; WT=3; HET=3 and KO=4. **(B)** Western blot of ileal IECs probing for Mist1 protein. **(C)** Densitometry of Mist1 protein levels in ileal IECs, a protein shown to be important in the organization of DCVs in secretory cells. WT=8, HET=8, KO=8. Columns display mean ± SD. Brown-Forsythe ANOVA test and Dunnett's T3 post-hoc test.

Next, western blot analysis of Mist1, a protein shown to be important in the secretory apparatus and maturation of exocrine cells, including Paneth cells[204–206], was elevated in KO mice compared with WT and HET (Figures 25B and C).

Although it is unclear why Mist1 is induced in *Ptpn2*-KO mice, it could suggest an attempt to rescue the normal secretory function of Paneth cells in these mice. Supporting this idea, expression of transcription factor 4 (*Tcf4*) and *Tcf7l2*, regulators of α-defensins expression[207,208]; and *Mmp7*, a Paneth cell-specific matrix metallopeptidase 7 (matrilysin) responsible for cleavage and activation of pro-α-defensins in mice[70]; remained unchanged in the Nanostring® analysis (Figures 23A and B), indicating that some of the Paneth cell molecular markers were retained despite the loss of many phenotypic features. Collectively, these data suggest that constitutive *Ptpn2* loss results in a dramatic reduction of mature Paneth cells and depletion of Paneth cells-specific AMPs in *Ptpn2*-KO mice.

4.3.3. *IECs of Ptpn2-KO Mice Show Activation of the Apoptosis Pathway*

Given the dramatic alterations in Paneth cell phenotype in mice that lack whole-body *Ptpn2* activity, we sought to investigate whether the absence of Paneth cells in *Ptpn2*-KO mice was due to apoptotic cell death. Western blot analysis of IECs showed that levels of both total and activated (cleaved) isoforms of the pro-apoptotic marker caspase-3 were elevated in KO mice compared with WT and HET (Figure 26A and B). Moreover, levels of cleaved poly-(ADP-ribose) polymerase (PARP), a critical protein during DNA repair, were significantly altered between groups, although pairwise comparisons did not detect differences between groups, suggesting activation of the apoptotic pathway (Figure 26A and C). However, TUNEL staining which detects DNA fragmentation in the late stage of cell apoptosis failed to detect substantial differences in the localization of apoptotic IECs between genotypes, except for some sporadic apoptotic cells found in the crypt region of constitutive *Ptpn2*-KO mice (Figure 26D).

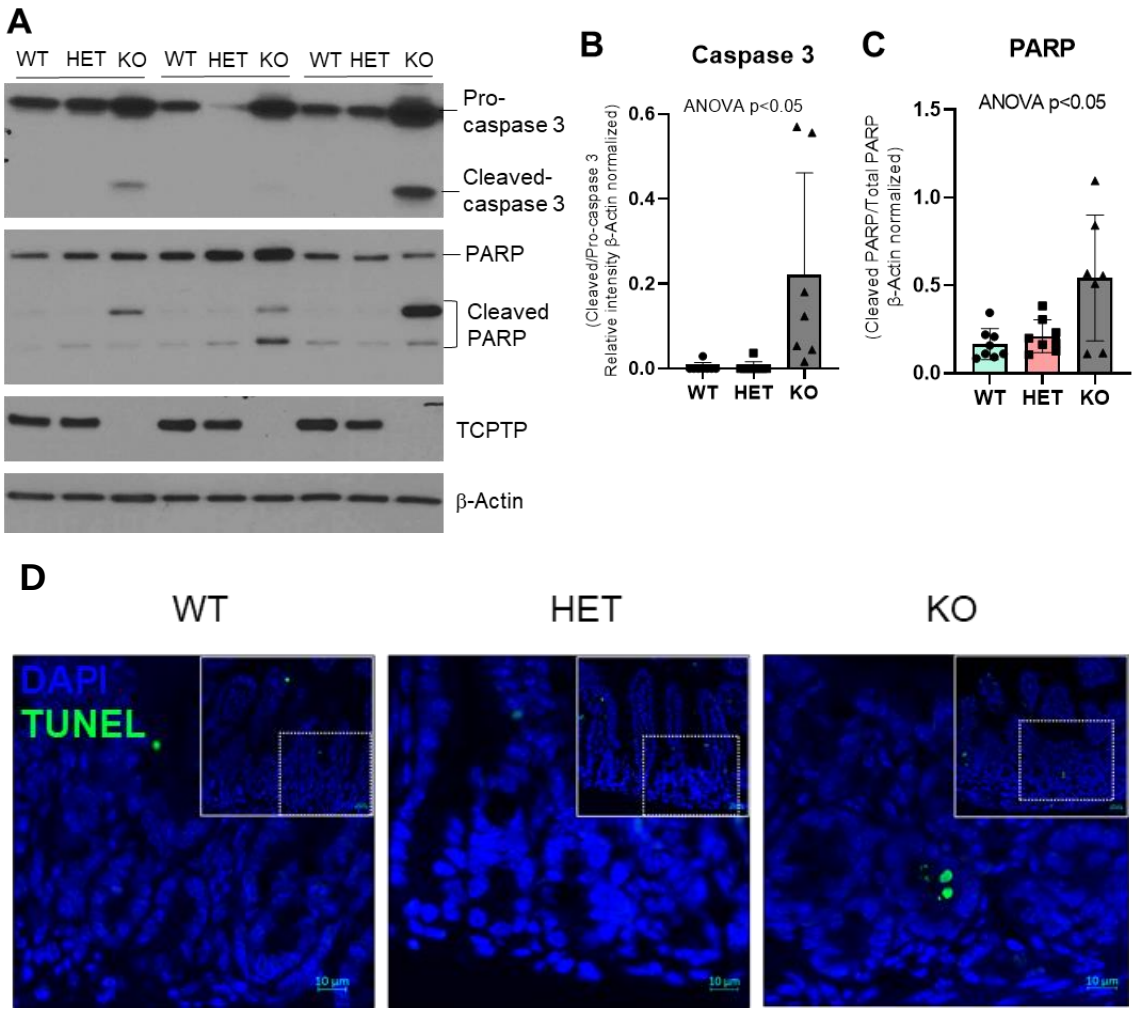

Figure 26. *Ptpn2*-KO mice have elevated levels of apoptotic immune cells. **(A)** Western blot of ileal IECs from constitutive *Ptpn2*-KO mice probing for pro-caspase 3 and cleaved caspase 3. **(B)** Densitometry and ratio of Caspase 3 isoforms. Columns show mean ± SD of relative intensity. Brown-Forsythe ANOVA test and Dunnett's T3 post-hoc test. **(C)** Densitometry and ratio of PARP isoforms. Brown-Forsythe ANOVA test and Dunnett's T3 post-hoc test. **(D)** TUNEL staining of ileal sections showing apoptotic cells (green) and cell nuclei (blue). N=4 per group.

As these crypt-localized TUNEL$^+$ cells did not appear to be IECs, we characterized immune cell viability in ileal tissues of these mice. Flow cytometric analysis identified increased proportions of dead CD3$^+$ immune cells and this was associated with increased number of dead CD4$^+$ and CD8$^+$ T-lymphocytes (Figures 27A-C). Collectively, these data identify increased activation of mucosal cell death mechanisms and a quantifiable increase in lymphocyte death in *Ptpn2*-KO mouse ileum.

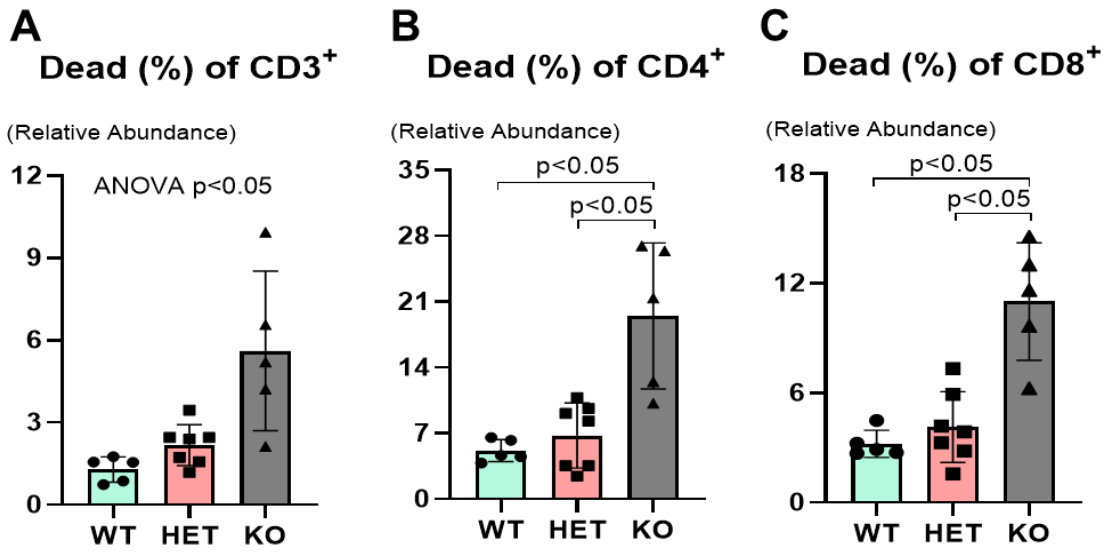

Figure 27. Flow cytometry of ileal mucosa cells stained for immune cell types and apoptotic marker showing elevated abundance of apoptotic **(A)** Lymphocytes (CD3$^+$), **(B)** T helper cells and (CD4$^+$), and **(C)** cytotoxic T cells (CD8$^+$). WT=8, HET=8, KO=8. Columns show mean ± SD. Brown-Forsythe ANOVA test and Dunnett's T3 post-hoc test.

4.3.4. *IEC-specific Ptpn2 Deletion Impairs Lysozyme Protein Levels Without Affecting Abundance of Paneth Cells*

To determine whether the Paneth cell defects in whole-body *Ptpn2* were a direct consequence of effects on epithelial cells, or an indirect consequence of effects on other (non-epithelial) cells, we used a tamoxifen-inducible villin-Cre transgenic *Ptpn2* deletion mouse line (*Ptpn2*$^{\Delta IEC}$). Tissues were harvested >30 days after recombinase induction by tamoxifen administration to minimize any potential residual effects from estrogen receptor activation[143]. H&E staining of ileal sections revealed and morphometric analysis of intestinal parameters, such as crypt depth, crypt width and villus length were similar between both groups (Figures 28 and 29).

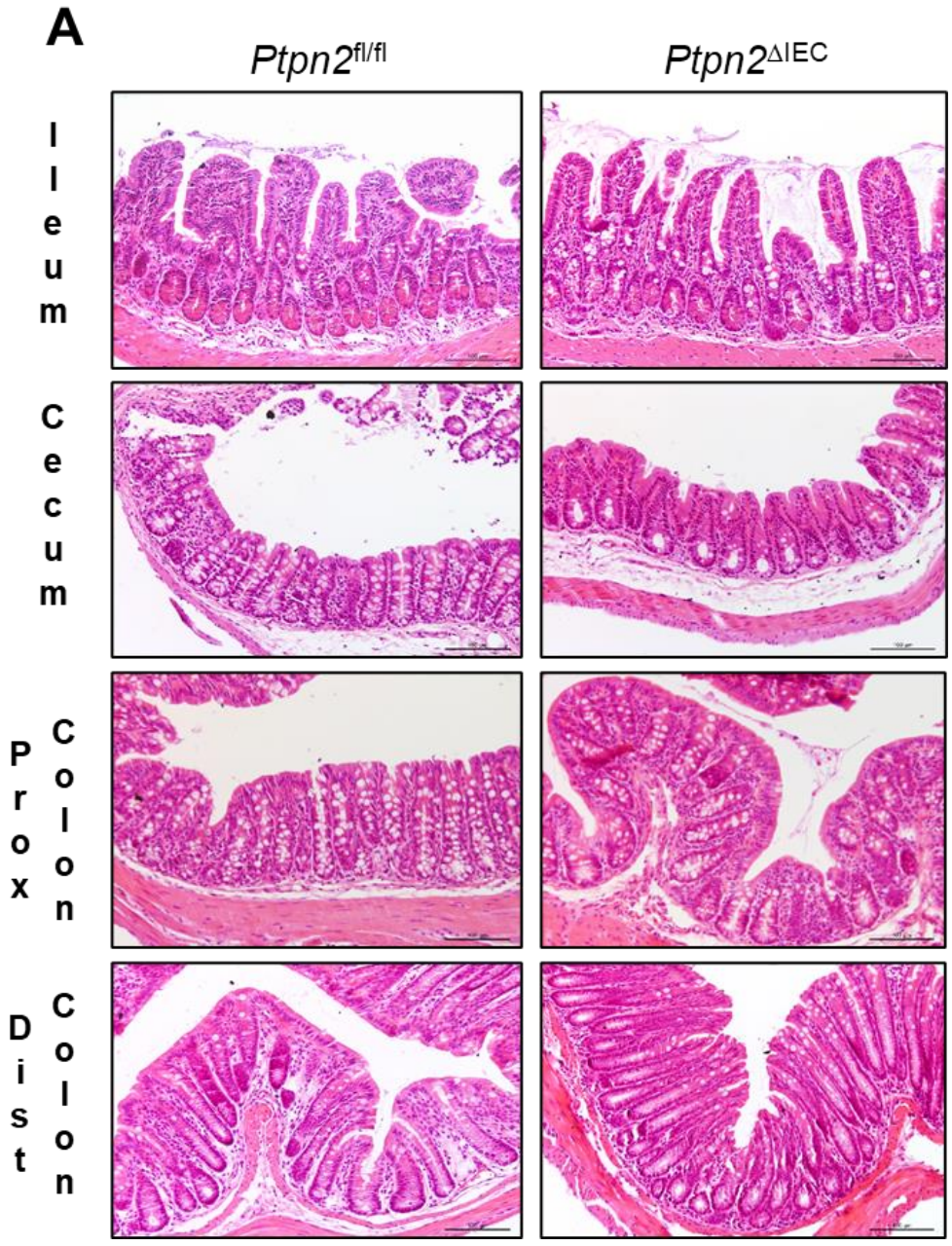

Figure 28. Morphological analysis of the intestinal mucosa architecture of *Ptpn2*$^{fl/fl}$ and *Ptpn2*$^{\Delta IEC}$ mice. **(A)** H&E staining of ileum, cecum, proximal and distal colon.

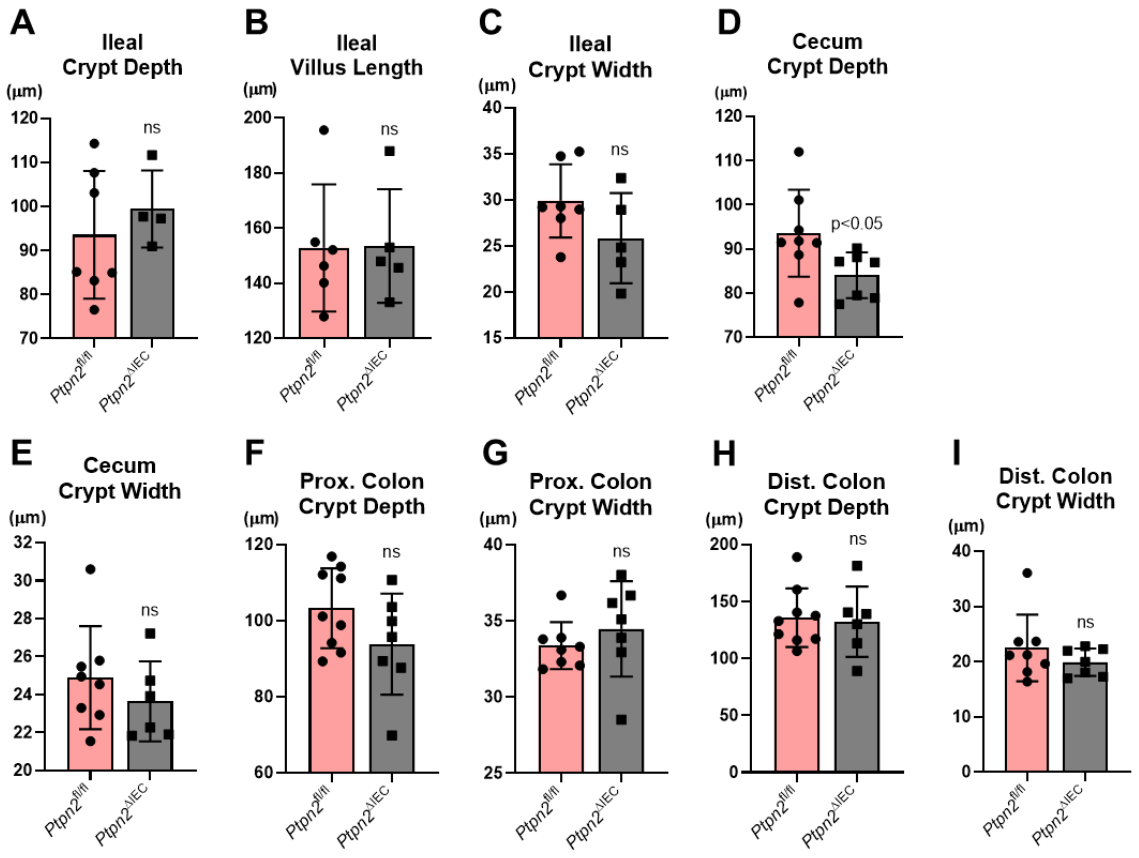

Figure 29. Morphometric analysis of intestinal structures of tamoxifen-inducible tissue-specific *Ptpn2*-deletion. Morphometric analysis of **(A)** ileal crypt depth; **(B)** ileal villus length; **(C)** ileal crypt depth; **(D)** cecal crypt width; **(E)** cecal crypt width; **(F)** proximal colon crypt depth; **(G)** proximal colon crypt width; **(H)** distal colon crypt depth; **(I)** distal colon crypt width. Each data point indicates the average value of a single mouse. $Ptpn2^{fl/fl}$=7, $Ptpn2^{\Delta IEC}$=5. Columns show mean ± standard deviation. Two-tailed unpaired student's t-test.

Paneth cells were present at the crypt base and displayed abundant cytosolic granules in both *Ptpn2*$^{\Delta IEC}$ mice and *Ptpn2*$^{fl/fl}$ controls (Figure 30A). The overall number of Paneth cells was not reduced by IEC-specific *Ptpn2* deletion (Figure 30B). However, when ileal sections were stained for lysozyme and *Ulex europaeus agglutinin-1* (UEA-1), a marker of lectins that is normally used to stain Paneth cell granules, both markers were dramatically reduced at the crypt base in *Ptpn2*$^{\Delta IEC}$ mice compared to controls (Figure 30A). Reduced levels of lysozyme protein in *Ptpn2*$^{\Delta IEC}$ mice were confirmed by Western blotting using isolated IECs (Figures 30C-D), whereas Mist1 protein levels were unchanged between groups (Figures 30C and E). Together, these data show that epithelial *Ptpn2* is critical for Paneth cell function with respect to lysozyme production, however, loss of epithelial *Ptpn2* is not sufficient to cause Paneth cell depletion.

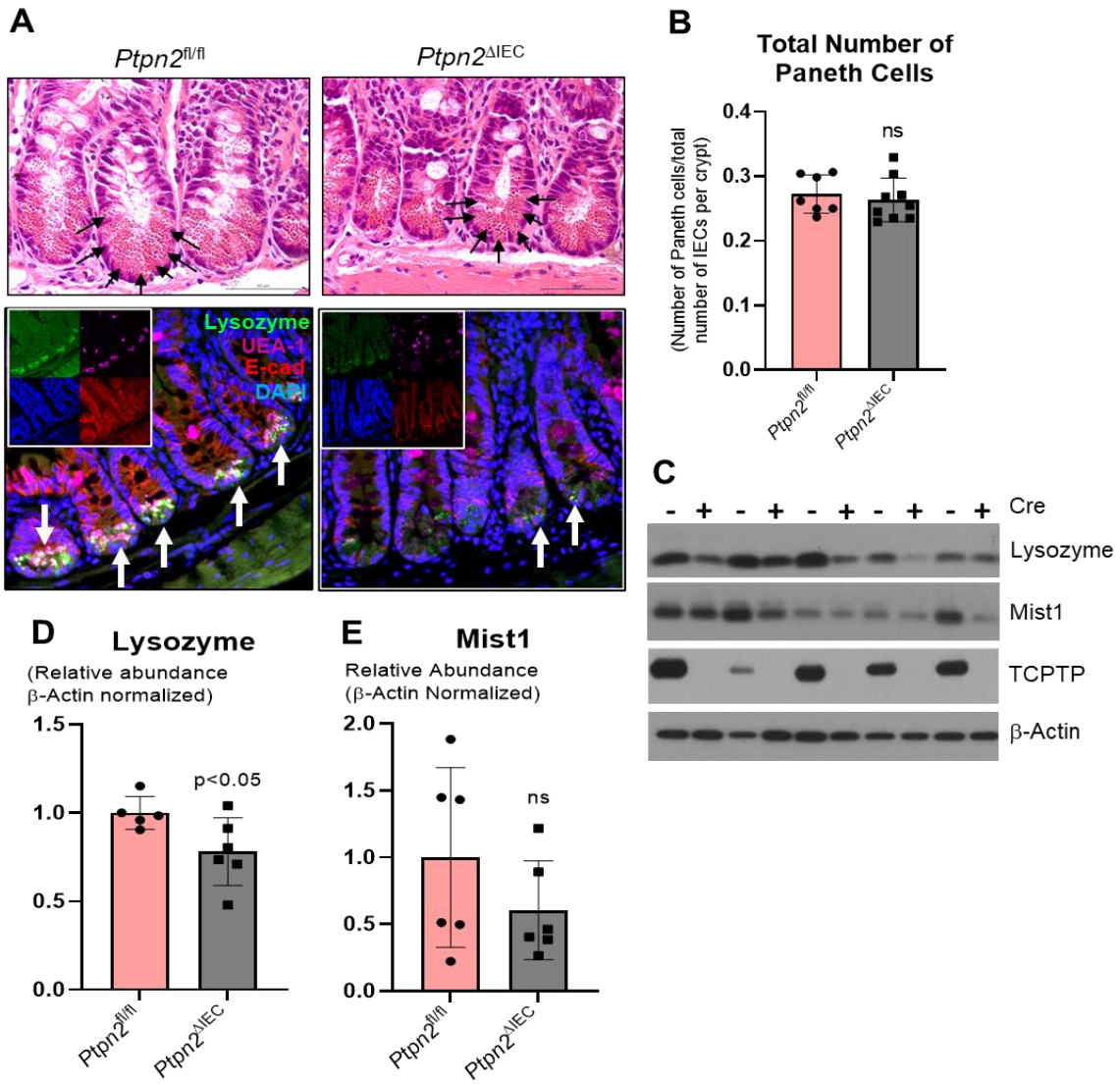

Figure 30. Paneth cell number is not affected by IEC-*Ptpn2* deletion but impairs production of lysozyme. **(A)** H&E staining of ileal sections showing abundant Paneth cells and cytosolic granules at the base of the crypt of *Ptpn2*$^{fl/fl}$ and *Ptpn2*$^{\Delta IEC}$ mice. Staining of ileal sections from *Ptpn2*$^{fl/fl}$ and *Ptpn2*$^{\Delta IEC}$ mice with Paneth cell marker lysozyme (green); UEA-1, a marker of Paneth cell dense core vesicles (magenta); cell nuclei (blue); and marker of intestinal epithelial cells E-cadherin (red). *Ptpn2*$^{fl/fl}$=7, *Ptpn2*$^{\Delta IEC}$=9. **(B)** Counting of total number of Paneth cells present in the ileum of *Ptpn2*$^{fl/fl}$ and *Ptpn2*$^{\Delta IEC}$ mice displayed as ratio of Paneth cells over total number of IECs per crypt. **(C)** Western blot of IECs probing for lysozyme and Mist1 proteins. **(D)** Densitometry of lysozyme protein levels in IECs comparing *Ptpn2*$^{fl/fl}$ and *Ptpn2*$^{\Delta IEC}$. **(E)** Densitometry of Mist1 protein levels in IECs comparing *Ptpn2*$^{fl/fl}$ and *Ptpn2*$^{\Delta IEC}$. *Ptpn2*$^{fl/fl}$=6, *Ptpn2*$^{\Delta IEC}$=6. Columns show mean ± SD. Two-tailed unpaired t-test.

4.3.5. *Constitutive Ptpn2-deficiency Increases Abundance of Ileal Immune Cells and Production of Paneth Cell Stimulatory Cytokines*

Because whole-body *Ptpn2*-KO mice failed to express several Paneth cell-associated AMPs, and were unable to form cytosolic granules, we investigated whether the ileal mucosa lacks stimulatory factors required for Paneth cell maturation, expression, and secretion of AMPs by evaluating immune cell infiltration and expression of immune cell-derived cytokines that stimulate Paneth cells. Flow cytometry analysis revealed increased abundance of neutrophils, macrophages, and TNF-α/IFN-γ expressing cytotoxic ($CD8^+$) and T helper ($CD4^+$) cells in the ileal mucosa of *Ptpn2*-KO mice in comparison with WT and HET mice (Figures 31A-D). Moreover, the abundance of $CD4^+$ T-cells positive for IFN-γ and IL-22 was also elevated (Figures 31C-E). These data indicate that the ileal mucosa contains abundant immune cells that express stimulatory cytokines that can promote PC function and stimulate secretion of AMPs. Furthermore, gene expression of cytokine receptors, *Il22ra1*, *Il10rb* and *Ifngr1* in IECs was unchanged (GEO database - accession number GSE181531), suggesting that IECs were not functionally uncoupled from cytokine stimulation, at least at the gene expression level.

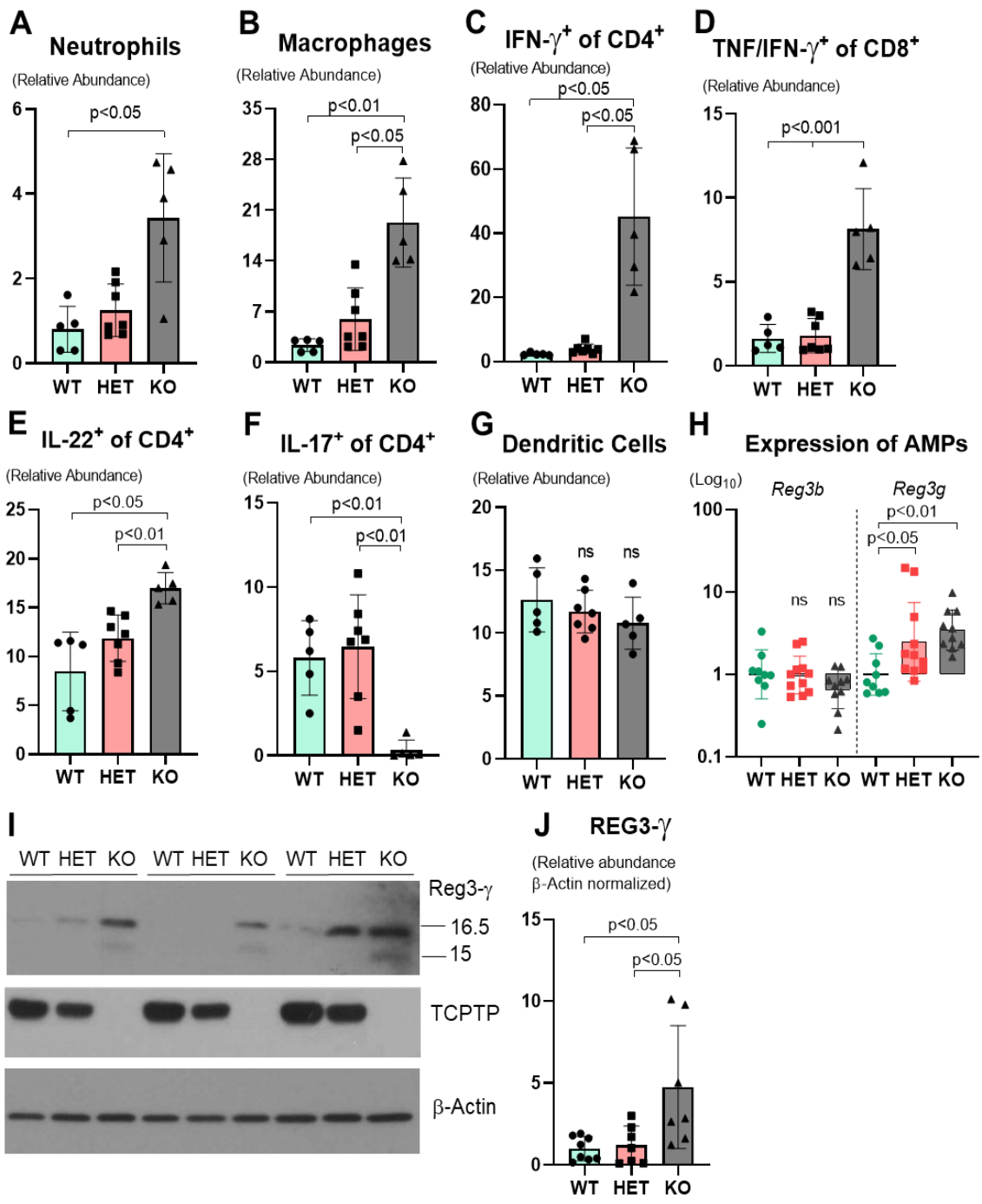
A
Neutrophils
(Relative Abundance)
p<0.05
WT HET KO
B
Macrophages
(Relative Abundance)
p<0.01
p<0.05
C
IFN-γ+ of CD4+
(Relative Abundance)
p<0.05
p<0.05
D
TNF/IFN-γ+ of CD8+
(Relative Abundance)
p<0.001
E
IL-22+ of CD4+
(Relative Abundance)
p<0.05
p<0.01
F
IL-17+ of CD4+
(Relative Abundance)
p<0.01
p<0.01
G
Dendritic Cells
(Relative Abundance)
ns
ns
H
Expression of AMPs
(Log10)
Reg3b
Reg3g
p<0.01
p<0.05
ns
ns
I
WT HET KO WT HET KO WT HET KO
Reg3-γ
16.5
15
TCPTP
β-Actin
J
REG3-γ
(Relative abundance
β-Actin normalized)
p<0.05
p<0.05

Figure 31. Flow cytometry of immune cells in the ileal mucosa of *Ptpn2*-KO mice stained for immune cell types and pro-inflammatory cytokines upon stimulation. **(A)** Relative abundance of neutrophils. **(B)** Relative abundance of macrophages. **(C)** Relative abundance of T helper cells ($CD4^+$) positive for IFN-γ. **(D)** Relative abundance of cytotoxic cells ($CD8^+$) positive for TNF and IFN-γ. **(E)** Relative abundance of T helper cells ($CD4^+$) positive for IL-22. **(F)** Relative abundance of T helper cells ($CD4^+$) positive for IL-17. **(G)** Relative abundance of dendritic cells ($CD11c^+$). WT=5, HET=7, KO=5. All columns show average ± SD. Brown-Forsythe ANOVA and Tukey's post-hoc test. **(H)** RT-qPCR gene expression of Paneth cell non-specific antimicrobial peptides, *Reg3b* and *Reg3g*. WT=9, HET=11, KO=10. Columns show geometric mean ± geometric standard deviation in a Log_{10} scale. One-way ANOVA and Tukey's post-hoc test. **(I)** Western blot of ileal IECs probing for Reg3-γ. **(J)** Densitometry of Reg3-γ protein levels in ileal IECs. Only the upper band (16.5 kDa) was measured as has been shown that cleavage of Reg3-γ by trypsin to generate the shorter active isoform (~15 kDa) occurs only after both proteins are released into the luminal space. WT=8, HET=7, KO=7. Columns show mean ± SD. One-way ANOVA and Tukey's post-hoc test.

Conversely, abundance of $CD4^+$ T-cells primed to express IL-17 was dramatically reduced in *Ptpn2*-KO mice in comparison with WT and HET (Figure 31F), whereas no change was detected in the abundance of ileal dendritic cells, a specialized antigen-presenting cell that orchestrates innate and adaptive immune responses (Figure 31G). Since pro-inflammatory cytokines should exert a global response on the ileal mucosa rather than targeting an individual IEC subtype, we analyzed the expression of two AMPs that are not Paneth cell-specific, *Reg3b* and *Reg3g* by RT-qPCR. Expression of *Reg3b* was unchanged, whereas the expression of *Reg3g* was induced in both *Ptpn2*-HET and KO mice compared with WT (Figure 31H). Western blots of ileal IECs confirmed that REG3-γ protein level was elevated in *Ptpn2*-KO mice compared to WT and HET mice (Figures 31I and J), suggesting that the deficit in the expression of Paneth cell-specific AMPs indicates a selective effect on Paneth cells.

4.3.6. *Constitutive Ptpn2-deletion Disrupts ER Architecture, Increases Levels of ER Stress and Unfolded Protein Response Markers Without Affecting Abundance of Autophagy Proteins*

Paneth cells respond to intestinal microbes by discharging AMP-filled granules into the luminal space[209]. Regarding secretion of lysozyme by Paneth cells, commensal bacteria seem to have a critical role in recruiting lysozyme into secretory granules, whereas depletion of commensals directs lysozyme to lysosomal degradation[199]. Bel et al, showed that lysozyme is secreted via secretory autophagy pathway during bacterial infection of the intestine, and when autophagy was disrupted in *Atg16l1*-deficient mice, lysozyme secretion was hindered[210]. Therefore, we tested whether the lysozyme deficit observed in constitutive *Ptpn2*-deficient mice was associated with impaired autophagy activation and/or autophagosome formation. Levels of the autophagy-related proteins Beclin-1, ATG3, ATG5, ATG7, ATG12, and the product of another IBD-associated gene, ATG16L1, were unchanged in IECs from whole-body *Ptpn2*-KO mice (Figure 32A-G).

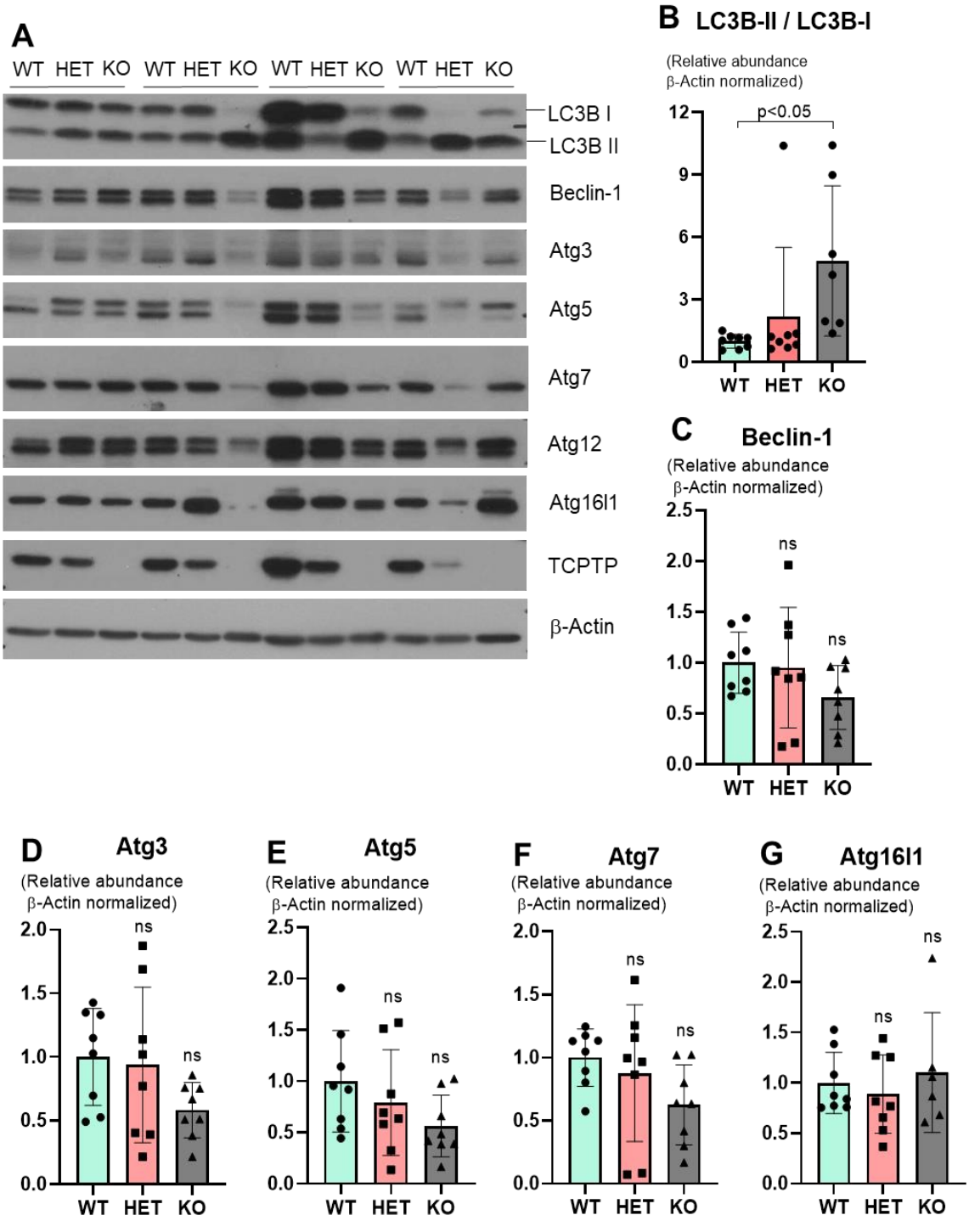
A
WT HET KO WT HET KO WT HET KO WT HET KO
LC3B I
LC3B II
Beclin-1
Atg3
Atg5
Atg7
Atg12
Atg16l1
TCPTP
β-Actin
B LC3B-II / LC3B-I
(Relative abundance β-Actin normalized)
p<0.05
C Beclin-1
(Relative abundance β-Actin normalized)
D Atg3
(Relative abundance β-Actin normalized)
E Atg5
(Relative abundance β-Actin normalized)
F Atg7
(Relative abundance β-Actin normalized)
G Atg16l1
(Relative abundance β-Actin normalized)
ns
WT HET KO

Figure 32. Evaluation of autophagy markers in the constitutive *Ptpn2*-deficient mice. **(A)** Western blot of ileal IECs probing for autophagy markers LC3B-I and -II, Beclin-1, ATG3, ATG5 (antibody detects total levels of free ATG5 and conjugated with ATG12), ATG7, ATG12 and ATG16L1. Densitometry of **(B)** LC3B-I and -II depicted as ratio between the two isoforms; **(C)** Beclin-1; **(D)** ATG3; **(E)** total ATG5; **(F)** ATG7; and **(G)** ATG16L1 protein levels. WT=8, HET=8, KO=8. Columns show mean ± SD. One-way ANOVA and Tukey post-hoc test.

Surprisingly, we observed elevated levels of autophagosome formation as evidenced by an increased ratio of LC3B isoforms, the lipidated LC3B-II over LC3B-I, suggesting increased autophagosome formation in *Ptpn2*-KO mice (Figure 32A and B). Although unexpected, our data suggested that the impairment in lysozyme production is independent of autophagy. On the other hand, to identify if the endoplasmic reticulum (ER)-driven protein secretory pathway was disrupted[211,212], we investigated whether Paneth cells in whole-body *Ptpn2*-deficient mice were undergoing ER stress. TEM images revealed that the ER architecture in Paneth cells was abnormal in constitutive *Ptpn2*-HET mice and dramatically disrupted in *Ptpn2*-KO mice, with ribosomes 'floating' in the cytosol having dissociated from ER cisternae (Figure 33A), which is a typical feature of cells undergoing ER stress. Protein levels of the ER stress-associated protein, Bip, and the unfolded protein response marker, Xbp-1s, were variable in *Ptpn2*-KO and -HET mice, whereas no change in phosphorylated-eIF2-α was observed (Figures 34A-D). Conversely, levels of CHOP protein, a late-stage ER stress marker and inducer of apoptosis, were increased in IECs from constitutive *Ptpn2*-KO mice in comparison with WT and HET mice (Figures 34A and E).

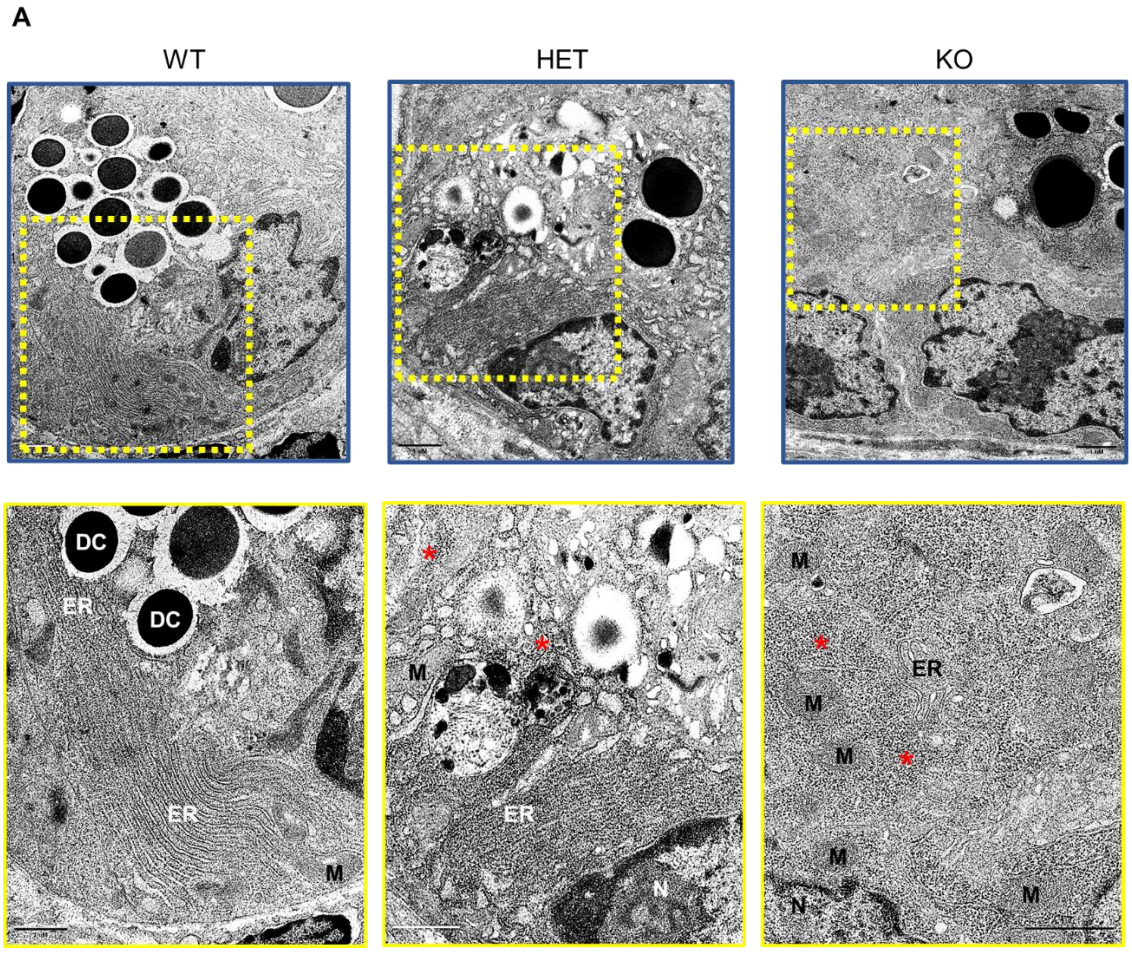

Figure 33. Constitutive *Ptpn2* deletion disrupts Paneth cell ER architecture. **(A)** Transmission electron microscopy (TEM) images. The upper row outlined in blue shows the Paneth cell cytosol. The yellow box with dashed lines shows the region further magnified. (DC) = Dense Core Vesicles; (N) = nucleus; (M) = mitochondria; (ER) = endoplasmic reticulum; (*) = ribosomes. WT=3, HET=3 and KO=4.

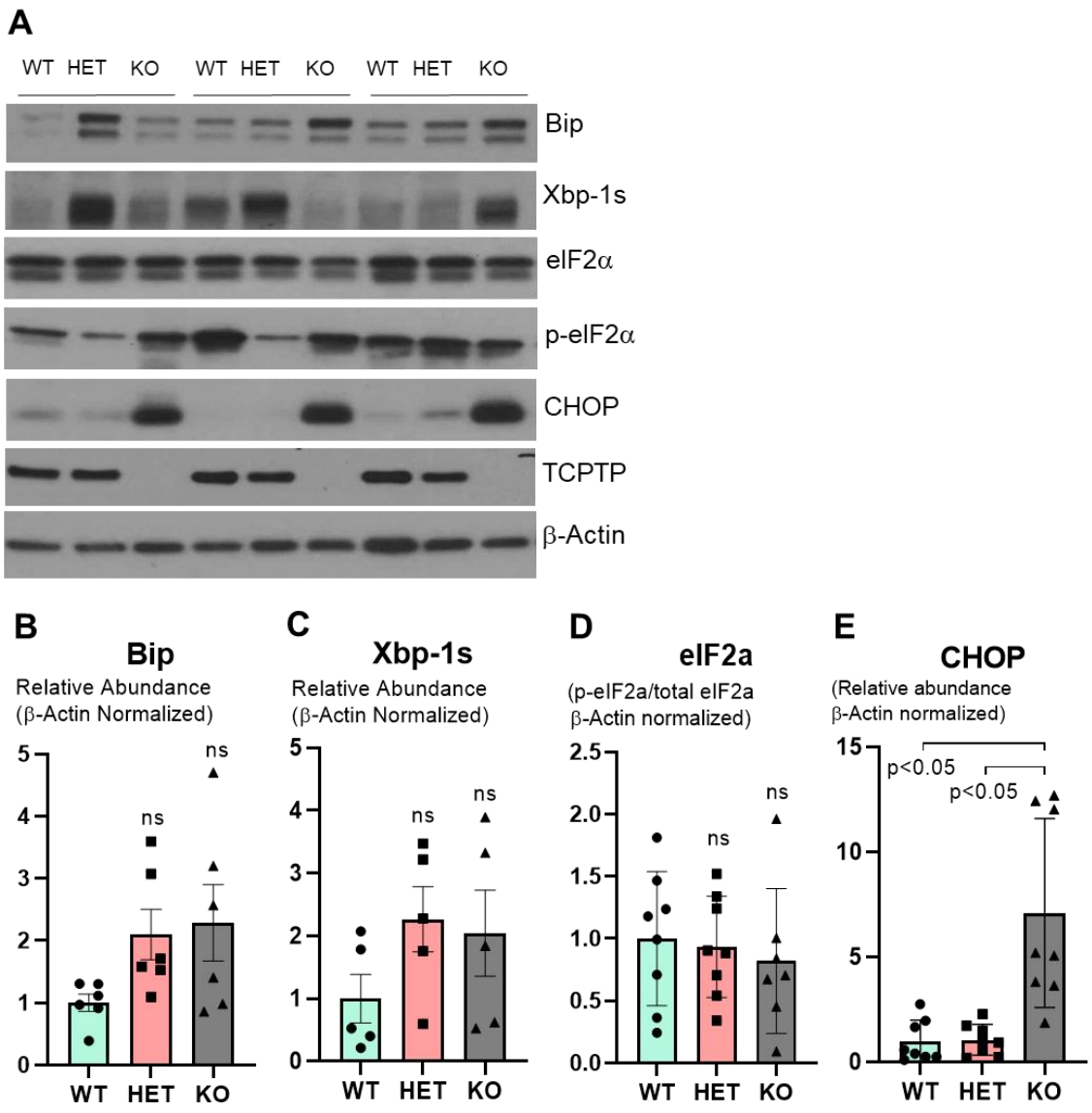

Figure 34. Constitutive *Ptpn2* loss increases ER stress marker CHOP protein levels in ileal IECs. **(A)** Western blot of ileal IECs probing for early ER stress marker Bip, unfolded protein response marker Xbp-1s, translation initiation factor isoforms eIF2-α and p-eIF2α, and ER stress marker CHOP protein in constitutive *Ptpn2*-deficient mice. Densitometry of **(B)** Bip, **(C)** Xbp-1s **(D)** eIF2-α ratio **(E)** CHOP protein levels. WT=8, HET=8, KO=8. Columns show mean ± standard deviation. One-way ANOVA and Tukey's post-hoc test.

In mice lacking *Ptpn2* only in the intestinal epithelium, we observed a substantial difference in the abundance of Xbp-1s protein between males and females (higher) in *Ptpn2*$^{\Delta IEC}$ and *Ptpn2*$^{fl/fl}$ mice (Figure 35A).

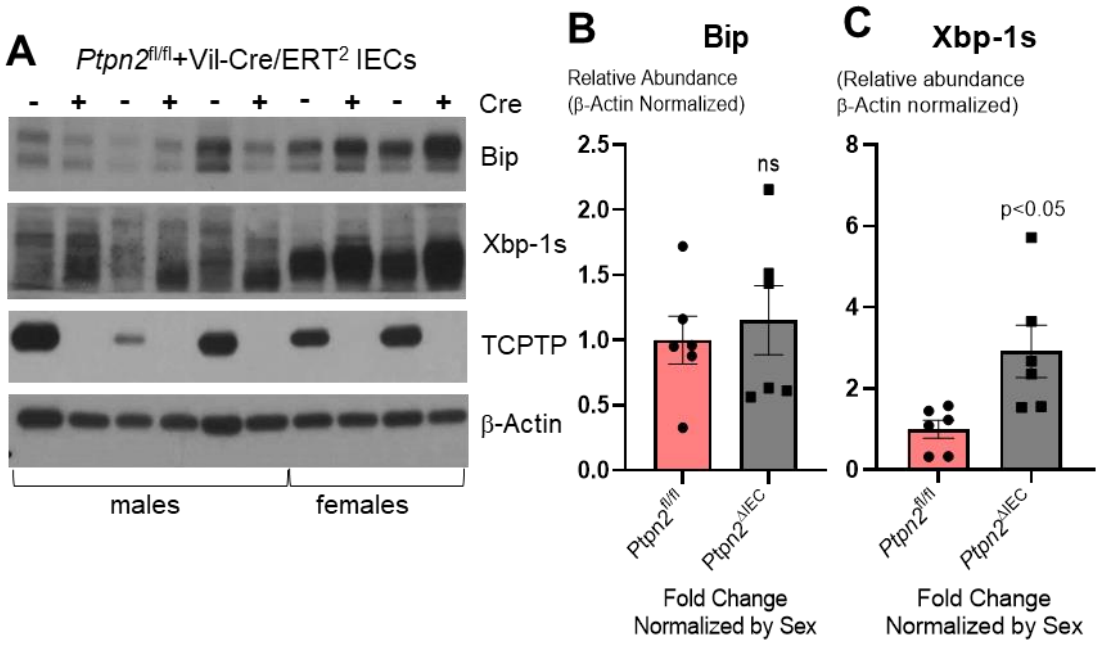

Figure 35. Specific *Ptpn2* deletion in IECs increases level of ER stress marker Xbp-1s. **(A)** Western blot of ileal IECs probing for ER stress markers in male and female *Ptpn2*$^{fl/fl}$ and *Ptpn2*$^{\Delta IEC}$ mice. **(B)** Densitometry of Bip protein levels and **(C)** Xbp-1s. Note the difference in band intensity between males and females. Here, data was normalized by sex. *Ptpn2*$^{fl/fl}$=6, *Ptpn2*$^{\Delta IEC}$=6. Columns show mean ± standard error of the mean. Two-tailed unpaired t-test.

When normalized by sex, levels of Xbp-1s were significantly higher in *Ptpn2*$^{\Delta IEC}$ compared to *Ptpn2*$^{fl/fl}$ mice (Figures 35B and C), indicating activation of the unfolded protein response in IECs of *Ptpn2*$^{\Delta IEC}$ mice. In

summary, *Ptpn2* loss in vivo provoked increased ER stress, activation of the unfolded protein response and compromised the ER architecture of Paneth cells which likely affects protein synthesis, including production of AMPs. Moreover, the elevated levels of CHOP protein in IECs suggest suppression of the unfolded protein response by increasing protein synthesis, which could lead to cell death through oxidative stress and ATP depletion[213,214].

4.3.7. *Constitutive Ptpn2 Deletion Does Not Affect Expression of Intestinal Epithelial Stem Cell Markers*

Paneth cells play a critical role in supporting the small intestinal stem cell niche[215]. Hence, we investigated whether the function of intestinal stem cells was also compromised in *Ptpn2*-KO mice. Western blot analysis of Olfm4 in IECs did not reveal alterations in the protein levels of this intestinal stem cell marker (Figures 36A-B). Additionally, gene expression of *Ephb3*, a marker of the ISC compartment, *Ascl2*, a gene that controls stem cell renewal in the crypts, and *Bmi1*, a marker of quiescent intestinal stem cell, were unaltered (Figure 23E and Figure 36C).

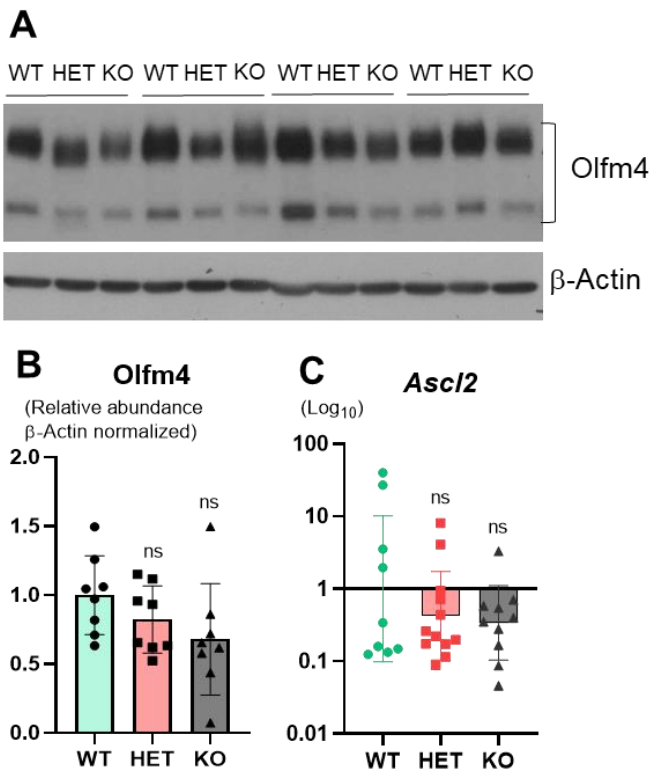

Figure 36. Constitutive *Ptpn2* deficiency does not seem to alter intestinal stem cell markers and self-renewal. **(A)** Western blot of ileal IECs probing for Olfm4, an intestinal stem cell marker. Per antibody manufacturer, Olfm4 in the small intestine typically displays two bands that belong to Olfm4 protein with molecular weight ranging from 85-90 and 70kDa. **(B)** Densitometry of both bands from Olfm4 protein level in ileal IECs. Columns show mean ± standard deviation. WT=8, HET=8, KO=8. One-way ANOVA and Tukey post-hoc test. **(C)** RT-qPCR analysis of *Ascl2* gene, responsible for intestinal stem cell renewal in the crypts. WT=9, HET=11, KO=10. Columns show geometric mean ± geometric standard deviation. One-way ANOVA and Tukey post-hoc test.

This indicates that the expression of the stem cell compartment markers was not affected, even though the increased number of proliferative cells suggest higher activity of intestinal stem cells while markers of quiescent stem cells remained unchanged. Next, we evaluated the expression of differentiation

factors involved in the commitment of secretory *vs.* absorptive lineages. Notably, fibroblast growth factor receptor 3, *Fgfr3*, a differentiation factor shown to be critical for Paneth cell development was downregulated (Figure 23C)[216,217]. Conversely, *Sfrp1* which encodes Secreted Frizzled Related Protein 1, and *Ccnd1* which encodes Cyclin-D1, genes with direct roles in cell cycle and differentiation of the intestinal epithelium, were markedly upregulated (Figure 23C). Altogether, our data suggest an imbalance in the expression of differentiation factors associated with the Paneth cell lineage, whereas expression of intestinal stem cell markers did not seem to be affected.

4.4. Discussion

Ptpn2 modulates the intestinal microbiome and restricts the expansion of a mouse-specific adherent-invasive *E. coli* (*m*AIEC), which has >90% genetic similarity to the human IBD-associated AIEC, LF82[142,218]. *Ptpn2* is also critically involved in the maintenance of intestinal barrier function through epithelial-macrophage crosstalk[139,36]. Here, we identified a possible mechanism to explain how loss of *Ptpn2* contributes to bacterial dysbiosis. We report that ileal IECs showed dramatic downregulation of critical genes associated with Paneth cell function, whereas analysis of morphological features and molecular markers confirmed that Paneth cells were nearly ablated in the ileum of constitutive *Ptpn2*-KO mice. Given the essential role of Paneth cells in the first line of enteric defense by modulating the gut microbiome through a large spectrum of AMPs secreted into the luminal space, the loss of AMP production by Paneth cells is likely a critical factor in the observed changes in microbiota composition.

Human Paneth cells abundantly express two α-defensin genes, *DEFA5* (HD5) and *DEFA6* (HD6), as well as lysozyme, secretory phospholipase A_2, and regenerating islet-derived protein 3-α (REG3A)[219]. HD5 has antibiotic activity against $Gram^+$ and $Gram^-$ bacteria, including *Staphylococcus aureus*

and *Salmonella typhimurium* as shown in transgenic mice expressing human *DEFA5*[220,221]. HD6 lacks direct antimicrobial activity, forming nanonets that trap bacteria instead[222]. Murine Paneth cells, on the other hand, express at least 19 different α-defensin isoforms[223,224]. The expression of α-defensins by Paneth cells in mice does not seem to be dependent on bacterial stimuli, but rather is regulated by transcription factors linked to IEC differentiation, including *Tcf4* and *Tcf7l2*, which are under control of the Wnt/Beta-catenin pathway[208]. In our study, we observed that these transcription factors that are critical in the development of Paneth cells were not affected in constitutive *Ptpn2*-KO mice (Figure 23D), suggesting that the deficit in AMP expression could be inherently connected to loss of Paneth cells in the ileal mucosa. Moreover, Paneth cells are the primary source of intestinal C-type lysozyme, encoded by the *Lyz1* gene, which hydrolyzes the bacterial wall component peptidoglycan (PGN), common to both $Gram^+$ and $Gram^-$ bacteria, resulting in the release of MDP, an important agonist of Nod1 and Nod2[18]. Unlike α-defensins, lysozyme levels are regulated by commensal bacteria stimulation of Nod2, as demonstrated by germ-free and *Nod2*-KO mice where lysozyme is rerouted from secretion to protein degradation[199]. Although *Lyz1*$^{-/-}$ mice displayed expansion of the mucolytic bacteria *Ruminococcus gnavus*, a

Crohn's disease-associated pathobiont, they had diminished mucosal sensing and responses to MDP, accompanied by a reduced basal inflammatory response, suggesting the importance of lysozyme activity in tuning of the immune system[225]. Consequently, the impact caused by a lack of mature Paneth cells could go beyond the impairment in the production of AMP to also affect lysozyme-mediated priming of the enteric immune response to bacterial products.

While Paneth cell-specific AMPs (*Lyz*, *Defa6* and *Pla2g2a*) were reduced, expression of AMP produced by other IECs were either induced (*Reg3g*), or unchanged (*Reg3b*), suggesting that the deficit in the expression of AMPs is Paneth cell-specific. With respect to the different effects on *Reg3g* and *Reg3b* expression, this could be due to a lack of IL-17 stimulation which is required for *Reg3b* induction. Paneth cell stimulation by IL-22 is essential for Paneth cell maturation and regulation of microbiota-dependent Il-17 immune responses. IL-17 and IL-22 tend to act synergistically in Paneth cells, albeit by distinct cellular mechanisms[226,227]. Despite abundant IL-22-expressing $CD4^+$ cells in the ileal mucosa, this was not sufficient to promote Paneth cell maturation or expression of Paneth cell-specific AMPs.

Studies with IBD patient and transgenic mice show that genetic variants, or deletion of IBD-associated genes, such as *ATG16L1*, *NOD2* and *LRRK2*, are detrimental to Paneth cell morphology and function, leading to dysbiosis[197–200.] In addition, deletion of the transcription factor X-box binding protein-1 (*Xbp1*) in IECs, a marker of unfolded protein response, leads to Paneth cell impairment and spontaneous enteritis[228]. However, mice with constitutive homozygotic *Ptpn2* deficiency develop severe systemic inflammation succumbing between three and five weeks of age[163]. Our group has recently shown that constitutive *Ptpn2*-KO mice have elevated pro-inflammatory cytokines (IFN-γ, TNF-α, and IL-6) in the serum and in large intestinal mucosa[143]. In this paper, we showed that immune cells primed to secrete stimulatory cytokines that induce PC function (IFN-γ, TNF-α and IL-22) were abundant in the ileal mucosa of *Ptpn2*-KO mice, indicating that Paneth cells seem to be extremely sensitive to inflammatory conditions. As an example, IFN-γ induces potent extrusion of secretory granules, and Paneth cell nucleus expulsion leading to apoptosis, if stimulation by IFN-γ is sustained[229,230]. We also identified that *Ptpn2* deletion in IECs alone is sufficient to impair lysozyme production without affecting overall Paneth cell number, in addition to promoting activation of the unfolded protein

response. Thus, the ablation of Paneth cells in constitutive *Ptpn2*-KO mice may reflect the elevated inflammatory status, and likely contribution of non-epithelial cells (i.e. immune cells) in these mice that is not seen in *Ptpn2*$^{\Delta IEC}$ mice.

In our study, gene expression of *Tcf4* and *Tcf7l2*, transcription factors that control expression of α-defensins, and *Mmp7*, another Paneth cell-associated gene critical in cleaving and activating AMPs, was unaltered in ileal IECs (GEO database - accession number GSE181531). This could indicate an impairment in Paneth cell maturation. Moreover, levels of Mist1 protein were elevated in *Ptpn2*-KO mice compared with WT and HET counterparts. Mist1 belongs to a helix-loop-helix (bHLH) family of transcription factors that bind DNA in several developmentally regulated genes[231], and play a role in the regulation of differentiation and maturation of the secretory machinery of exocrine cells[232]. Studies using *Mist1*-KO mice showed that Paneth cells develop an immature phenotype with abnormal DCVs and secretory apparatus without affecting the expression of lysozyme[204]. As Mist1 seems to be critical in maturation of Paneth cells and in the organization of their secretory granules, this might suggest that the elevated levels of Mist1 could

be an attempt to rescue the normal secretory function of Paneth cells in whole-body *Ptpn2*-deficient mice.

Our group has shown that loss-of-function *PTPN2* variants impair autophagosome formation in T_{84} IECs and THP-1 monocytes in response to the bacterial wall component MDP, or the inflammatory cytokines IFN-γ+TNF *in vitro*[233,234]. However, we did not observe changes in the levels of autophagy proteins, nor in autophagosome formation in isolated IECs from *Ptpn2*-KO mice, indicating that the lysozyme deficit in Paneth cells is not due to autophagy impairment. Spalinger et al, have shown that *m*AIEC replicate and survive in macrophages lacking *Ptpn2* activity, however autophagosome formation was rescued after stimulation with rapamycin, showing that the defective autophagy present in *Ptpn2*-deficient macrophages *in vivo* can be bypassed by stimulatory factors[144]. One possible explanation for the different effects on autophagy in whole-body vs. macrophage specific loss of *Ptpn2* is that the elevated ER stress could be the stimulus to activate autophagy in whole body *Ptpn2*-KO mice since there is extensive crosstalk between these two cellular processes[235]. Constitutive *Ptpn2*-deletion resulted in disruption of the ER architecture in Paneth cells, indicating ER stress that could compromise correct protein processing and

folding. Of note, we did not observe increased phosphorylation of eIF2-α that is normally elevated during ER stress. IFN-γ induces potent phosphorylation of eIF2-α at serine 51 (Ser51) in exocrine cells[236]. However, in agreement with our findings, *PTPN2* knockdown in HT-29 IECs showed no change in eIF2-α phosphorylation following tunicamycin-induced ER stress[237]. Moreover, we observed a dramatic increase in the levels of CHOP, which plays an essential role in inducing cell cycle arrest and apoptosis during ER stress[214,238]. CHOP promotes cell death by GADD34-mediated dephosphorylation of eIF2-α[214], thus stimulating protein synthesis under ER stress, increasing oxidative stress, ATP depletion, which collectively culminates in apoptosis[213]. Additionally, Bettaieb et al., reported that *Ptpn2* knockdown in MIN6 cells mitigated ER stress-induced phosphorylation of eIF2-α[239]. Consequently, constitutive *Ptpn2*-deficiency seems to promote cell death by sustaining ER stress instead of inhibiting it.

The enhanced proliferation of IECs in constitutive *Ptpn2*-KO mice was focused on the crypt region, while ileal villus length, but not crypt depth, was increased. Moreover, the apoptosis marker cleaved caspase-3 was increased in IECs, although TUNEL staining did not detect substantial differences in the number of apoptotic cells between genotypes. We attribute

the lack of TUNEL signal due to the nature of the assay, where apoptotic cells are only detected at a late stage, possibly when IECs are likely being ejected from the epithelium in an orchestrated fashion[240,241]. Regardless of whether there is or is not an increase in IEC apoptosis, functionally there does not appear to be a dramatic effect on intestinal barrier properties as constitutive *Ptpn2*-KO mice displayed no increase in intestinal permeability to rhodamine B isothiocyanate-70kD dextran (RD70), a molecular probe for the unrestricted permeability route indicating epithelial damage or shedding[36,143]. Additionally, we cannot rule out that the elevated activation of caspase-3 and PARP detected by the western blot, could be due to the presence of immune cells in our IEC-enriched sample isolation, as higher abundance of the CD45 immune cell marker was found in some KO samples (Figure 5). In addition, flow cytometry analysis identified a significantly elevated abundance of apoptotic immune cells in *Ptpn2*-KO mouse ileum. Furthermore, CHOP activity can lead to cell death independent of the caspase pathway activation, which in this case would not be detected by TUNEL staining[242]. Collectively, our data indicate a more rapid turnover of ileal IECs without causing non-specific defects in epithelial barrier permeability.

IEC lineage tracing studies, and mouse models of colitis (DSS), have identified that Paneth cells possess some level of cell plasticity, and can reacquire intestinal stem cell characteristics to repopulate the intestinal stem cell compartment depleted of $Lgr5^+$ intestinal stem cells[243,244]. Thus, we hypothesized that depletion of Paneth cells could be due to their ability to dedifferentiate and repopulate the stem cell zone shifting to a stem-like cell. Consistent with our Nanostring dataset showing that gene expression of intestinal stem cell markers, *Lgr5* and *Olfm4* were not significantly altered, protein levels of Olfm4 were unchanged. In addition, gene expression of the stem cell compartment marker (*Ephb3*), and of intestinal stem cell renewal activity (*Ascl2*) were not significantly altered. Moreover, gene expression of a quiescent stem cell marker, *Bmi1*, was unchanged, suggesting that quiescent cells remained dormant[245]. Therefore, it seems unlikely that depletion of Paneth cells in *Ptpn2*-deficient mice is the result of a phenotypic shift in an attempt to rescue/repopulate the stem cell zone.

In conclusion, the present study shows that *Ptpn2* is a regulator of ileal intestinal epithelial cell homeostasis and a critical mediator of Paneth cell viability and antimicrobial protein expression in mice. Collectively, our data suggest that the ileal mucosa of *Ptpn2*-deficient mice undergoes rapid

turnover likely affecting the maturation of Paneth cells. Conversely, the remnant Paneth cells undergo ER stress that could lead to cell death. Thus, our study identifies that loss of *Ptpn2* activity causes Paneth cell dysfunction that may explain the intestinal dysbiosis and pathobiont expansion observed in *Ptpn2*-deficient mice.

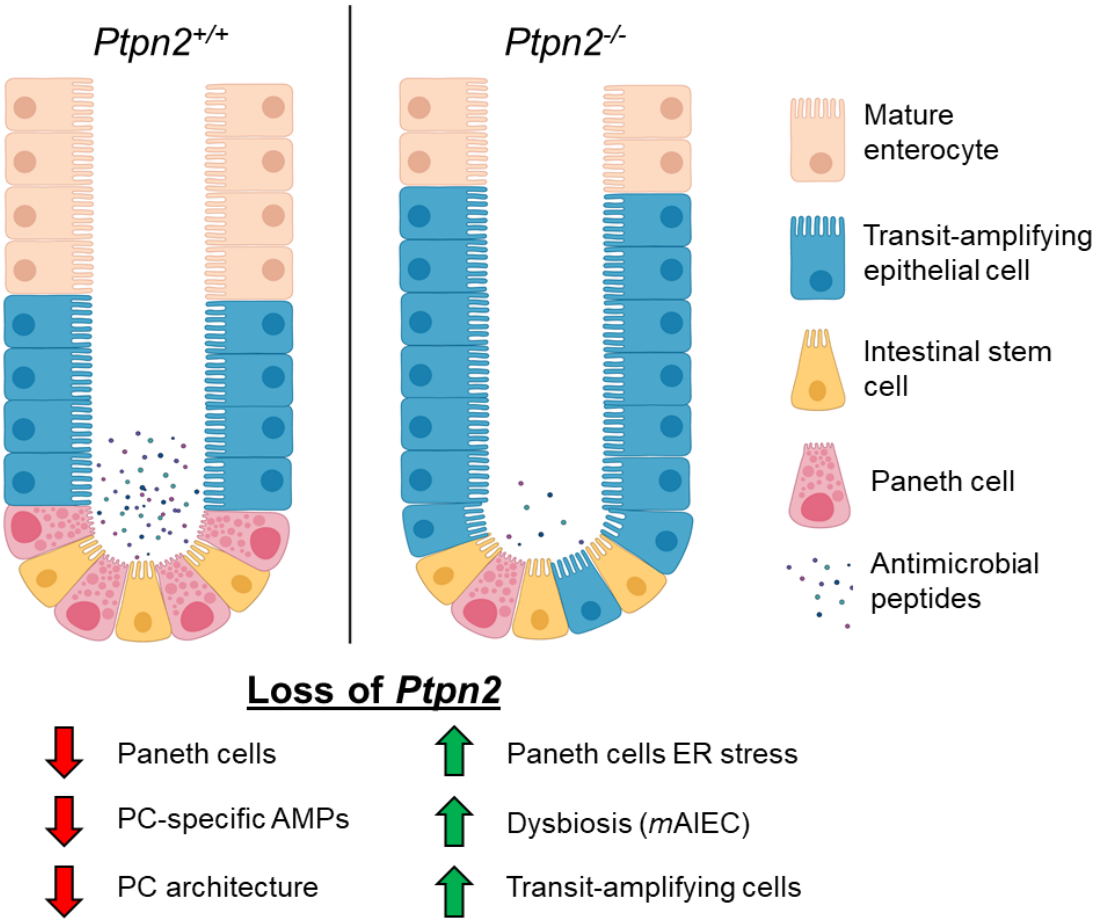

Figure 37. Graphical summary regarding Paneth cell number, function, and viability in constitutive *Ptpn2*-deficient mice.

5. Constitutive *Ptpn2*-regulates Goblet Cell Number and Function in a Region-specific Manner

5.1. Introduction

As mentioned previously, the mucus layer limits bacterial contact with the underlying epithelium by creating a gel-forming mucus barrier that prevents bacterial penetration. The MUC2 mucin produced by intestinal goblet cells, is the major gel-forming component of the mucus barrier. The importance of the mucus layer to intestinal homeostasis is underlined by the phenotypes in *Muc2*$^{-/-}$ mice, where the colon is devoid of a mucus layer thereby allowing bacteria in direct contact with the epithelium. This results in epithelial hyperproliferation, immune cell activation and development of spontaneous colitis[30,33,246]

Despite much focus, the mechanisms involved in the activation and secretory functions of goblet cells are not fully understood. There are different goblet cell subtypes that can be categorized based on their location and function. For example, surface colonic goblet cells secrete continuously to maintain the inner mucus layer, whereas goblet cells localized in the crypts appear to secrete mucin proteins only upon stimulation[247]. Much of

our understanding of goblet cell functions are derived from investigations of helminth infections that demonstrated immune cell-derived cytokines IL-4, IL-5, IL-9, and IL-13 induce goblet cell hyperplasia and hypersecretion, where IL-13 seems to be a major effector cytokine[24,248]. Apart from helminth infections, IL-10 has also been shown to have a direct effect on goblet cells, by modulating mucin synthesis and misfolding, whereas *Il10*$^{-/-}$ mice develop chronic enterocolitis with decreased production of Muc2[249–251].

The renewal rate of the inner mucus layer has been estimated to be as fast as 1 hour, which is considerably faster than renewal of the epithelial cell layer[247]. Like Paneth cells, goblet cells have an adapted secretory system enabling them to synthesize and store large quantities of their products. As such, these cells are especially susceptible to ER stress when subjected to ongoing challenge, such as inflammation[252].

Since we demonstrated that Paneth cells display disrupted ER architecture in *Ptpn2*-KO mice, in addition to activation of the unfolded protein response in ileal isolated IECs from *Ptpn2*$^{\Delta IEC}$ mice, we investigated whether goblet cell number, and/or function is altered in *Ptpn2*-deficient mice, in such a way as to potentially weaken the protective mucus layer and increase susceptibility to microbial infection.

5.2. Methods

For this study, we evaluated intestinal morphology and number of goblet cells through histology and immunofluorescence. Western blotting was performed using colonic whole-tissue lysates as opposed to isolated intestinal epithelial cells. However, partial transcriptome analysis using nanostring was performed using isolated IECs as reported in the previous chapter. Flow cytometry was performed on immune cells isolated from cecal and colonic mucosa as described in detail in the methods chapter. The experiments and data shown in this chapter will be included in a follow up paper focused on goblet cell subtypes, and structural aspects of the mucus layer.

5.3. Results

5.3.1. *Whole-body Ptpn2-KO Mice Display Increased Number of Proliferating Cells and Apoptotic Cells in the Colonic Mucosa*

We demonstrated in Chapter 3 that whole-body *Ptpn2*-KO mice display increased crypt depth in the cecum and proximal colon (Figures 12A and Figure 13E-J)[143]. Moreover, we observed increased villus length in the ileum of *Ptpn2*-KO mice, while elevated numbers of proliferating cells were found in the crypts (Figure 21A-B). We further noted that increased crypt depth in the *Ptpn2*-KO mice was also accompanied by elevated numbers of proliferating cells in the proximal and distal colon (Figures 38A-C).

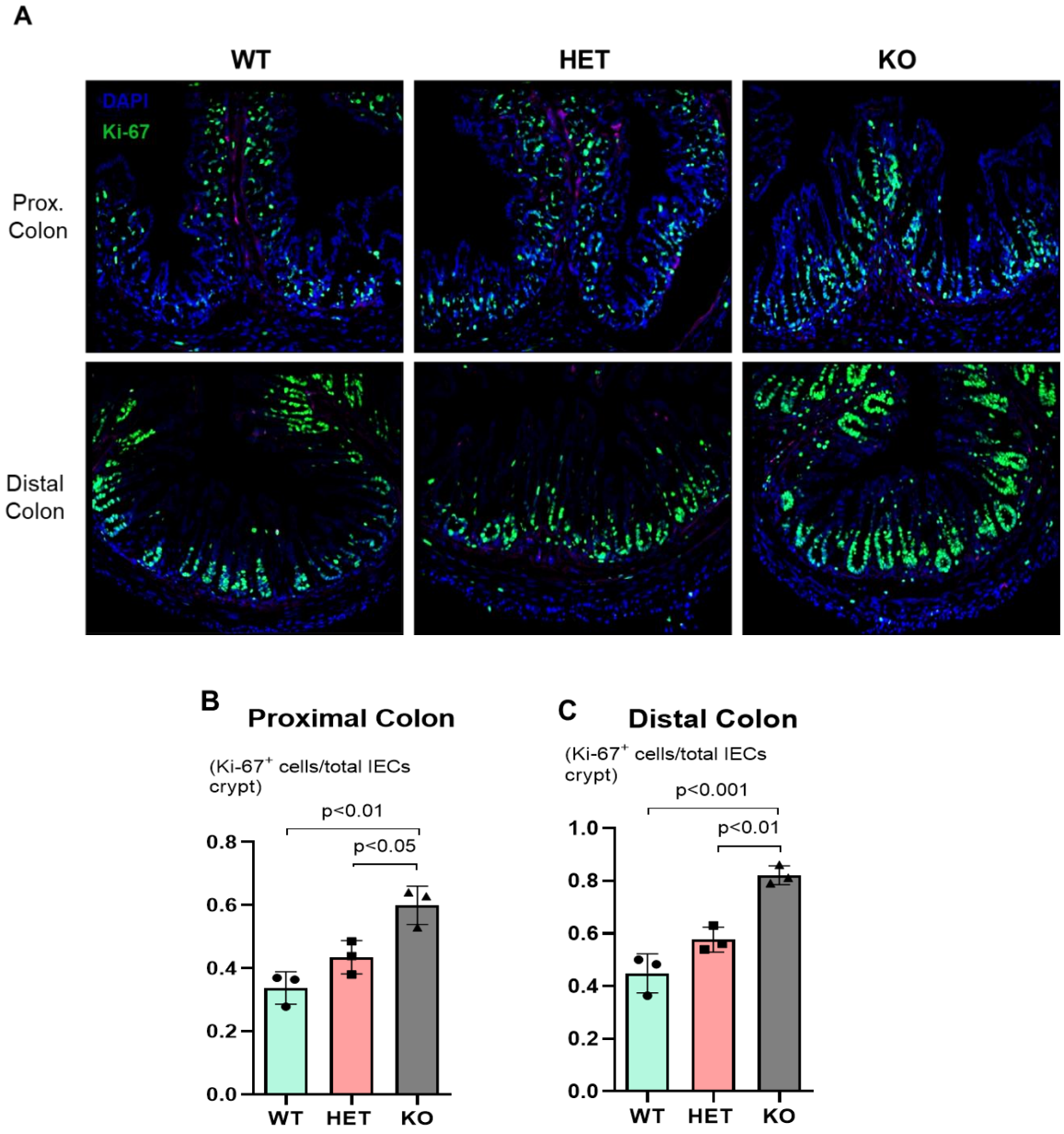

Figure 38. *Ptpn2*-KO mice displayed elevated numbers of proliferating colonic IECs. **(A)** Immunofluorescence imaging of proximal and distal colon sections staining for the proliferation marker Ki-67 (green) and cell nuclei (blue). **(B)** Quantification of Ki-67$^+$ IECs in the proximal colon. **(C)** Quantification of Ki-67$^+$ IECs in the distal colon. WT=3, HET=3, KO=3. Columns show mean ± SD. One-way ANOVA and Tukey post-hoc test.

Our investigation of the ileum segment revealed elevated activation of the apoptosis pathway in isolated IECs (Figure 26A-C), however TUNEL staining was not different indicating no increase in DNA fragmentation in the ileal epithelium (Figure 26D). Thus, we wanted to confirm that the intestinal epithelium layer is intact in the large intestine of *Ptpn2*-deficient mice. In contrast to the ileal segment, TUNEL staining was elevated in the proximal and distal colon of *Ptpn2*-KO mice compared with WT and HET (Figure 39A). Due to the nature of the assay, we were not able to use these data to clearly determine whether the apoptotic cells were IECs or of a different lineage. Next, our preliminary western blot analysis of colonic whole-tissue lysates showed elevated levels of both, total and activated (cleaved) isoforms of the pro-apoptotic marker caspase-3, in KO mice compared with WT and HET (Figure 39B).

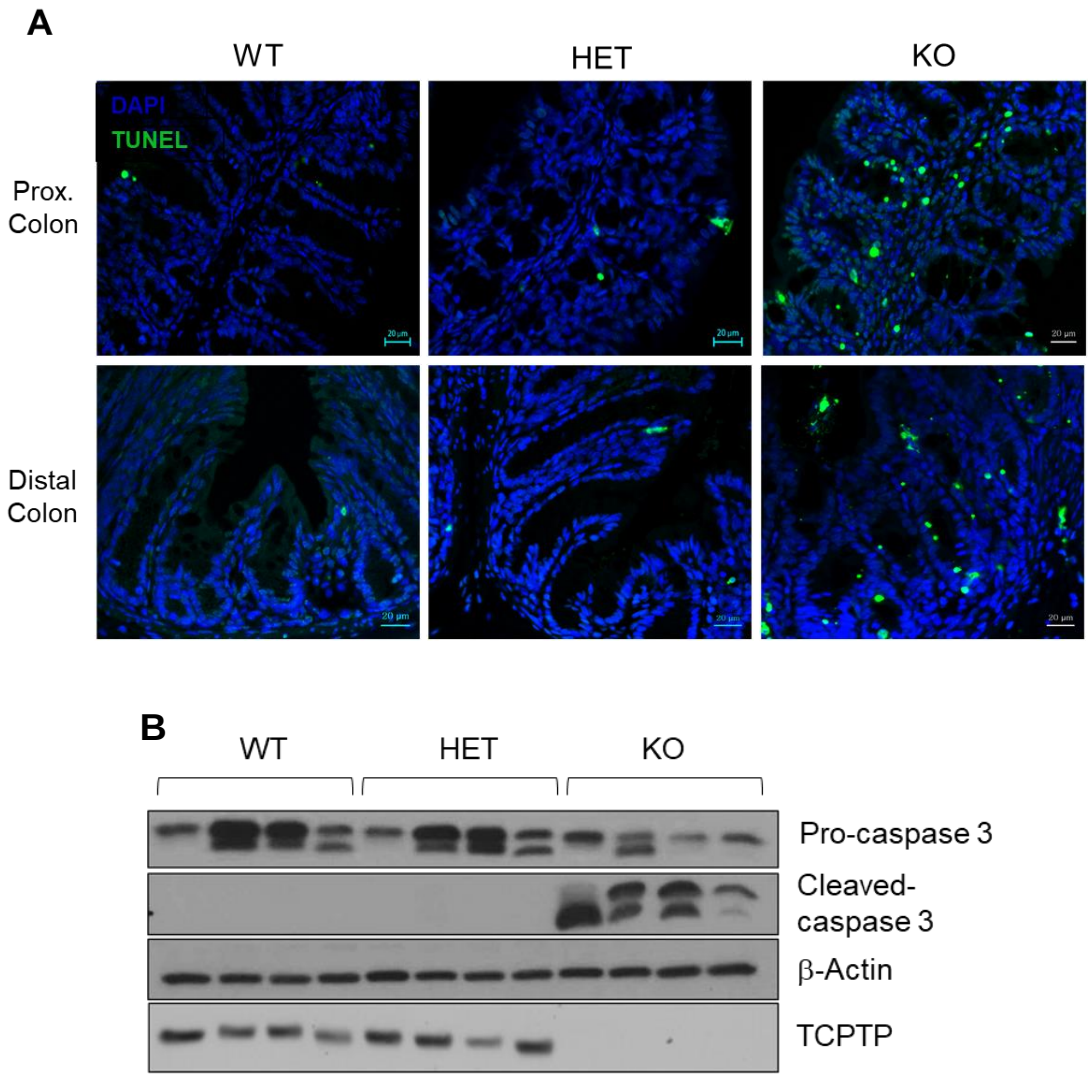

Figure 39. Colonic mucosa of whole-body *Ptpn2*-KO mice showed elevated levels of apoptotic cells. **(A)** TUNEL staining of proximal and distal colon sections showing apoptotic cells (green) and cell nuclei (blue). N=3 per group. **(B)** Western blot of colon whole-tissue lysates from constitutive *Ptpn2*-KO mice probing for pro-caspase 3 and cleaved caspase 3. Flow cytometry of colonic mucosa cells stained for immune cell types and apoptotic marker showing elevated abundance of apoptotic.

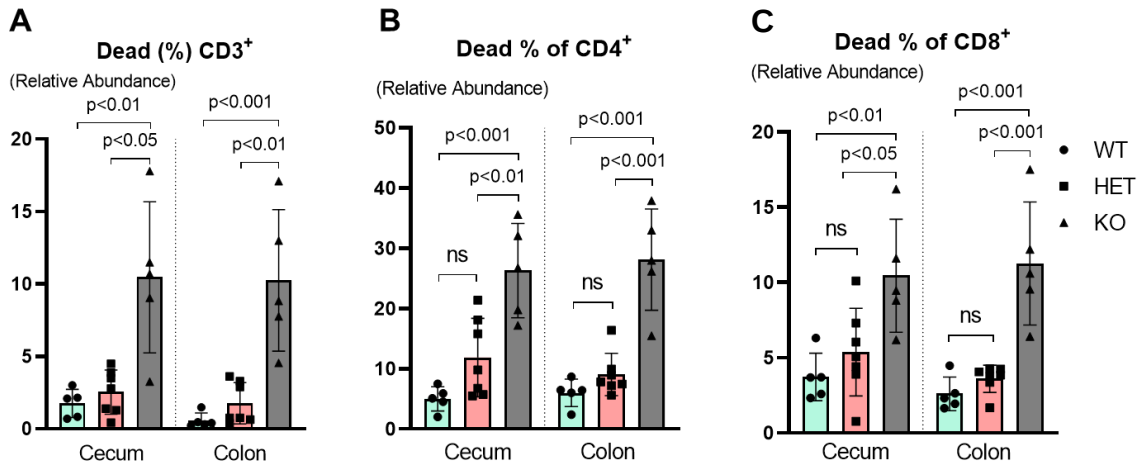

Figure 40. *Ptpn2*-KO mice have elevated levels of apoptotic immune cells in the colonic mucosa. **(A)** Lymphocytes ($CD3^+$), **(B)** T helper cells and ($CD4^+$), and **(C)** cytotoxic T cells ($CD8^+$). WT=8, HET=8, KO=8. Columns show mean ± SD. One-way ANOVA and Tukey's post hoc.

To determine if *Ptpn2* loss increased immune cell apoptosis, as observed in the small intestine (Chapter 4, Figure 27), we characterized immune cell viability in the colonic mucosa of these mice. Flow cytometric analysis identified increased proportions of dead $CD3^+$ immune cells in *Ptpn2*-KO mice and this was associated with increased numbers of dead $CD4^+$ and $CD8^+$ T-lymphocytes (Figures 40A-C). Collectively, these data identify increased activation of cell death mechanisms and a quantifiable increase in lymphocyte death in *Ptpn2*-KO mouse large intestine.

5.3.2. *The Intestinal Epithelium Shows Variable Number of Goblet Cells in Different Segments of the Intestinal Tract*

Next, to assess the number of goblet cells in the intestinal epithelium we performed Periodic-acid Schiff's (PAS) staining on four segments of the intestinal tract (ileum, cecum, proximal and distal colon). Figure 41A shows mucus-filled goblet cells identified by the magenta color and indicated by black arrows. Quantification of the goblet cells showed reduced numbers in the ileal crypt of the small intestine but not on the villi (Figures 42A-B). In the large intestine, the number of goblet cells was reduced in the cecum of *Ptpn2*-KO mice in comparison with HET mice (Figure 42C), whereas the proximal and distal colon did not show significant changes, although there was substantial variability in *Ptpn2*-KO mice (Figure 42D-E). Additionally, we observed occasional cryptitis in the distal colon of *Ptpn2*-KO mice, as indicated by red arrows on Figure 41A.

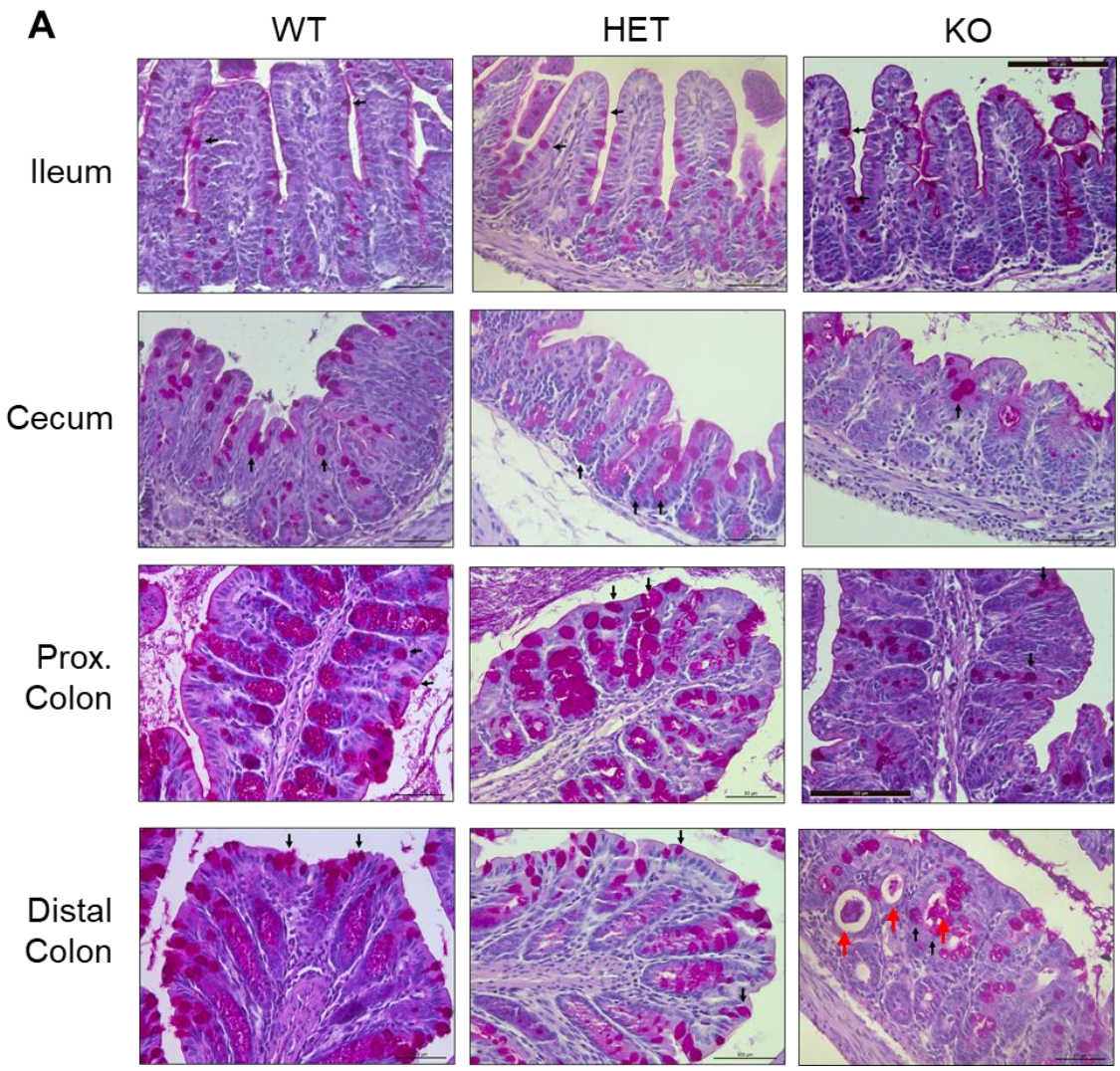

Figure 41. (A) Evaluation of goblet cell numbers in the intestinal mucosa of whole-body *Ptpn2*-deficient mice. PAS staining of ileum, cecum, proximal and distal colon from whole-body *Ptpn2*-deficient mice. Black arrows indicate mucin-filled goblet cells. Red arrows indicate cryptitis.

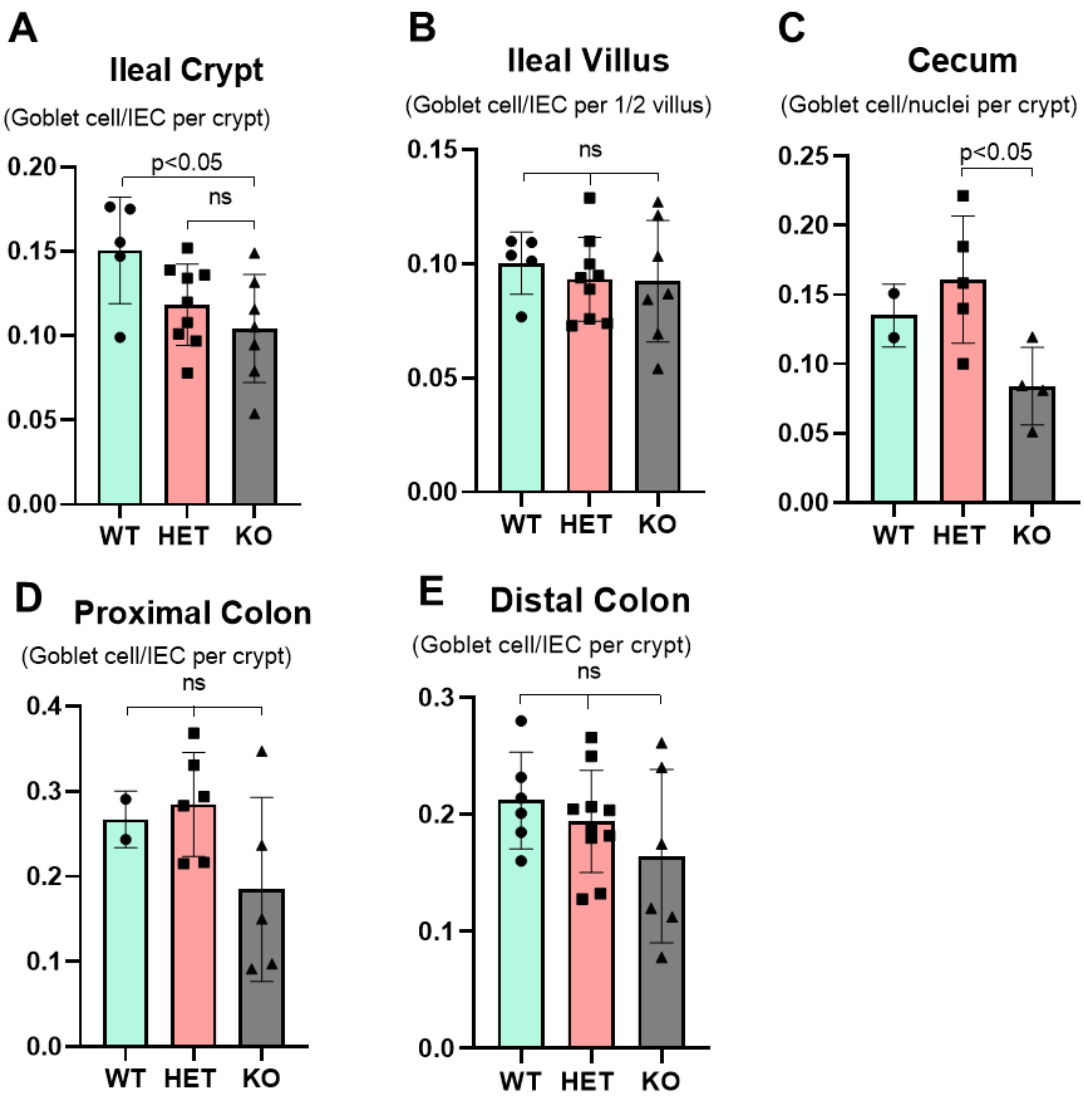

Figure 42. Quantification of intestinal goblet cells. **(A)** Quantification of ileal goblet cells found in the crypts normalized by total number of IECs per crypts. **(B)** Quantification of ileal goblet cells in the villus normalized by total number of IECs per villus. **(C)** Quantification of cecal goblet cells normalized by total number of IECs per crypt. **(D)** Quantification of proximal colon goblet cells normalized by total number of IECs per crypt. **(E)** Quantification of distal colon goblet cells normalized by total number of IECs per crypt. Columns show mean ± SD. One-way ANOVA and Tukey's post hoc.

To evaluate whether constitutive *Ptpn2*-deficiency affects the integrity and efficiency of the mucus barrier, we performed a specific tissue fixation that enables visualization of the mucus layer as described in the methods chapter. By measuring the thickness of the mucus layer, we can assess its integrity and uniformity in covering the colonic epithelium, as demonstrated in Figure 43A[110,253].

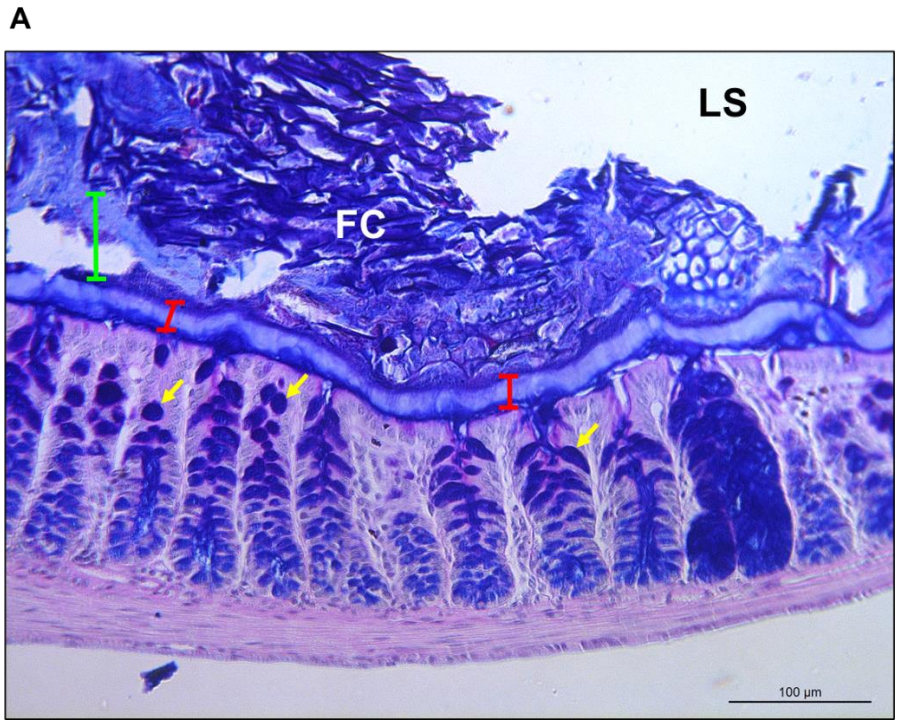

Figure 43. (A) Evaluation of the mucus layer in the distal colon of *Ptpn2*-deficient mice. Yellow arrows indicate mucin-filled goblet cells. Red bars indicate the gel-forming inner adherent mucus layer, whereas the green bar indicates the region of outer loose mucus layer. (FC)= fecal content; (LS)= luminal space. Tissue was fixed with Methacarn fixative and stained with alcian blue.

In order to determine the efficiency of the mucus barrier in preventing bacterial adherence to the epithelial lining in *Ptpn2*-KO mice (vs. WT), future studies should focus on performing fluorescent *in situ* hybridization (FISH), thereby enabling us to quantify bacterial penetrability of the mucus layer and identify differences between genotypes[25,26,29].

5.3.3. *Whole-body Ptpn2-KO Mice do not Show Gene Expression Alterations in Goblet Cell Function, Induction, or Differentiation*

Since the number of goblet cells was reduced in the ileal and cecal crypts of *Ptpn2*-KO mice, and to better understand how constitutive *Ptpn2* deficiency affects the function and differentiation of IEC subtypes, we expanded our Nanostring® transcriptome analysis to isolated IECs from the cecum and distal colon regions, as described in Chapter 2. Principal component analysis showed that cecal IECs from *Ptpn2*-KO mice do not cluster together with WT and HET samples, suggesting that the gene expression profile of *Ptpn2*-KO samples is unique, as previously observed with ileal samples (Figure 44A; red ellipse). Moreover, the same analysis revealed that the littermate effect was also present among these samples, as shown by principal components 3 and 4 (Figure 44A; yellow, purple, and maroon ellipses).

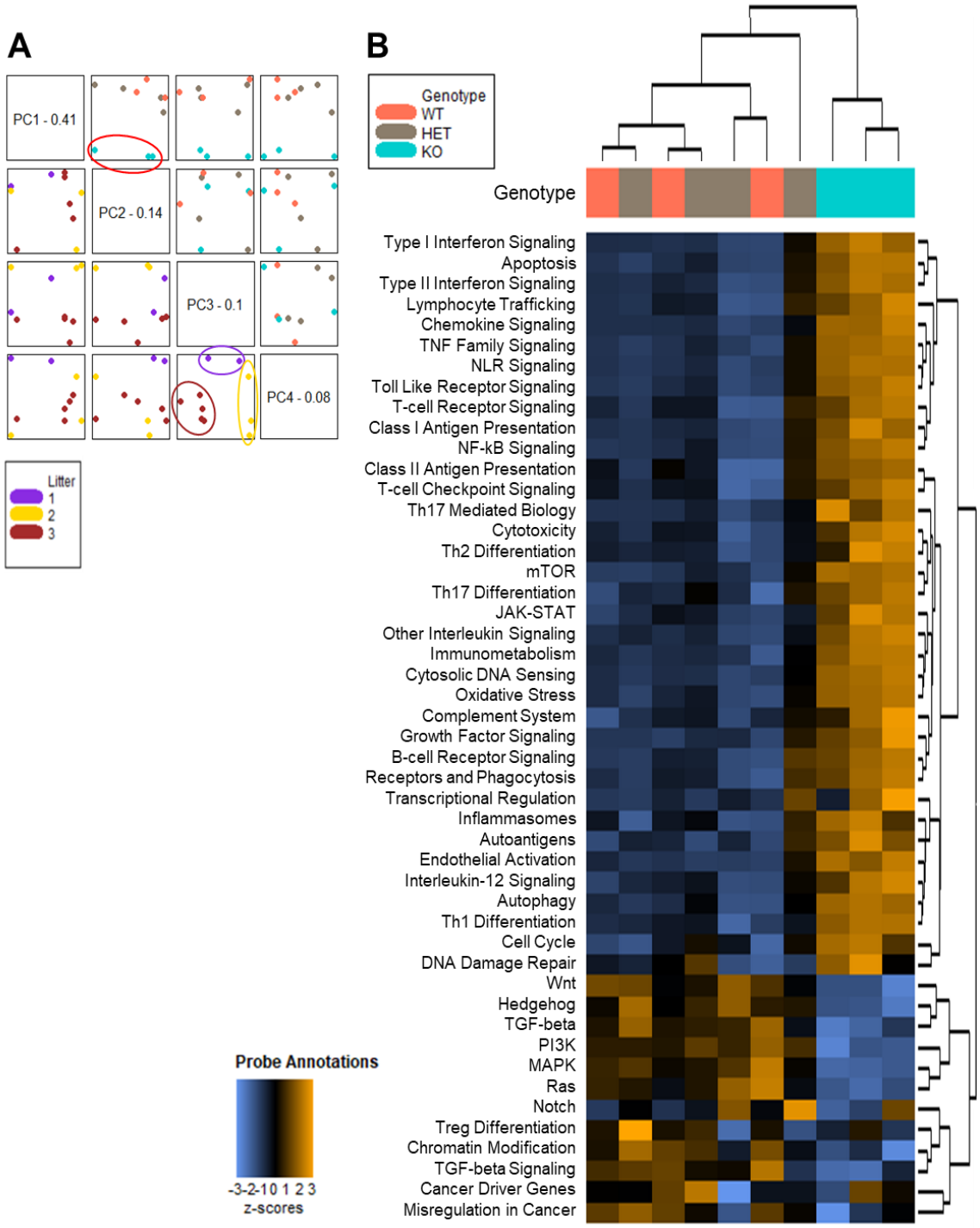
A
PC1 - 0.41
PC2 - 0.14
PC3 - 0.1
PC4 - 0.08
Litter
1
2
3
B
Genotype
WT
HET
KO
Genotype
Type I Interferon Signaling
Apoptosis
Type II Interferon Signaling
Lymphocyte Trafficking
Chemokine Signaling
TNF Family Signaling
NLR Signaling
Toll Like Receptor Signaling
T-cell Receptor Signaling
Class I Antigen Presentation
NF-kB Signaling
Class II Antigen Presentation
T-cell Checkpoint Signaling
Th17 Mediated Biology
Cytotoxicity
Th2 Differentiation
mTOR
Th17 Differentiation
JAK-STAT
Other Interleukin Signaling
Immunometabolism
Cytosolic DNA Sensing
Oxidative Stress
Complement System
Growth Factor Signaling
B-cell Receptor Signaling
Receptors and Phagocytosis
Transcriptional Regulation
Inflammasomes
Autoantigens
Endothelial Activation
Interleukin-12 Signaling
Autophagy
Th1 Differentiation
Cell Cycle
DNA Damage Repair
Wnt
Hedgehog
TGF-beta
PI3K
MAPK
Ras
Notch
Treg Differentiation
Chromatin Modification
TGF-beta Signaling
Cancer Driver Genes
Misregulation in Cancer
Probe Annotations
-3-2-10 1 2 3
z-scores

Figure 44. Partial transcriptome analysis of isolated cecal IECs by Nanostring®. Data consolidated from two different panels: 'AutoImmune Profiling' and 'PanCancer Pathways' with the addition of 60 custom targets. **(A)** Principal Component Analysis (PCA) had the upper quadrants, above the diagonal line, color-coded with the genotype of each sample indicating that gene expression of *Ptpn2*-KO mice is unique. The red ellipse indicates how data points from KO mice cluster apart from WT and HET mice. Lower quadrants were color-coded with littermates, indicating that littermates clustered together as indicated by red, purple and yellow ellipses. Data was normalized by littermates (co-housed mice) as a covariate. **(B)** Heatmap of pathway scores is a high-level overview of how the cellular pathway scores change across samples. Orange indicates high scores; blue indicates low scores. Scores are displayed in the same scale by Z-transformation. Each column represents an individual sample.

Figure 44B summarizes the overall effect of *Ptpn2* deletion on cell pathways, revealing upregulation of 37 signaling cascades and downregulation of 12. Next, Nanostring® analysis of isolated IECs from the distal colon revealed a similar overall gene expression profile between genotypes, with principal component analysis showing that *Ptpn2*-KO samples do not cluster with WT and HET samples, corresponding to an approximate 17% difference on the transcriptome profile by this covariant (Figure 45A).

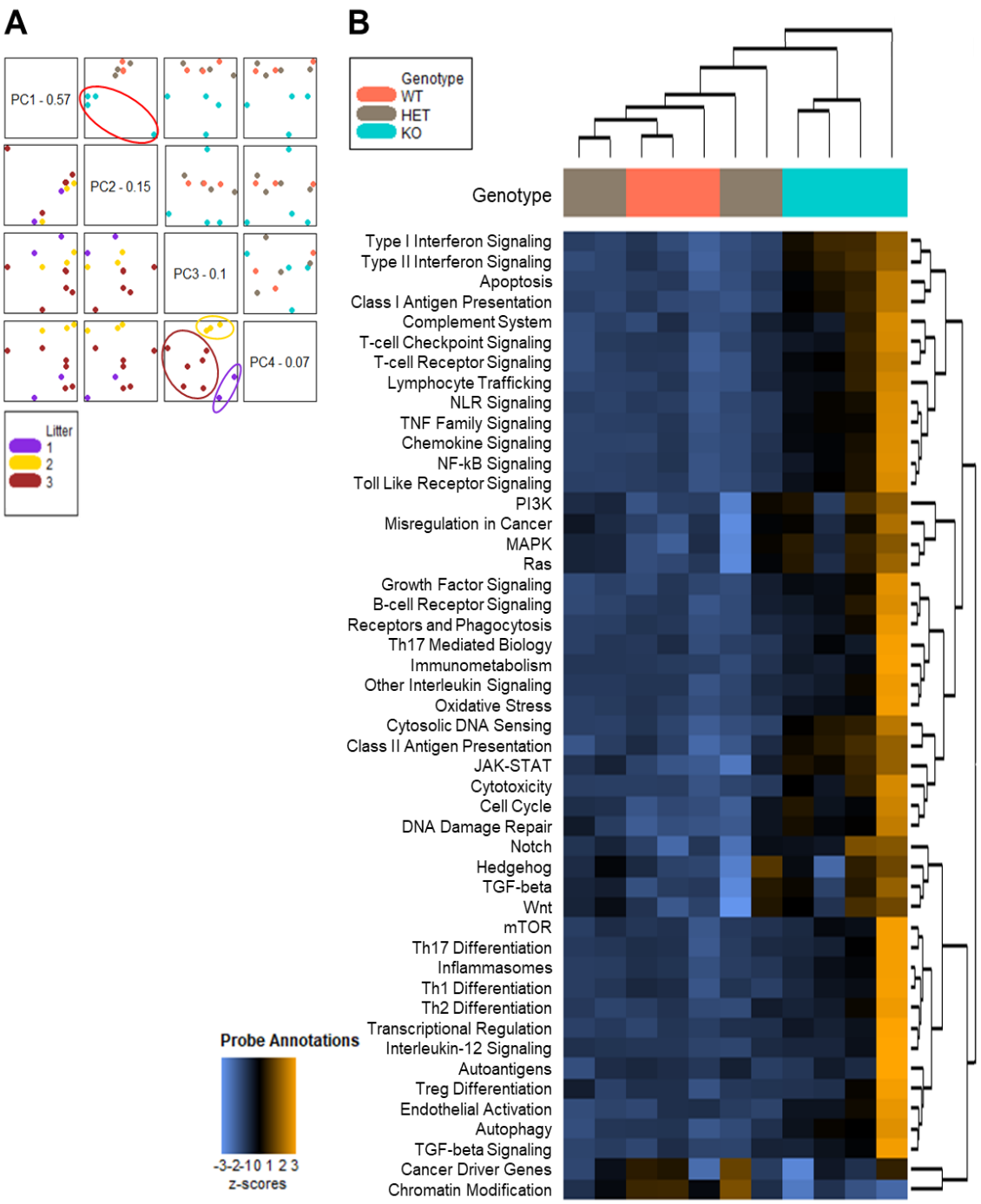
A
PC1 - 0.57
PC2 - 0.15
PC3 - 0.1
PC4 - 0.07
Litter
1
2
3
B
Genotype
WT
HET
KO
Genotype
Type I Interferon Signaling
Type II Interferon Signaling
Apoptosis
Class I Antigen Presentation
Complement System
T-cell Checkpoint Signaling
T-cell Receptor Signaling
Lymphocyte Trafficking
NLR Signaling
TNF Family Signaling
Chemokine Signaling
NF-kB Signaling
Toll Like Receptor Signaling
PI3K
Misregulation in Cancer
MAPK
Ras
Growth Factor Signaling
B-cell Receptor Signaling
Receptors and Phagocytosis
Th17 Mediated Biology
Immunometabolism
Other Interleukin Signaling
Oxidative Stress
Cytosolic DNA Sensing
Class II Antigen Presentation
JAK-STAT
Cytotoxicity
Cell Cycle
DNA Damage Repair
Notch
Hedgehog
TGF-beta
Wnt
mTOR
Th17 Differentiation
Inflammasomes
Th1 Differentiation
Th2 Differentiation
Transcriptional Regulation
Interleukin-12 Signaling
Autoantigens
Treg Differentiation
Endothelial Activation
Autophagy
TGF-beta Signaling
Cancer Driver Genes
Chromatin Modification
Probe Annotations
-3 -2 -1 0 1 2 3
z-scores

Figure 45. Partial transcriptome analysis of isolated IECs from the distal colon by Nanostring®. Data consolidated from two different panels: 'AutoImmune Profiling' and 'PanCancer Pathways' with the addition of 60 custom targets. **(A)** Principal Component Analysis (PCA) had the upper quadrants, above the diagonal line, color-coded with the genotype of each sample indicating that gene expression of *Ptpn2*-KO mice is unique. The red ellipse indicates how data points from KO mice cluster apart from WT and HET mice. Lower quadrants were color-coded with littermates, indicating that littermates clustered together as indicated by red, purple and yellow ellipses. Data was normalized by littermates (co-housed mice) as a covariate. **(B)** Heatmap of pathway scores is a high-level overview of how the cellular pathway scores change across samples. Orange indicates high scores; blue indicates low scores. Scores are displayed in the same scale by Z-transformation. Each column represents an individual sample.

Figure 46A shows the differential expression of goblet cell-associated genes from the intestinal segments analyzed (ileum, cecum, and distal colon). Unexpectedly, apart from *Atoh1*, an early secretory cell lineage differentiation factor found downregulated in the distal colon, no other genes associated with goblet cell function (*Muc2* and *Muc5b*) or associated with maturation/differentiation of goblet cells (*Spdef*, *Hes1*, *Elf3*, *Cdh1*, and *Klf4*) were altered. Furthermore, when analyzing the expression of cytokines and their receptors that reportedly induce goblet cell function, no significant differences were found.

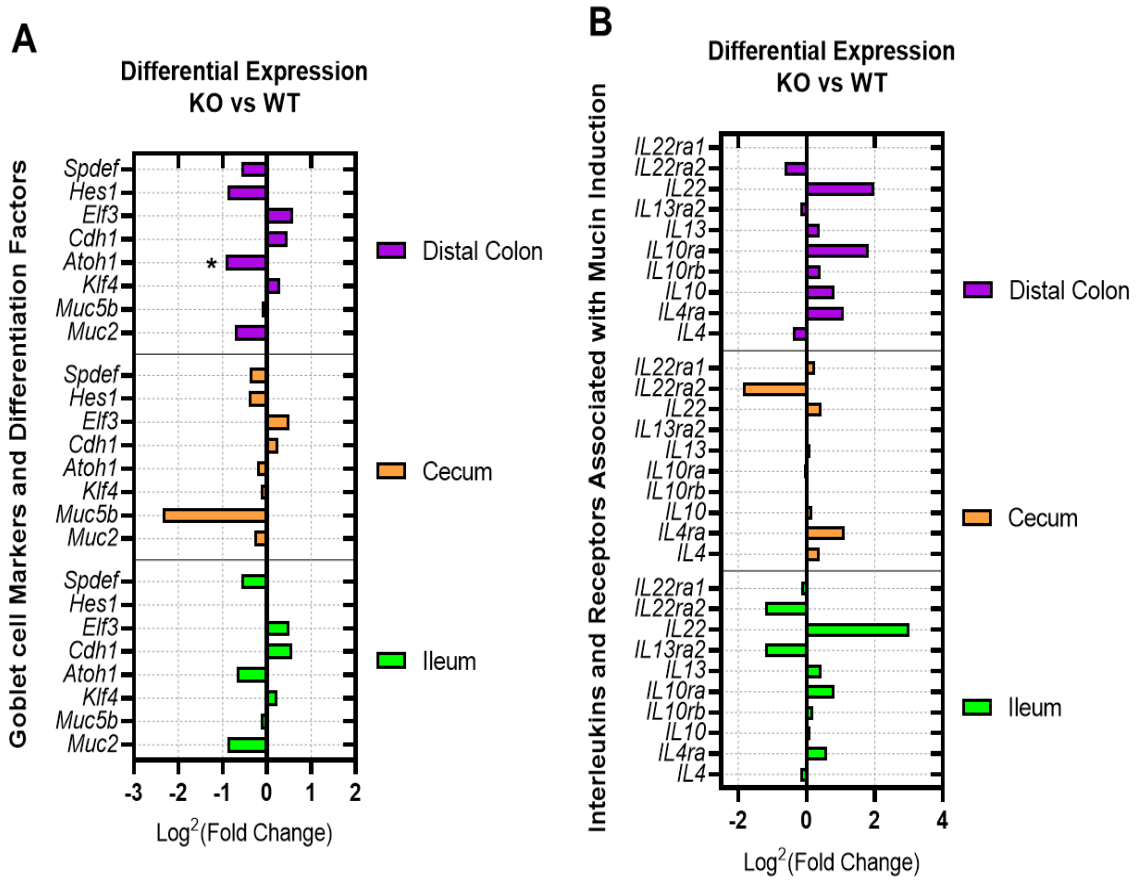

Figure 46. Differential expression of goblet cell-associated differentiation and stimulatory factors from ileum, cecum, and distal colon. **(A)** KO vs. WT differential expression of goblet cell-associated differentiation factors epithelial markers, differentiation factors and function. WT=3, HET=3, KO=4. (*) Indicates targets statistically significant (α <0.05; FDR <0.1). **(B)** Differential expression of goblet cell-stimulatory cytokines and their receptors (KO vs. WT); (*) Indicates targets statistically significant (α <0.05; FDR <0.1).

5.3.4. *IECs from the Distal Colon of Ptpn2-KO Mice Have Decreased Expression of Intestinal Stem Cell and Tuft Cell Markers*

Further analysis of the Nanostring® dataset from cecal and distal colon IECs, revealed that expression of the intestinal stem cell marker *Lgr5*, and expression of the tuft cell marker *Dclk1* were significantly downregulated in the distal colon but not in the cecum (Figures 47A-B).

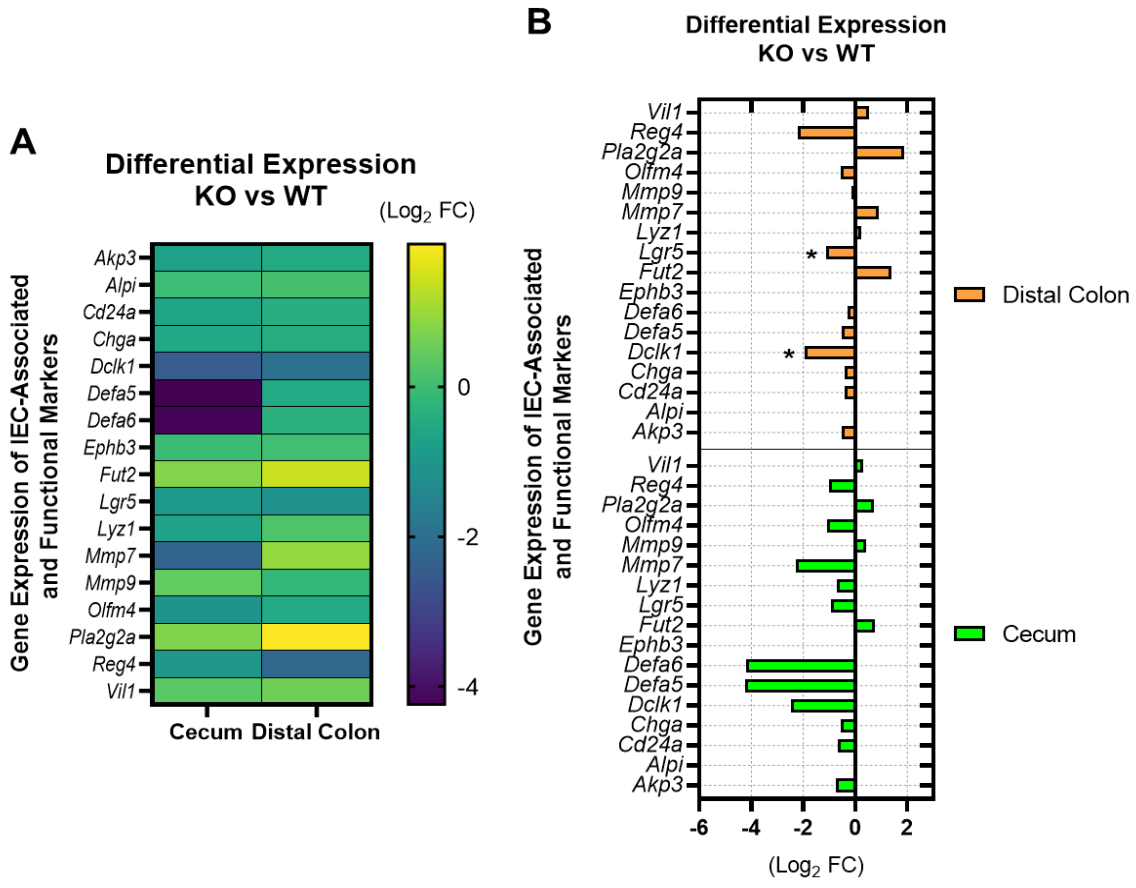

Figure 47. Differential gene expression of IEC-associated and functional markers from cecum and distal colon isolated IECs. **(A)** Heatmap differential gene expression contrasting the FC differences cecum and distal colon. **(B)** Bar representation of gene fold change (FC) where (*) indicates targets statistically significant (α <0.05; FDR <0.1).

Figure 48 lists the genes included in our analysis that reportedly play a role in IEC differentiation. In the cecum, only the expression of *Sfrp1*, which encodes secreted frizzled related protein 1, was upregulated (Figure 48A).

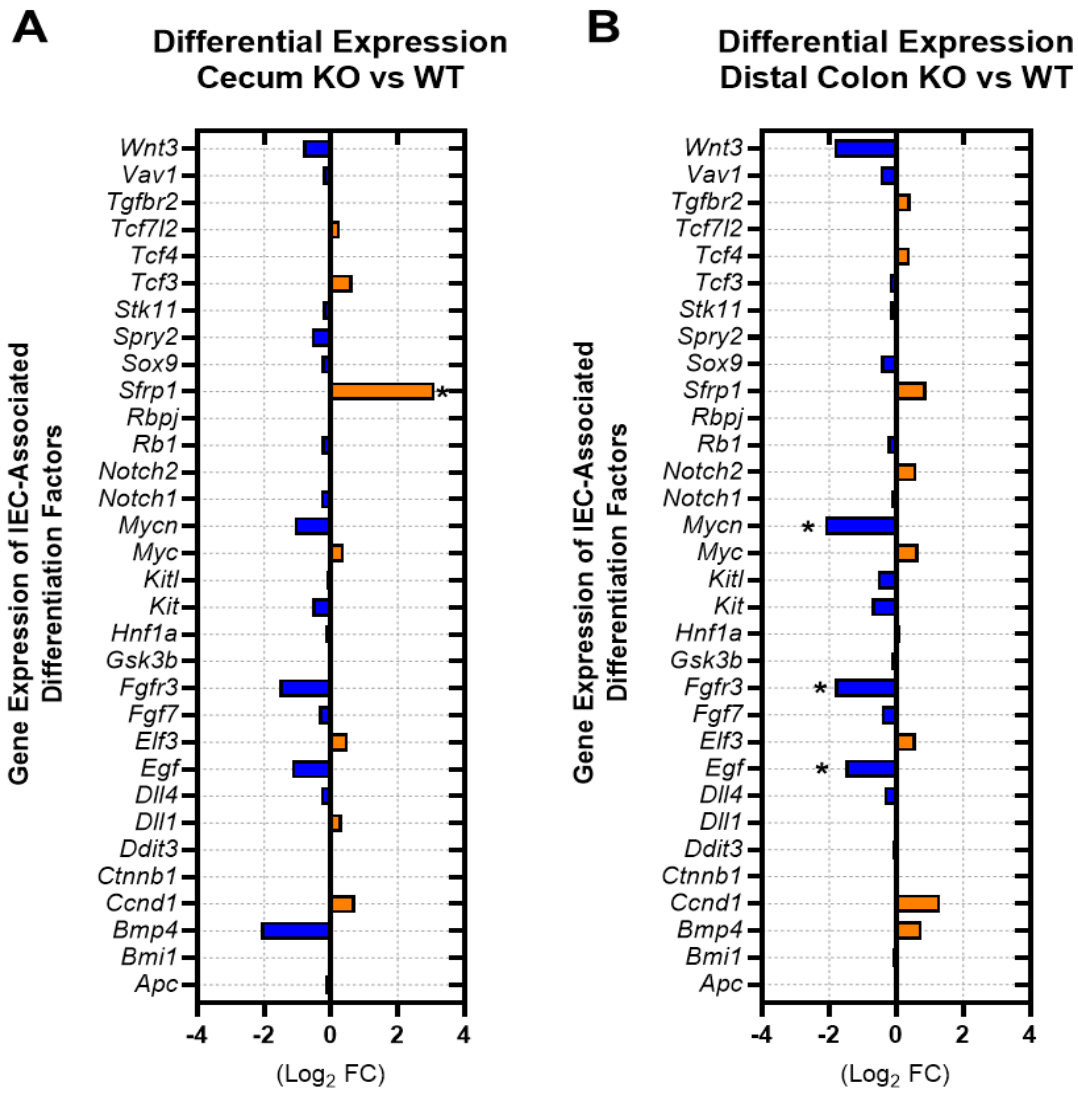

Figure 48. Differential expression of IEC differentiation factors. (A) Isolated Cecal IECs, and (B) isolated distal colon IECs. (*) Indicates targets statistically significant (α <0.05; FDR <0.1).

In contrast, colonic expression of intestinal stem cell-associated genes, *Egf*, *Fgfr3*, and *Mycn*, were downregulated (Figure 48B). This suggests, along with downregulation of *Lgr5* shown in Figure 47A, that numbers and/or activity of the fast-cycling intestinal stem cells could be impaired in the distal colon of *Ptpn2*-KO mice.

5.3.5. *Large Intestinal Mucosa of Ptpn2-KO Mice Have Elevated Abundance of Immune Cells and Immune Cell-derived Pro-Inflammatory Cytokines*

Because whole-body *Ptpn2*-KO mice failed to induce hyperproliferation and activity of goblet cells, we sought to determine whether the cecal and colonic mucosa of these mice have immune cell-derived cytokines that modulate goblet cell activity. Flow cytometry analysis revealed increased abundance of neutrophils, macrophages, and TNF-α/IFN-γ expressing cytotoxic ($CD8^+$) and T helper ($CD4^+$) cells in the cecal and colonic mucosa of *Ptpn2*-KO mice in comparison with WT and HET mice (Figures 49A-D). Moreover, the abundance of $CD4^+$ T-cells positive for IFN-γ and IL-22 was also elevated (Figures 49C and E). These data indicate that the ileal mucosa

contains abundant immune cells that express cytokines during tissue inflammation.

Conversely, abundance of ileal $CD4^+$ T-cells primed to express IL-4, a cytokine reported to induce goblet cell hyperplasia and secretion of effector molecules[248], was decreased in *Ptpn2*-KO mice in comparison with HET (Figure 49F), while a more robust IL-4 reduction of $CD4^+$ T-cells was found in the colon of KO mice compared with WT and HET mice, whereas no change was detected in the cecum. Furthermore, abundance of Tregs primed to express IL-10, an anti-inflammatory cytokine that contributes to proper goblet cell function, was decreased in *Ptpn2*-KO mice in all intestinal segments analyzed (Figure 49G).

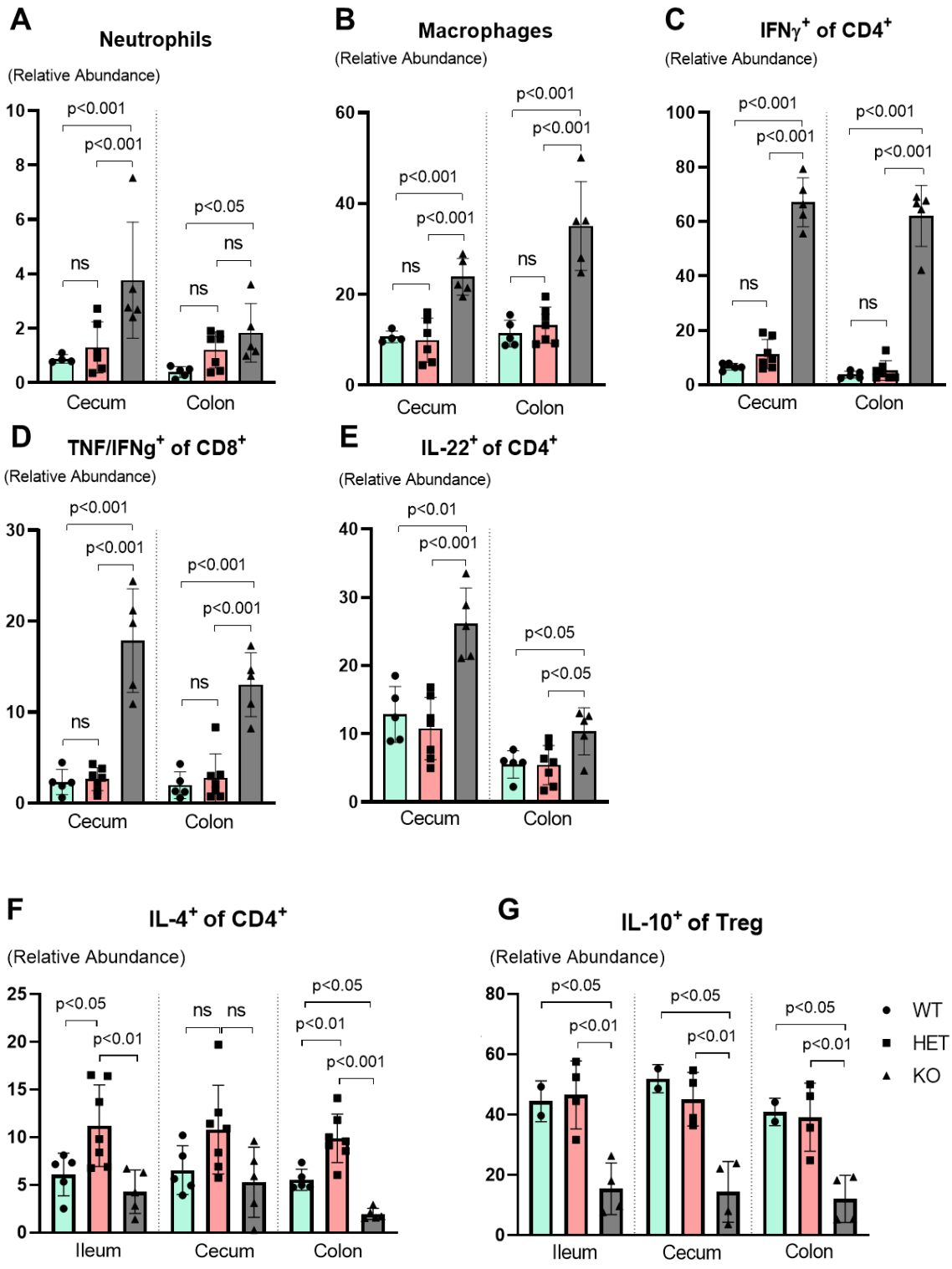
A
Neutrophils
(Relative Abundance)
p<0.001
p<0.001
ns
p<0.05
ns
ns
Cecum
Colon
B
Macrophages
(Relative Abundance)
p<0.001
p<0.001
p<0.001
p<0.001
ns
ns
Cecum
Colon
C
IFNγ+ of CD4+
(Relative Abundance)
p<0.001
p<0.001
p<0.001
p<0.001
ns
ns
Cecum
Colon
D
TNF/IFNg+ of CD8+
(Relative Abundance)
p<0.001
p<0.001
p<0.001
p<0.001
ns
ns
Cecum
Colon
E
IL-22+ of CD4+
(Relative Abundance)
p<0.01
p<0.001
p<0.05
p<0.05
Cecum
Colon
F
IL-4+ of CD4+
(Relative Abundance)
p<0.05
p<0.01
ns ns
p<0.05
p<0.01
p<0.001
Ileum
Cecum
Colon
G
IL-10+ of Treg
(Relative Abundance)
p<0.05
p<0.01
p<0.05
p<0.01
p<0.05
p<0.01
Ileum
Cecum
Colon
WT
HET
KO

Figure 49. Flow cytometry of immune cells in the cecal and colonic mucosa stained for immune cell types and pro-inflammatory cytokines upon stimulation. **(A)** Relative abundance of neutrophils. **(B)** Relative abundance of macrophages. **(C)** Relative abundance of T helper cells ($CD4^+$) positive for IFN-γ. **(D)** Relative abundance of cytotoxic cells ($CD8^+$) positive for TNF and IFN-γ. **(E)** Relative abundance of T helper cells ($CD4^+$) positive for IL-22. **(F)** Relative abundance of T helper cells ($CD4^+$) positive for IL-4. **(G)** Relative abundance of Tregs positive for IL-10. All columns show mean ± SD. One-way ANOVA and Tukey's post hoc.

5.4. Discussion

Here we showed that constitutive *Ptpn2*-deletion negatively affects the number of goblet cells in the ileal and cecal crypts of mice. Regarding the proximal and distal colon segments, we did not detect significant changes in the number of goblet cells, although there was great variability between samples, and even between regions of the same tissue section, suggesting that these effects could be region-specific. Furthermore, we detected cryptitis in several regions of the distal colon, showing an ongoing and disease-relevant inflammatory process within the crypts. However, this impairment in the number of goblet cells was not accompanied by a diminished expression of *Muc2* nor *Muc5b*. Thus, it is possible that the remaining goblet cells were able to increase gene transcription to compensate for the reduction in the number of goblet cells. In line with this, it has been reported that in transgenic mice with nearly 60% of colonic goblet cells depletion, the expression of *Muc2* mRNA was comparable to those of control mice, suggesting that the remaining goblet cells were able to compensate for the deficit in the number of cells[254]. However, evidence that this transcriptional compensation results in higher protein synthesis is still missing.

Similar to our observations in the ileum, we found elevated numbers of proliferating cells in the proximal and distal colon of *Ptpn2*-KO mice that was accompanied by increased crypt length in the cecum and proximal colon, suggesting that there are dynamic changes occurring in the IECs. Also, we reported that there is increased apoptosis activation along with elevated DNA fragmentation in the intestinal mucosa of the proximal and distal colon of *Ptpn2*-KO mice. While we could not distinguish the identity of the cells undergoing apoptosis through TUNEL staining, flow cytometry data showed increased apoptotic immune cells in the colonic mucosa. Despite the presence of apoptotic immune cells, and possibly IECs, previous studies by our group showed that *Ptpn2*-KO mice had not increase in unrestricted intestinal permeability, a physiological feature that occurs when epithelial damage is present. This suggests that our findings could be associated with a more rapid turnover of the colonic epithelium without causing breaches in the epithelial barrier even though the level of apoptosis is higher in *Ptpn2*-KO mice compared with WT and HET[36,143].

Patients with ulcerative colitis (UC) display a defective mucus layer associated with reduced number of goblet cells in the colon[103,110,253]. However, the underlying mechanisms of this pathophysiological feature and

its potential causal role in inflammation is poorly understood. For instance, the UC phenotype has been replicated in UC-derived organoids, forming a thin and non-continuous mucus layer compared with healthy subject-derived organoids even in the absence of a pro-inflammatory environment[255]. Additionally, patients with CD normally display enhanced goblet cell differentiation and a thicker mucus layer in the colon despite the elevated inflammatory status[256]. Of note, germ-free mice have been reported to show fewer and smaller goblet cells with a thinner colonic mucus layer[77,256]. However, when the intestinal microbiota is reconstituted, the activity of goblet cells increases generating a normal mucus layer, which is thought to be mediated by a variety of pro-inflammatory cytokines[257]. The consensus is that both inflammatory cytokines and gut microbiota are essential for proper goblet cell function and mucus layer assembly, albeit by unknown mechanisms.

In vitro studies using different cell lineages have shown that several pro-inflammatory cytokines stimulate synthesis and secretion of mucin proteins, such as IL-1, IL-6 and TNF-α[77]. IFN-γ has been shown to stimulate goblet cell secretion but without inducing expression of mucin proteins[258]. However, even though there was increased levels of circulating IFN-γ and

TNF-α, in addition to elevated levels of mucosal IFN-γ, TNF-α, and IL-6 in the colon of *Ptpn2*-KO mice[143], expression of *Muc2* and *Muc5b* were unchanged.

Conversely, studies with helminth infections have shown that goblet cells display a remarkable response to type 2 inflammation signaling, mainly driven by IL-4 and IL-13[248]. In our study, we showed that expression of cytokine receptors associated with type 2 inflammatory response was unchanged in IECs, suggesting that IECs were not functionally uncoupled from cytokine stimulation, at least at the gene expression level. However, flow cytometry data showed that the abundance of IL-4 in $CD4^+$ T-helper cells was decreased in the ileal and colonic mucosa of *Ptpn2*-KO mice. Interestingly, lack of IL-4 stimulation also affected macrophage differentiation, favoring the development of inflammation-promoting M1-like macrophages, and a corresponding decrease in anti-inflammatory M2-like macrophages in whole-body *Ptpn2*-KO mice[36,143].

With respect to an additional member of the epithelial secretory lineage, we also identified that expression of the tuft cell marker *Dclk1*, was downregulated in the distal colon of *Ptpn2*-KO mice, whereas in the other intestinal segments this downregulation fell short of statistical significance.

During helminth infection, tuft cell-derived IL-25 activates innate lymphoid cell type 2 (ILC2) to secrete IL-13, which promotes differentiation of transit-amplifying cells into tuft and goblet cells[89]. In addition, tuft cell induction of a type 2 immune response leads to goblet cell hyperplasia and smooth muscle hypercontractility, a mechanism best known as 'sweep and weep' that promotes parasite expulsion[88,259]. Although these investigations were performed with helminth infections, it is unclear what role these cytokines exert on goblet cells during intestinal inflammation. Since the function of tuft cells is intrinsically connected with that of goblet cells, it would be of interest to investigate whether the lack of goblet cell stimulation could be associated with functionally deficient tuft cells.

Another notable finding was that the abundance of anti-inflammatory IL-10^{+} Tregs was decreased in all intestinal segments. IL-10 plays a direct role on goblet cell activity by decreasing ER stress in these cells, modulating mucin protein synthesis and misfolding[250]. Moreover, decreased Muc2 levels have been observed in *Il10*$^{-/-}$ mice while the colonic mucus layer is penetrable by bacteria-size beads[113,260]. This is relevant to our study since IL-10 was able to rescue proper Muc2 folding and secretion in a mouse model with a *Muc2* missense mutation that results in ER stress and spontaneous chronic

colitis[261]. Since we demonstrated that Paneth cells display disrupted ER, and *Ptpn2*$^{\Delta IEC}$ mice have shown elevated levels of the unfolded protein response marker, it is reasonable to consider that the failure in induction of *Muc2* expression could be associated with ER stress. Consistent with this, it has been reported that DSS-induced colitis results in goblet cell hypersecretion accompanied by ER stress and apoptosis of goblet cells that precedes epithelial damage[249]. Furthermore, specific *Xbp1* deletion in IECs of mice, led to nearly 30% reduction in the number of ileal goblet cells, indicating that goblet cells are susceptible to ER stress and that is detrimental to goblet cell viability[228].

Finally, the expression of goblet cell-associated differentiation factors was unchanged, suggesting that the reduction in the number of goblet cells is not due to a lack of differentiation factors associated with this cell lineage. Conversely, expression of the intestinal stem cell marker *Lgr5*, and intestinal stem cell factors *Egf*, *Mycn*, and *Fgfr3* were downregulated, indicating that the number and/or activity of rapid-cycling intestinal stem cells could be affected in the distal colon of *Ptpn2*-KO mice.

6. Conclusion

6.1. Summary

This dissertation has demonstrated that indeed constitutive *Ptpn2* function is critical for the maintenance of IECs homeostasis. Whole-body *Ptpn2* deletion showed a higher proliferative intestinal epithelium, accompanied with morphological changes, and increased activation of the apoptosis pathway in the immune cells of the intestinal mucosa. The elevated abundance of immune cells present in the intestinal mucosa, contributes to the pro-inflammatory environment, with immune cells primed to secrete TNF-α, IFN-γ, and IL-22. Despite these phenotypical alterations, the intestinal epithelium remained intact without major breaches in the intestinal epithelial lining, suggesting that the changes reported above occur in an orchestrated manner that does not cause a critical failure in the gut barrier. This is supported by previous studies demonstrating that *Ptpn2*-KO mice do not display changes in intestinal permeability mediated by the unrestricted pathway[144].

Nevertheless, we observed phenotypical alterations at the IEC subtype level. This was more pronounced in the distal ileum, where the number of Paneth cells and the production of Paneth cell-specific AMPs were markedly

reduced. Thus, this study identifies a possible mechanism that contributes to gut dysbiosis of constitutive *Ptpn2*-deficient mice, which in turn leads to expansion of a disease-relevant *m*AIEC and immune-cell activation.

In addition, I demonstrated that the number of goblet cells is impaired in a region-specific manner in *Ptpn2*-KO mice. Given the elevated pro-inflammatory profile of the intestinal mucosa in these mice, it is surprising that expression of *Muc2* was not induced. In line with this, decreased abundance of immune cell-derived IL-4 and IL-10 were found in the colonic mucosa. However, it remains to be determined whether this potential lack of goblet cell stimuli is sufficient to cause an impairment in the mucosal barrier that would facilitate bacterial penetration.

6.2. Future studies

Our findings regarding Paneth cell phenotypes in mice with constitutive *Ptpn2* loss leave two major lingering questions. First, are the phenotypical changes observed in Paneth cells a result of the inflammatory status of the intestinal mucosa, or a direct effect of *Ptptn2* loss? We began to address this question using the inducible-specific *Ptpn2* deletion in IECs, which showed that despite no change in Paneth cell numbers, the abundance of

antimicrobial lysozyme protein was impaired. Additionally, we detected higher levels of the unfolded protein response Xbp-1s in *Ptpn2*$^{\Delta IEC}$ mice. Therefore, it seems that impairment in Paneth cell function begins before mucosal inflammation is established. To test this hypothesis, we plan to challenge *Ptpn2*$^{fl/fl}$ and *Ptpn2*$^{\Delta IEC}$ mice with a series of Paneth cell-stimulatory factors, such as: LPS (gavaged), cytokines IFN-γ, IL-22, and a combination of IFN-γ+IL-22 that can be administered intraperitoneally. By doing so, we can evaluate whether impairment in function and number of Paneth cells is aggravated by these inflammatory molecules. For this investigation, we will expand the number of readouts of Paneth cell function in the *Ptpn2*$^{\Delta IEC}$ mice and evaluate expression of other Paneth cell-specific markers and AMPs (*Defa1*, *Defa5*, *Defa6*, *Mmp7*, *Pla2g2a*). Additionally, we can extend our transmission electron microscopy analysis to evaluate the dense core vesicles and ER structure in these mice after challenge.

The other major question is: what causes the depletion of Paneth cells in constitutive *Ptpn2* mice? Is this due to Paneth cell death (apoptosis, necroptosis, CHOP-driven cell death), or to a deficient differentiation process? To begin answering this question, we will investigate the number and function of Paneth cells using constitutive *Ptpn2*-derived enteroids. This

will allow us to compare the development of Paneth cells in enteroids derived from *Ptpn2*-WT and *Ptpn2*-KO mice in an inflammation-free setting. Then, by challenging the enteroids with the same Paneth cell-stimulatory molecules described above, we can assess how Paneth cell-enriched enteroids behave under those conditions.

The investigation of goblet cell function must be expanded and completed in several areas: (a) increase the sample size for goblet cell counting, particularly in the WT group; (b) morphological analysis and characterization of the mucus layer in the colon; (c) perform fluorescent *in situ* hybridization to detect bacterial penetration of the mucus layer and intestinal mucosa; (d) evaluate gene expression and cytokine levels in the intestinal mucosa of goblet cell-stimulatory factors, such as IL-4, IL-5, IL-9, IL-10, and IL-13; and (e) further characterize the number and function of tuft cells in the colon of *Ptpn2*-KO mice and identify if this contributes to goblet cell function. Once a more comprehensive characterization of the mucus layer/goblet cell function is complete, then we can develop experiments with mechanistic approaches to better understand how *Ptpn2* loss contributes to impaired mucus layer/goblet cell function at the molecular level. This could potentially include studies with the JAK

inhibitor, tofacitinib, which we have shown can reverse JAK-STAT-mediated processes that are elevated in *PTPN2*-deficient *in vitro* and *in vivo* models.

6.3. Conclusions

Figure 50 summarizes the working concept of this dissertation, showing that *Ptpn2* is a critical regulator of IEC subtypes in mice and how loss of *Ptpn2* contributes to impaired intestinal homeostasis. Further, this investigation makes a substantial contribution to our understanding of how *PTPN2* loss-of-function contributes to higher susceptibility to bacterial infection.

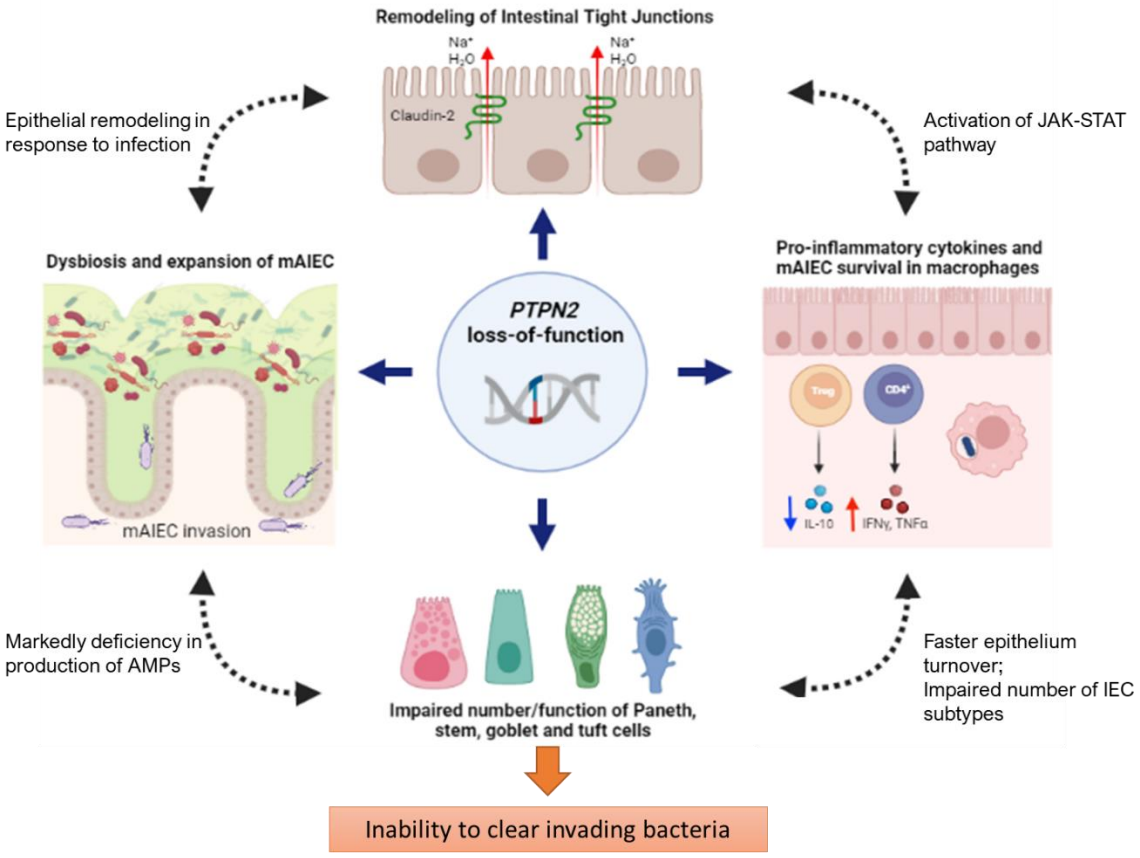

Figure 50. *PTPN2* loss-of-function results in impaired number and function of intestinal epithelial cell subtypes, contributing to elevated susceptibility to infection.

References

1. Marchiando AM, Graham WV, Turner JR. Epithelial barriers in homeostasis and disease. *Annu Rev Pathol Mech Dis*. 2010;5:119-144. doi:10.1146/annurev.pathol.4.110807.092135

2. Peled JU, Hanash AM, Jenq RR. Role of the intestinal mucosa in acute gastrointestinal GVHD. *Hematology*. 2016;2016(1):119-127. doi:10.1182/asheducation-2016.1.119

3. Ley RE, Peterson DA, Gordon JI. Ecological and evolutionary forces shaping microbial diversity in the human intestine. *Cell*. 2006;124(4):837-848. doi:10.1016/j.cell.2006.02.017

4. Maynard CL, Elson CO, Hatton RD, Weaver CT. Reciprocal interactions of the intestinal microbiota and immune system. *Nature*. 2012;489(7415):231-241. doi:10.1038/nature11551

5. Okumura R, Takeda K. Roles of intestinal epithelial cells in the maintenance of gut homeostasis. *Exp Mol Med*. 2017;49(5):338. doi:10.1038/emm.2017.20

6. Edelblum KL, Turner JR. Epithelial Cells: Structure, Transport, and Barrier Function. Structure, Transport, and Barrier Function. In: *Mucosal Immunology: Fourth Edition*. Vol 1-2. ; 2015:187-210. doi:10.1016/B978-0-12-415847-4.00012-4

7. Eroschenko VP. *Atlas of Histology with Functional Correlations*. 11th ed. Wolters Kluwer Health/Lippincott Williams & Wilkins; 2008. Accessed August 20, 2021. http://medcontent.metapress.com/index/A65RM03P4874243N.pdf

8. Miller TL, Wolin MJ. Pathways of acetate, propionate, and butyrate formation by the human fecal microbial flora. *Appl Environ Microbiol*. 1996;62(5):1589-1592. doi:10.1128/AEM.62.5.1589-1592.1996

9. Turner JR. Intestinal mucosal barrier function in health and disease. *Nat Rev Immunol*. 2009;9(11):799–809. doi:10.1038/nri2653

10. Cario E, Gerken G, Podolsky DK. Toll-like receptor 2 enhances ZO-1-associated intestinal epithelial barrier integrity via protein kinase C. *Gastroenterology*. 2004;127(1):224-238. doi:10.1053/j.gastro.2004.04.015

11. Fitzgerald KA, Kagan JC. Toll-like Receptors and the Control of Immunity. *Cell*. 2020;180(6):1044-1066. doi:10.1016/j.cell.2020.02.041

12. Rakoff-Nahoum S, Paglino J, Eslami-Varzaneh F, Edberg S, Medzhitov R. Recognition of commensal microflora by toll-like receptors is required for intestinal homeostasis. *Cell*. 2004;118(2):229-241. doi:10.1016/j.cell.2004.07.002

13. Nenci A, Becker C, Wullaert A, et al. Epithelial NEMO links innate immunity to chronic intestinal inflammation. *Nat 2006 4467135*. 2007;446(7135):557-561. doi:10.1038/nature05698

14. Greten FR, Eckmann L, Greten TF, et al. IKKβ Links Inflammation and Tumorigenesis in a Mouse Model of Colitis-Associated Cancer. *Cell*. 2004;118(3):285-296. doi:10.1016/J.CELL.2004.07.013

15. Philpott DJ, Sorbara MT, Robertson SJ, Croitoru K, Girardin SE. NOD proteins: Regulators of inflammation in health and disease. *Nat Rev Immunol*. 2014;14(1):9-23. doi:10.1038/nri3565

16. Hugot JP, Chamaillard M, Zouali H, et al. Association of NOD2 leucine-rich repeat variants with susceptibility to Crohn's disease. *Nature*. 2001;411(6837):599-603. doi:10.1038/35079107

17. Ogura Y, Bonen DK, Inohara N, et al. A frameshift mutation in NOD2 associated with susceptibility to Crohn's disease. *Nature*. 2001;411(6837):603-606. doi:10.1038/35079114

18. Balasubramanian I, Gao N. From sensing to shaping microbiota: Insights into the role of NOD2 in intestinal homeostasis and progression of crohn's disease. *Am J Physiol - Gastrointest Liver Physiol*. 2017;313(1):G7-G13. doi:10.1152/ajpgi.00330.2016

19. Cooney R, Baker J, Brain O, et al. NOD2 stimulation induces autophagy in dendritic cells influencing bacterial handling and antigen presentation. *Nat Med*. 2010;16(1):90-97. doi:10.1038/nm.2069

20. Duerr CU, Salzman NH, Dupont A, et al. Control of intestinal Nod2-mediated peptidoglycan recognition by epithelium-associated lymphocytes. *Mucosal Immunol*. 2011;4(3):325-334. doi:10.1038/mi.2010.71

21. Marcobal A, Southwick AM, Earle KA, Sonnenburg JL. A refined palate: Bacterial consumption of host glycans in the gut. *Glycobiology*. 2013;23(9):1038-1046. doi:10.1093/glycob/cwt040

22. McGuckin MA, Lindén SK, Sutton P, Florin TH. Mucin dynamics and enteric pathogens. *Nat Rev Microbiol*. 2011;9(4):265-278. doi:10.1038/nrmicro2538

23. Corfield AP. Mucins: A biologically relevant glycan barrier in mucosal protection. *Biochim Biophys Acta - Gen Subj*. 2015;1850(1):236-252. doi:10.1016/j.bbagen.2014.05.003

24. Johansson MEV, Hansson GC. Immunological aspects of intestinal mucus and mucins. *Nat Rev Immunol*. 2016;16(10):639-649. doi:10.1038/nri.2016.88

25. Van Der Waaij LA, Harmsen HJM, Madjipour M, et al. Bacterial population analysis of human colon and terminal ileum biopsies with 16S rRNA-based fluorescent probes: Commensal bacteria live in suspension and have no direct contact with epithelial cells. *Inflamm Bowel Dis*. 2005;11(10):865-871. doi:10.1097/01.mib.0000179212.80778.d3

26. Ermund A, Schütte A, Johansson MEV, Gustafsson JK, Hansson GC. Studies of mucus in mouse stomach, small intestine, and colon. I. Gastrointestinal mucus layers have different properties depending on location as well as over the Peyer's patches. *Am J Physiol - Gastrointest Liver Physiol*. 2013;305(5):341-347. doi:10.1152/ajpgi.00046.2013

27. Birchenough GMH, Johansson MEV, Gustafsson JK, Bergström JH, Hansson GC. New developments in goblet cell mucus secretion and function. *Mucosal Immunol*. 2015;8(4):712-719. doi:10.1038/mi.2015.32

28. McGuckin MA, Thornton DJ, Whitsett JA. Mucins and Mucus. In: *Mucosal Immunology: Fourth Edition*. Vol 1-2. ; 2015:231-250. doi:10.1016/B978-0-12-415847-4.00014-8

29. Johansson MEV, Holmén Larsson JM, Hansson GC. The two mucus layers of colon are organized by the MUC2 mucin, whereas the outer layer is a legislator of host-microbial interactions. *Proc Natl Acad Sci U S A*. 2011;108(SUPPL. 1):4659-4665. doi:10.1073/pnas.1006451107

30. Van der Sluis M, De Koning BAE, De Bruijn ACJM, et al. Muc2-Deficient Mice Spontaneously Develop Colitis, Indicating That MUC2 Is Critical for Colonic Protection. *Gastroenterology*. 2006;131(1):117-129. doi:10.1053/j.gastro.2006.04.020

31. Kawashima H. Roles of the gel-forming MUC2 mucin and its O-glycosylation in the protection against colitis and colorectal cancer. *Biol Pharm Bull*. 2012;35(10):1637-1641. doi:10.1248/bpb.b12-00412

32. Johansson MEV, Phillipson M, Petersson J, Velcich A, Holm L, Hansson GC. The inner of the two Muc2 mucin-dependent mucus layers in colon is devoid of bacteria. *Proc Natl Acad Sci U S A*. 2008;105(39):15064-15069. doi:10.1073/pnas.0803124105

33. Bergstrom KSB, Kissoon-Singh V, Gibson DL, et al. Muc2 protects against lethal infectious colitis by disassociating pathogenic and commensal bacteria from the colonic mucosa. *PLoS Pathog*. 2010;6(5). doi:10.1371/journal.ppat.1000902

34. Peterson LW, Artis D. Intestinal epithelial cells: Regulators of barrier function and immune homeostasis. *Nat Rev Immunol*. 2014;14(3):141-153. doi:10.1038/nri3608

35. De Schepper S, Verheijden S, Aguilera-Lizarraga J, et al. Self-Maintaining Gut Macrophages Are Essential for Intestinal Homeostasis. *Cell*. 2018;175(2):400-415.e13. doi:10.1016/j.cell.2018.07.048

36. Spalinger MR, Sayoc-Becerra A, Santos AN, et al. PTPN2 Regulates Interactions Between Macrophages and Intestinal Epithelial Cells to Promote Intestinal Barrier Function. *Gastroenterology*. 2020;159(5):1763-1777.e14. doi:10.1053/j.gastro.2020.07.004

37. Rescigno M, Sabatino A Di. Dendritic cells in intestinal homeostasis and disease. *J Clin Invest*. 2009;119(9):2441-2450. doi:10.1172/JCI39134

38. Stagg AJ. Intestinal Dendritic Cells in Health and Gut Inflammation. *Front Immunol*. 2018;9:2883. doi:10.3389/fimmu.2018.02883

39. Chieppa M, Rescigno M, Huang AYC, Germain RN. Dynamic imaging of dendritic cell extension into the small bowel lumen in response to epithelial cell TLR engagement. *J Exp Med*. 2006;203(13):2841-2852. doi:10.1084/jem.20061884

40. Spits H, Artis D, Colonna M, et al. Innate lymphoid cells-a proposal for uniform nomenclature. *Nat Rev Immunol*. 2013;13(2):145-149. doi:10.1038/nri3365

41. Eberl G, Colonna M, Santo JPD, McKenzie ANJ. Innate lymphoid cells: A new paradigm in immunology. *Science (80-).* 2015;348(6237). doi:10.1126/science.aaa6566

42. Edelblum KL, Shen L, Weber CR, et al. Dynamic migration of γδ intraepithelial lymphocytes requires occludin. *Proc Natl Acad Sci U S A*. 2012;109(18):7097-7102. doi:10.1073/pnas.1112519109

43. Cheroutre H, Lambolez F, Mucida D. The light and dark sides of intestinal intraepithelial lymphocytes. *Nat Rev Immunol*. 2011;11(7):445-456. doi:10.1038/nri3007

44. Xu W, He B, Chiu A, et al. Epithelial cells trigger frontline immunoglobulin class switching through a pathway regulated by the inhibitor SLPI. *Nat Immunol*. 2007;8(3):294-303. doi:10.1038/ni1434

45. He B, Xu W, Santini PA, et al. Intestinal Bacteria Trigger T Cell-Independent Immunoglobulin A2 Class Switching by Inducing Epithelial-Cell Secretion of the Cytokine APRIL. *Immunity*. 2007;26(6):812-826. doi:10.1016/j.immuni.2007.04.014

46. Fagarasan S, Honjo T. Intestinal IgA synthesis: Regulation of front-line body defences. *Nat Rev Immunol*. 2003;3(1):63-72. doi:10.1038/nri982

47. LEBLOND CP, WALKER BE. Renewal of cell populations. *Physiol Rev*. 1956;36(2):255-276. doi:10.1152/physrev.1956.36.2.255

48. Martini E, Krug SM, Siegmund B, Neurath MF, Becker C. Mend Your Fences: The Epithelial Barrier and its Relationship With Mucosal Immunity in Inflammatory Bowel Disease. *Cmgh*. 2017;4(1):33-46. doi:10.1016/j.jcmgh.2017.03.007

49. Barker N. Adult intestinal stem cells: Critical drivers of epithelial homeostasis and regeneration. *Nat Rev Mol Cell Biol*. 2014;15(1):19-33. doi:10.1038/nrm3721

50. Beumer J, Clevers H. Cell fate specification and differentiation in the adult mammalian intestine. *Nat Rev Mol Cell Biol*. 2021;22(1):39-53. doi:10.1038/s41580-020-0278-0

51. Mah AT, Yan KS, Kuo CJ. Wnt pathway regulation of intestinal stem cells. *J Physiol*. 2016;594(17):4837-4847. doi:10.1113/JP271754

52. Stanger BZ, Datar R, Murtaugh LC, Melton DA. Direct regulation of intestinal fate by Notch. *Proc Natl Acad Sci U S A*. 2005;102(35):12443-12448. doi:10.1073/pnas.0505690102

53. Fre S, Huyghe M, Mourikis P, Robine S, Louvard D, Artavanis-Tsakonas S. Notch signals control the fate of immature progenitor cells in the intestine. *Nature*. 2005;435(7044):964-968. doi:10.1038/nature03589

54. Van Es JH, Sato T, Van De Wetering M, et al. Dll1 + secretory progenitor cells revert to stem cells upon crypt damage. *Nat Cell Biol*. 2012;14(10):1099-1104. doi:10.1038/ncb2581

55. Batlle E, Henderson JT, Beghtel H, et al. β-catenin and TCF mediate cell positioning in the intestinal epithelium by controlling the expression of EphB/EphrinB. *Cell*. 2002;111(2):251-263. doi:10.1016/S0092-8674(02)01015-2

56. Sailaja BS, He XC, Li L. The regulatory niche of intestinal stem cells. *J Physiol*. 2016;594(17):4827-4836. doi:10.1113/JP271931

57. Scoville DH, Sato T, He XC, Li L. Current View: Intestinal Stem Cells and Signaling. *Gastroenterology*. 2008;134(3):849-864. doi:10.1053/j.gastro.2008.01.079

58. Crosnier C, Stamataki D, Lewis J. Organizing cell renewal in the intestine: Stem cells, signals and combinatorial control. *Nat Rev Genet*. 2006;7(5):349-359. doi:10.1038/nrg1840

59. Barker N, Van Es JH, Kuipers J, et al. Identification of stem cells in small intestine and colon by marker gene Lgr5. *Nature*. 2007;449(7165):1003-1007. doi:10.1038/nature06196

60. Sato T, Van Es JH, Snippert HJ, et al. Paneth cells constitute the niche for Lgr5 stem cells in intestinal crypts. *Nature*. 2011;469(7330):415-418. doi:10.1038/nature09637

61. Meran L, Baulies A, Li VSW. Intestinal Stem Cell Niche: The Extracellular Matrix and Cellular Components. *Stem Cells Int*. 2017;2017. doi:10.1155/2017/7970385

62. Sato T, Vries RG, Snippert HJ, et al. Single Lgr5 stem cells build crypt-villus structures in vitro without a mesenchymal niche. *Nature*. 2009;459(7244):262-265. doi:10.1038/nature07935

63. Clevers HC, Bevins CL. Paneth Cells: Maestros of the Small Intestinal Crypts. *Annu Rev Physiol*. 2013;75(1):289-311. doi:10.1146/annurev-physiol-030212-183744

64. Smith NR, Gallagher AC, Wong MH. Defining a stem cell hierarchy in the intestine: markers, caveats and controversies. *J Physiol*. 2016;594(17):4781-4790. doi:10.1113/JP271651

65. Castillo-Azofeifa D, Fazio EN, Nattiv R, et al. Atoh1 + secretory progenitors possess renewal capacity independent of Lgr5 + cells during colonic regeneration. *EMBO J*. 2019;38(4):e99984. doi:10.15252/embj.201899984

66. Cunliffe RN, Rose FRAJ, Keyte J, Abberley L, Chan WC, Mahida YR. Human defensin 5 is stored in precursor form in normal Paneth cells and is expressed by some villous epithelial cells and by metaplastic Paneth cells in the colon in inflammatory bowel disease. *Gut*. 2001;48(2):176-185. doi:10.1136/gut.48.2.176

67. Tanaka M, Saito H, Kusumi T, et al. Spatial distribution and histogenesis of colorectal Paneth cell metaplasia in idiopathic inflammatory bowel disease. *J Gastroenterol Hepatol*. 2001;16(12):1353-1359. doi:10.1046/j.1440-1746.2001.02629.x

68. Simmonds N, Furman M, Karanika E, Phillips A, Bates AW. Paneth cell metaplasia in newly diagnosed inflammatory bowel disease in children. *BMC Gastroenterol*. 2014;14(1):1-6. doi:10.1186/1471-230X-14-93

69. Selsted ME, Ouellette AJ. Mammalian defensins in the antimicrobial immune response. *Nat Immunol*. 2005;6(6):551-557. doi:10.1038/ni1206

70. Weeks CS, Tanabe H, Cummings JE, et al. Matrix metalloproteinase-7 activation of mouse paneth cell pro-α-defensins: SER43 ↓ ILE44 proteolysis enables membrane-disruptive activity. *J Biol Chem*. 2006;281(39):28932-28942. doi:10.1074/jbc.M602041200

71. Chairatana P, Nolan EM. Human α-Defensin 6: A Small Peptide That Self-Assembles and Protects the Host by Entangling Microbes. *Acc Chem Res*. 2017;50(4):960-967. doi:10.1021/acs.accounts.6b00653

72. Gregorieff A, Stange DE, Kujala P, et al. The Ets-Domain Transcription Factor Spdef Promotes Maturation of Goblet and Paneth Cells in the Intestinal Epithelium. *Gastroenterology*. 2009;137(4):1333-1345.e3. doi:10.1053/J.GASTRO.2009.06.044

73. Katz JP, Perreault N, Goldstein BG, et al. The zinc-finger transcription factor Klf4 is required for terminal differentiation of goblet cells in the colon. *Development*. 2002;129(11):2619-2628. doi:10.1242/dev.129.11.2619

74. Yu T, Chen X, Zhang W, et al. Krüppel-like factor 4 regulates intestinal epithelial cell morphology and polarity. *PLoS One*. 2012;7(2). doi:10.1371/journal.pone.0032492

75. Schneider MR, Dahlhoff M, Horst D, et al. A key role for E-cadherin in intestinal homeostasis and paneth cell maturation. *PLoS One*. 2010;5(12). doi:10.1371/journal.pone.0014325

76. Ye DZ, Kaestner KH. Foxa1 and Foxa2 Control the Differentiation of Goblet and Enteroendocrine L- and D-Cells in Mice. *Gastroenterology*. 2009;137(6):2052-2062. doi:10.1053/j.gastro.2009.08.059

77. Deplancke B, Gaskins HR. Microbial modulation of innate defense: Goblet cells and the intestinal mucus layer. In: *American Journal of Clinical Nutrition*. Vol 73. Oxford Academic; 2001:1131S-1141S. doi:10.1093/ajcn/73.6.1131s

78. Wlodarska M, Thaiss CA, Nowarski R, et al. NLRP6 inflammasome orchestrates the colonic host-microbial interface by regulating goblet cell mucus secretion. *Cell*. 2014;156(5):1045-1059. doi:10.1016/j.cell.2014.01.026

79. Specian RD, Neutra MR. Mechanism of rapid mucus secretion in goblet cells stimulated by acetylcholine. *J Cell Biol*. 1980;85(3):626-640. doi:10.1083/jcb.85.3.626

80. Haber AL, Biton M, Rogel N, et al. A single-cell survey of the small intestinal epithelium. *Nature*. 2017;551(7680):333-339. doi:10.1038/nature24489

81. Smirnova MG, Guo L, Birchall JP, Pearson JP. LPS up-regulates mucin and cytokine mRNA expression and stimulates mucin and cytokine secretion in goblet cells. *Cell Immunol*. 2003;221(1):42-49. doi:10.1016/S0008-8749(03)00059-5

82. Knoop KA, Newberry RD. Goblet cells: multifaceted players in immunity at mucosal surfaces. *Mucosal Immunol*. 2018;11(6):1551-1557. doi:10.1038/s41385-018-0039-y

83. Knoop KA, McDonald KG, McCrate S, McDole JR, Newberry RD. Microbial sensing by goblet cells controls immune surveillance of luminal antigens in the colon. *Mucosal Immunol*. 2015;8(1):198-210. doi:10.1038/mi.2014.58

84. Middelhoff M, Westphalen CB, Hayakawa Y, et al. Dclk1-expressing tuft cells: Critical modulators of the intestinal niche? *Am J Physiol - Gastrointest Liver Physiol*. 2017;313(4):G285-G299. doi:10.1152/ajpgi.00073.2017

85. Reid L, Meyrick B, Antony VB, Chang LY, Crapo JD, Reynolds HY. The mysterious pulmonary brush cell: A cell in search of a function. In: *American Journal of Respiratory and Critical Care Medicine*. Vol 172. American Thoracic Society; 2005:136-139. doi:10.1164/rccm.200502-203WS

86. Nadjsombati MS, McGinty JW, Lyons-Cohen MR, et al. Detection of Succinate by Intestinal Tuft Cells Triggers a Type 2 Innate Immune Circuit. *Immunity*. 2018;49(1):33-41.e7. doi:10.1016/j.immuni.2018.06.016

87. Gerbe F, Sidot E, Smyth DJ, et al. Intestinal epithelial tuft cells initiate type 2 mucosal immunity to helminth parasites. *Nature*. 2016;529(7585):226-230. doi:10.1038/nature16527

88. Schneider C, O'Leary CE, Locksley RM. Regulation of immune responses by tuft cells. *Nat Rev Immunol*. 2019;19(9):584-593. doi:10.1038/s41577-019-0176-x

89. Von Moltke J, Ji M, Liang HE, Locksley RM. Tuft-cell-derived IL-25 regulates an intestinal ILC2-epithelial response circuit. *Nature*. 2016;529(7585):221-225. doi:10.1038/nature16161

90. Worthington JJ, Reimann F, Gribble FM. Enteroendocrine cells-sensory sentinels of the intestinal environment and orchestrators of mucosal immunity. *Mucosal Immunol*. 2018;11(1):3-20. doi:10.1038/mi.2017.73

91. Bellono NW, Bayrer JR, Leitch DB, et al. Enterochromaffin Cells Are Gut Chemosensors that Couple to Sensory Neural Pathways. *Cell*. 2017;170(1):185-198.e16. doi:10.1016/j.cell.2017.05.034

92. Mellitzer G, Beucher A, Lobstein V, et al. Loss of enteroendocrine cells in mice alters lipid absorption and glucose homeostasis and impairs postnatal survival. *J Clin Invest*. 2010;120(5):1708-1721. doi:10.1172/JCI40794

93. Snoeck V, Goddeeris B, Cox E. The role of enterocytes in the intestinal barrier function and antigen uptake. *Microbes Infect*. 2005;7(7-8):997-1004. doi:10.1016/j.micinf.2005.04.003

94. Johansen FE, Kaetzel CS. Regulation of the polymeric immunoglobulin receptor and IgA transport: New advances in environmental factors that stimulate pIgR expression and its role in mucosal immunity. *Mucosal Immunol*. 2011;4(6):598-602. doi:10.1038/mi.2011.37

95. Cash HL, Whitham C V., Behrendt CL, Hooper L V. Symbiotic bacteria direct expression of an intestinal bactericidal lectin. *Science (80-)*. 2006;313(5790):1126-1130. doi:10.1126/science.1127119

96. Xiao Y, Huang X, Zhao Y, et al. Interleukin-33 Promotes REG3γ Expression in Intestinal Epithelial Cells and Regulates Gut Microbiota. *Cell Mol Gastroenterol Hepatol*. 2019;8(1):21-36. doi:10.1016/j.jcmgh.2019.02.006

97. Litvak Y, Byndloss MX, Bäumler AJ. Colonocyte metabolism shapes the gut microbiota. *Science (80-)*. 2018;362(6418). doi:10.1126/science.aat9076

98. Bennett KM, Walker SL, Lo DD. Epithelial microvilli establish an electrostatic barrier to microbial adhesion. *Infect Immun*. 2014;82(7):2860-2871. doi:10.1128/IAI.01681-14

99. Corr SC, Gahan CCGM, Hill C. M-cells: Origin, morphology and role in mucosal immunity and microbial pathogenesis. *FEMS Immunol Med Microbiol*. 2008;52(1):2-12. doi:10.1111/j.1574-695X.2007.00359.x

100. Wood MB, Rios D, Ifor X, Williams R, Williams IR. TNF-augments RANKL-dependent intestinal M cell differentiation in enteroid cultures Wood MB, Rios D, Williams IR. TNF-augments RANKL-dependent intestinal M cell differentiation in enteroid cultures. *Am J Physiol Cell Physiol*. 2016;311:498-507. doi:10.1152/ajpcell.00108.2016.-Microfold

101. Bennett KM, Parnell EA, Sanscartier C, et al. Induction of Colonic M Cells during Intestinal Inflammation. *Am J Pathol*. 2016;186(5):1166-1179. doi:10.1016/j.ajpath.2015.12.015

102. Ananthakrishnan AN. Epidemiology and risk factors for IBD. *Nat Rev Gastroenterol Hepatol*. 2015;12(4):205-217. doi:10.1038/nrgastro.2015.34

103. Danese S, Fiocchi C. Ulcerative colitis. *N Engl J Med*. 2011;365(31):1713-1725.

104. Louis E, Collard A, Oger AF, Degroote E, Aboul Nasr El Yafi F, Belaiche J. Behaviour of Crohn's disease according to the Vienna classification: Changing pattern over the course of the disease. *Gut*. 2001;49(6):777-782. doi:10.1136/gut.49.6.777

105. Baumgart DC, Sandborn WJ. Crohn's disease. *Lancet*. 2012;380(9853):1590-1605. doi:10.1016/S0140-6736(12)60026-9

106. Neurath MF. Cytokines in inflammatory bowel disease. *Nat Rev Immunol*. 2014;14(5):329-342. doi:10.1038/nri3661

107. Antoni L, Nuding S, Wehkamp J, Stange EF. Intestinal barrier in inflammatory bowel disease. *World J Gastroenterol*. 2014;20(5):1165-1179. doi:10.3748/wjg.v20.i5.1165

108. Wehkamp J, Salzman NH, Porter E, et al. Reduced Paneth cell α-defensins in ileal Crohn's disease. *Proc Natl Acad Sci U S A*. 2005;102(50):18129-18134. doi:10.1073/pnas.0505256102

109. Wehkamp J, Stange EF. Paneth's disease. *J Crohn's Colitis*. 2010;4(5):523-531. doi:10.1016/j.crohns.2010.05.010

110. Pullan RD, Thomas GAO, Rhodes M, et al. Thickness of adherent mucus gel on colonic mucosa in humans and its relevance to colitis. *Gut*. 1994;35(3):353-359. doi:10.1136/gut.35.3.353

111. Larsson JMH, Karlsson H, Crespo JG, et al. Altered O-glycosylation profile of MUC2 mucin occurs in active ulcerative colitis and is associated with increased inflammation. *Inflamm Bowel Dis*. 2011;17(11):2299-2307. doi:10.1002/ibd.21625

112. Bankole E, Read E, Curtis MA, Neves JF, Garnett JA. The relationship between mucins and ulcerative colitis: A systematic review. *J Clin Med*. 2021;10(9):1935. doi:10.3390/jcm10091935

113. Johansson MEV, Gustafsson JK, Holmen-Larsson J, et al. Bacteria penetrate the normally impenetrable inner colon mucus layer in both murine colitis models and patients with ulcerative colitis. *Gut*. 2014;63(2):281-291. doi:10.1136/gutjnl-2012-303207

114. Eckburg PB, Bik EM, Bernstein CN, et al. Microbiology: Diversity of the human intestinal microbial flora. *Science (80-)*. 2005;308(5728):1635-1638. doi:10.1126/science.1110591

115. Gilbert JA, Blaser MJ, Caporaso JG, Jansson JK, Lynch S V, Knight R. Current understanding of the human microbiome. *Nat Med*. 2018;24(4):392-400. doi:10.1038/nm.4517

116. Cani PD. Gut microbiota-at the intersection of everything? *Nat Rev Gastroenterol Hepatol*. 2017;14(6):321-322. doi:10.1038/nrgastro.2017.54

117. Tamboli CP, Neut C, Desreumaux P, Colombel JF. Dysbiosis in inflammatory bowel disease. *Gut*. 2004;53(1):1-4. doi:10.1136/gut.53.1.1

118. King SJ, McCole DF. Epithelial-Microbial Diplomacy: Escalating Border Tensions Drive Inflammation in Inflammatory Bowel disease. *Intest Res*. 2019;17(2):177-191. doi:10.5217/ir.2018.00170

119. Frank DN, St. Amand AL, Feldman RA, Boedeker EC, Harpaz N, Pace NR. Molecular-phylogenetic characterization of microbial community imbalances in human inflammatory bowel diseases. *Proc Natl Acad Sci U S A*. 2007;104(34):13780-13785. doi:10.1073/pnas.0706625104

120. Darfeuille-Michaud A, Neut C, Barnich N, et al. Presence of adherent Escherichia coli strains in ileal mucosa of patients with Crohn's disease. *Gastroenterology*. 1998;115(6):1405-1413. doi:10.1016/S0016-5085(98)70019-8

121. Glasser AL, Boudeau J, Barnich N, Perruchot MH, Colombel JF, Darfeuille-Michaud A. Adherent invasive Escherichia coli strains from patients with Crohn's disease survive and replicate within macrophages without inducing host cell death. *Infect Immun*. 2001;69(9):5529-5537. doi:10.1128/IAI.69.9.5529-5537.2001

122. Boudeau J, Barnich N, Darfeuille-Michaud A. Type 1 pili-mediated adherence of Escherichia coli strain LF82 isolated from Crohn's disease is involved in bacterial invasion of intestinal epithelial cells. *Mol Microbiol*. 2004;39(5):1272-1284. doi:10.1111/j.1365-2958.2001.02315.x

123. De Lange KM, Moutsianas L, Lee JC, et al. Genome-wide association study implicates immune activation of multiple integrin genes in inflammatory bowel disease. *Nat Genet*. 2017;49(2):256-261. doi:10.1038/ng.3760

124. Lees CW, Barrett JC, Parkes M, Satsangi J. New IBD genetics: common pathways with other diseases. *Gut*. 2011;60(12):1739-1753. doi:10.1136/gut.2009.199679

125. Khor B, Gardet A, Xavier RJ. Genetics and pathogenesis of inflammatory bowel disease. *Nature*. 2011;474(7351):307-317. doi:10.1038/nature10209

126. Moore F, Colli ML, Cnop M, et al. PTPN2, a candidate gene for type 1 diabetes, modulates interferon-γ- induced pancreatic β-cell apoptosis. *Diabetes*. 2009;58(6):1283-1291. doi:10.2337/db08-1510

127. Hsieh WC, Svensson MND, Zoccheddu M, et al. PTPN2 links colonic and joint inflammation in experimental autoimmune arthritis. *JCI Insight*. 2020;5(20). doi:10.1172/jci.insight.141868

128. Okada Y, Terao C, Ikari K, et al. Meta-analysis identifies nine new loci associated with rheumatoid arthritis in the Japanese population. *Nat Genet*. 2012;44(5):511-516. doi:10.1038/ng.2231

129. Wellcome T, Case T, Consortium C. Genome-wide association study of 14,000 cases of seven common diseases and 3,000 shared controls. *Nature*. 2007;447(7145):661-678. doi:10.1038/nature05911

130. Anderson CA, Boucher G, Lees CW, et al. Meta-analysis identifies 29 additional ulcerative colitis risk loci, increasing the number of confirmed associations to 47. *Nat Genet*. 2011;43(3):246-252. doi:10.1038/ng.764

131. Glas J, Wagner J, Seiderer J, et al. PTPN2 gene variants are associated with susceptibility to both Crohn's disease and ulcerative colitis supporting a common genetic disease background. *PLoS One*. 2012;7(3). doi:10.1371/journal.pone.0033682

132. Zhang JX, He JH, Wang J, et al. Associations between PTPN2 polymorphisms and susceptibility to ulcerative colitis and Crohn's disease: A meta-analysis. *Inflamm Res*. 2014;63(1):71-79. doi:10.1007/s00011-013-0673-5

133. Scharl M, Mwinyi J, Fischbeck A, et al. Crohn's disease-associated polymorphism within the PTPN2 gene affects muramyl-dipeptide-induced cytokine secretion and autophagy. *Inflamm Bowel Dis*. 2012;18(5):900-912. doi:10.1002/ibd.21913

134. Parlato M, Nian Q, Charbit-Henrion F, et al. Loss-of-Function Mutation in PTPN2 Causes Aberrant Activation of JAK Signaling Via STAT and Very Early Onset Intestinal Inflammation. *Gastroenterology*. 2020;159(5):1968-1971.e4. doi:10.1053/j.gastro.2020.07.040

135. Scharl M, Paul G, Weber A, et al. Protection of Epithelial Barrier Function by the Crohn's Disease Associated Gene Protein Tyrosine Phosphatase N2. *Gastroenterology*. 2009;137(6):2030-2040.e5. doi:10.1053/j.gastro.2009.07.078

136. Houtman M, Shchetynsky K, Chemin K, et al. T cells are influenced by a long non-coding RNA in the autoimmune associated PTPN2 locus. *J Autoimmun*. 2018;90:28-38. doi:10.1016/j.jaut.2018.01.003

137. Spalinger MR, Mccole DF, Rogler G, Scharl M. Role of Protein Tyrosine Phosphatases in Regulating the Immune System: Implications for Chronic Intestinal Inflammation. *Inflamm Bowel Dis*. 2015;21(3):645-655. doi:10.1097/MIB.0000000000000297

138. Marcil V, Mack DR, Kumar V, et al. Association Between the PTPN2 Gene and Crohn's DiseaseDissection of Potential Causal Variants. *Inflamm Bowel Dis*. 2013;19(6):1149-1155. doi:10.1097/MIB.0B013E318280B181

139. Sayoc-Becerra A, Krishnan M, Fan S, et al. The JAK-Inhibitor Tofacitinib Rescues Human Intestinal Epithelial Cells and Colonoids from Cytokine-Induced Barrier Dysfunction. *Inflamm Bowel Dis*. 2020;26(3):407-422. doi:10.1093/ibd/izz266

140. Krishnan M, McCole DF. T cell protein tyrosine phosphatase prevents STAT1 induction of claudin-2 expression in intestinal epithelial cells. *Ann N Y Acad Sci*. Published online 2017. doi:10.1111/nyas.13439

141. Spalinger MR, Crawford M, Bobardt SD, et al. Loss of protein tyrosine phosphatase non-receptor type 2 reduces IL-4-driven alternative macrophage activation. *Mucosal Immunol*. Published online August 21, 2021:1-10. doi:10.1038/s41385-021-00441-3

142. Shawki A, Ramirez R, Spalinger MR, et al. The autoimmune susceptibility gene, PTPN2, restricts expansion of a novel mouse adherent-invasive E. coli. *Gut Microbes*. 2020;11(6):1547-1566. doi:10.1080/19490976.2020.1775538

143. Marchelletta RR, Krishnan M, Spalinger MR, et al. T cell protein tyrosine phosphatase protects intestinal barrier function by restricting epithelial tight junction remodeling. *J Clin Invest*. 2021;131(17). doi:10.1172/JCI138230

144. Spalinger MR, Shawki A, Chatterjee P, et al. Autoimmune susceptibility gene PTPN2 is required for clearance of adherent-invasive Escherichia coli by integrating bacterial uptake and lysosomal defence. *Gut*. Published online 2021:1-12. doi:10.1136/gutjnl-2020-323636

145. Doody KM, Bourdeau A, Tremblay ML. T-cell protein tyrosine phosphatase is a key regulator in immune cell signaling: Lessons from the knockout mouse model and implications in human disease. *Immunol Rev*. 2009;228(1):325-341. doi:10.1111/j.1600-065X.2008.00743.x

146. Ibarra-Sánchez M de J, Simoncic PD, Nestel FR, Duplay P, Lapp WS, Tremblay ML. The T-cell protein tyrosine phosphatase. *Semin Immunol*. 2000;12(4):379-386. doi:10.1006/smim.2000.0220

147. Kamatkar S, Radha V, Nambirajan S, Reddy RS, Swarup G. Two splice variants of a tyrosine phosphatase differ in substrate specificity, DNA binding, and subcellular location. *J Biol Chem*. 1996;271(43):26755-26761. doi:10.1074/jbc.271.43.26755

148. Lam MHC, Michell BJ, Fodero-Tavoletti MT, Kemp BE, Tonks NK, Tiganis T. Cellular Stress Regulates the Nucleocytoplasmic Distribution of the Protein-tyrosine Phosphatase TCPTP. *J Biol Chem*. 2001;276(40):37700-37707. doi:10.1074/jbc.M105128200

149. Mosinger B, Tillmann U, Westphal H, Tremblay ML. Cloning and characterization of a mouse cDNA encoding a cytoplasmic protein-tyrosine-phosphatase. *Proc Natl Acad Sci U S A*. 1992;89(2):499-503. doi:10.1073/pnas.89.2.499

150. Tiganis T, Bennett AM, Ravichandran KS, Tonks NK. Epidermal Growth Factor Receptor and the Adaptor Protein p52Shc Are Specific Substrates of T-Cell Protein Tyrosine Phosphatase. *Mol Cell Biol*. 1998;18(3):1622-1634. doi:10.1128/mcb.18.3.1622

151. ten Hoeve J, de Jesus Ibarra-Sanchez M, Fu Y, et al. Identification of a Nuclear Stat1 Protein Tyrosine Phosphatase. *Mol Cell Biol*. 2002;22(16):5662-5668. doi:10.1128/mcb.22.16.5662-5668.2002

152. Simoncic PD, Lee-Loy A, Barber DL, Tremblay ML, McGlade CJ. The T cell protein tyrosine phosphatase is a negative regulator of Janus family kinases 1 and 3. *Curr Biol*. 2002;12(6):446-453. doi:10.1016/S0960-9822(02)00697-8

153. Galic S, Klingler-Hoffmann M, Fodero-Tavoletti MT, et al. Regulation of Insulin Receptor Signaling by the Protein Tyrosine Phosphatase TCPTP. *Mol Cell Biol*. 2003;23(6):2096-2108. doi:10.1128/mcb.23.6.2096-2108.2003

154. Matilla E, Pellinen T, Nevo J, Vuoriluoto K, Arjonen A, Ivaska J. Negative regulation of EGFR signalling through integrin-α1β1-mediated activation of protein tyrosine phosphatase TCPTP. *Nat Cell Biol*. 2005;7(1):78-85. doi:10.1038/ncb1209

155. Van Vliet C, Bukczynska PE, Puryer MA, et al. Selective regulation of tumor necrosis factor-induced Erk signaling by Src family kinases and the T cell protein tyrosine phosphatase. *Nat Immunol*. 2005;6(3):253-260. doi:10.1038/ni1169

156. Simoncic PD, Bourdeau A, Lee-Loy A, et al. T-Cell Protein Tyrosine Phosphatase (Tcptp) Is a Negative Regulator of Colony-Stimulating Factor 1 Signaling and Macrophage Differentiation. *Mol Cell Biol*. 2006;26(11):4149-4160. doi:10.1128/mcb.01932-05

157. Lu X, Chen J, Sasmono RT, et al. T-Cell Protein Tyrosine Phosphatase, Distinctively Expressed in Activated-B-Cell-Like Diffuse Large B-Cell Lymphomas, Is the Nuclear Phosphatase of STAT6. *Mol Cell Biol*. 2007;27(6):2166-2179. doi:10.1128/mcb.01234-06

158. Tiganis T. PTP1B and TCPTP - Nonredundant phosphatases in insulin signaling and glucose homeostasis. *FEBS J*. 2013;280(2):445-458. doi:10.1111/j.1742-4658.2012.08563.x

159. Wehkamp J, Salzman NH, Porter E, et al. Reduced Paneth cell α-defensins in ileal Crohn's disease. *Proc Natl Acad Sci U S A*. 2005;102(50):18129-18134. doi:10.1073/pnas.0505256102

160. Gersemann M, Becker S, Kübler I, et al. Differences in goblet cell differentiation between Crohn's disease and ulcerative colitis. *Differentiation*. 2009;77(1):84-94. doi:10.1016/j.diff.2008.09.008

161. Caruso R, Mathes T, Martens EC, et al. A specific gene-microbe interaction drives the development of Crohn's disease–like colitis in mice. *Sci Immunol*. 2019;4(34):eaaw4341. doi:10.1126/sciimmunol.aaw4341

162. Salzman NH, Bevins CL. Dysbiosis-A consequence of Paneth cell dysfunction. *Semin Immunol*. 2013;25(5):334-341. doi:10.1016/j.smim.2013.09.006

163. You-Ten KE, Muise ES, Itié A, et al. Impaired Bone Marrow Microenvironment and Immune Function in T Cell Protein Tyrosine Phosphatase–deficient Mice. *J Exp Med*. 1997;186(5):683-693. http://www.jem.org

164. Bourdeau A, Dubé N, Heinonen KM, Théberge JF, Doody KM, Tremblay ML. TC-PTP-deficient bone marrow stromal cells fail to support normal B lymphopoiesis due to abnormal secretion of interferon-γ. *Blood*. 2007;109(10):4220-4228. doi:10.1182/blood-2006-08-044370

165. El Marjou F, Janssen KP, Chang BHJ, et al. Tissue-specific and inducible Cre-mediated recombination in the gut epithelium. *Genesis*. 2004;39(3):186-193. doi:10.1002/gene.20042

166. Eriguchi Y, Nakamura K, Yokoi Y, et al. Essential role of IFN-γ in T cell-associated intestinal inflammation. *JCI insight*. 2018;3(18). doi:10.1172/jci.insight.121886

167. Johansson MEV, Hansson GC. Preservation of mucus in histological sections, immunostaining of mucins in fixed tissue, and localization of bacteria with FISH. *Methods Mol Biol*. 2012;842:229-235. doi:10.1007/978-1-61779-513-8_13

168. Satoh Y, Yamano M, Matsuda M, Ono K. Ultrastructure of Paneth cells in the intestine of various mammals. *J Electron Microsc Tech*. 1990;16(1):69-80. doi:10.1002/jemt.1060160109

169. Brazma A, Hingamp P, Quackenbush J, et al. Minimum information about a microarray experiment (MIAME) - Toward standards for microarray data. *Nat Genet*. 2001;29(4):365-371. doi:10.1038/ng1201-365

170. Barrett T, Wilhite SE, Ledoux P, et al. NCBI GEO: Archive for functional genomics data sets - Update. *Nucleic Acids Res*. 2013;41(D1):991-995. doi:10.1093/nar/gks1193

171. Spalinger MR, Manzini R, Hering L, et al. PTPN2 Regulates Inflammasome Activation and Controls Onset of Intestinal Inflammation and Colon Cancer. *Cell Rep*. 2018;22(7):1835-1848. doi:10.1016/j.celrep.2018.01.052

172. Huang H, Fang M, Jostins L, et al. Fine-mapping inflammatory bowel disease loci to single-variant resolution. *Nature*. 2017;547(7662):173-178. doi:10.1038/nature22969

173. Heinonen KM, Nestel FP, Newell EW, et al. T-cell protein tyrosine phosphatase deletion results in progressive systemic inflammatory disease. *Blood*. 2004;103(9):3457-3464. doi:10.1182/blood-2003-09-3153

174. Hassan SW, Doody KM, Hardy S, Uetani N, Cournoyer D, Tremblay ML. Increased susceptibility to dextran sulfate sodium induced colitis in the T cell protein tyrosine phosphatase heterozygous mouse. *PLoS One*. 2010;5(1). doi:10.1371/journal.pone.0008868

175. Spalinger MR, Schwarzfischer M, Scharl M. The Role of Protein Tyrosine Phosphatases in Inflammasome Activation. *Int J Mol Sci*. 2020;21(15):5481. doi:10.3390/ijms21155481

176. Katkeviciute E, Hering L, Montalban-Arques A, et al. Protein tyrosine phosphatase non-receptor type 2 controls colorectal cancer development. *J Clin Invest*. Published online October 1, 2020. doi:10.1172/jci140281

177. LaFleur MW, Nguyen TH, Coxe MA, et al. PTPN2 regulates the generation of exhausted CD8+ T cell subpopulations and restrains tumor immunity. *Nat Immunol*. 2019;20(10):1335-1347. doi:10.1038/s41590-019-0480-4

178. Spalinger MR, Manzini R, Hering L, et al. PTPN2 Regulates Inflammasome Activation and Controls Onset of Intestinal Inflammation and Colon Cancer. *CellReports*. 2018;22:1835-1848. doi:10.1016/j.celrep.2018.01.052

179. Lee H, Kim M, Baek M, et al. Targeted disruption of TC-PTP in the proliferative compartment augments STAT3 and AKT signaling and skin tumor development. *Sci Rep*. 2017;7. doi:10.1038/srep45077

180. Bruens L, Ellenbroek SIJ, van Rheenen J, Snippert HJ. In Vivo Imaging Reveals Existence of Crypt Fission and Fusion in Adult Mouse Intestine. *Gastroenterology*. 2017;153(3):674-677.e3. doi:10.1053/j.gastro.2017.05.019

181. Baker A-M, Gabbutt C, Williams MJ, et al. Crypt fusion as a homeostatic mechanism in the human colon. *Gut*. 2019;0:1-8. doi:10.1136/gutjnl-2018-317540

182. König J, Wells J, Cani PD, et al. Human intestinal barrier function in health and disease. *Clin Transl Gastroenterol*. 2016;7(10). doi:10.1038/ctg.2016.54

183. De Souza HSP, Fiocchi C. Immunopathogenesis of IBD: Current state of the art. *Nat Rev Gastroenterol Hepatol*. 2016;13(1):13-27. doi:10.1038/nrgastro.2015.186

184. Morón B, Spalinger M, Kasper S, et al. Activation of Protein Tyrosine Phosphatase Non-Receptor Type 2 by Spermidine Exerts Anti-Inflammatory Effects in Human THP-1 Monocytes and in a Mouse Model of Acute Colitis. *PLoS One*. 2013;8(9). doi:10.1371/journal.pone.0073703

185. Zhang YG, Wu S, Xia Y, Sun J. Salmonella Infection Upregulates the Leaky Protein Claudin-2 in Intestinal Epithelial Cells. *PLoS One*. 2013;8(3). doi:10.1371/journal.pone.0058606

186. Luettig J, Rosenthal R, Barmeyer C, Schulzke JD. Claudin-2 as a mediator of leaky gut barrier during intestinal inflammation. *Tissue Barriers*. 2015;3(1). doi:10.4161/21688370.2014.977176

187. Rosenthal R, Milatz S, Krug SM, et al. Claudin-2, a component of the tight junction, forms a paracellular water channel. *J Cell Sci*. 2010;123(11):1913-1921. doi:10.1242/JCS.060665

188. Barnich N, Carvalho FA, Glasser AL, et al. CEACAM6 acts as a receptor for adherent-invasive E. coli, supporting ileal mucosa colonization in Crohn disease. *J Clin Invest*. 2007;117(6):1566-1574. doi:10.1172/JCI30504

189. Zeissig S, Bürgel N, Günzel D, et al. Changes in expression and distribution of claudin 2, 5 and 8 lead to discontinuous tight junctions and barrier dysfunction in active Crohn's disease. *Gut*. 2007;56(1):61-72. doi:10.1136/gut.2006.094375

190. Tsai PY, Zhang B, He WQ, et al. IL-22 Upregulates Epithelial Claudin-2 to Drive Diarrhea and Enteric Pathogen Clearance. *Cell Host Microbe*. 2017;21(6):671-681.e4. doi:10.1016/j.chom.2017.05.009

191. Scharl M, Rudenko I, McCole DF. Loss of protein tyrosine phosphatase N2 potentiates epidermal growth factor suppression of intestinal epithelial chloride secretion. *AJP Gastrointest Liver Physiol*. 2010;299(4):G935-G945. doi:10.1152/ajpgi.00106.2010

192. Scharl M, McCole DF, Weber A, et al. Protein tyrosine phosphatase N2 regulates TNFα-induced signalling and cytokine secretion in human intestinal epithelial cells. *Gut*. 2011;60(2):189-197. doi:10.1136/gut.2010.216606

193. Spalinger MR, Sayoc-Becerra A, Ordookhanian C, et al. The JAK Inhibitor Tofacitinib Rescues Intestinal Barrier Defects Caused by Disrupted Epithelial-macrophage Interactions. *J Crohns Colitis*. 2021;15(3):471-484. doi:10.1093/ecco-jcc/jjaa182

194. Stappenbeck TS, McGovern DPB. Paneth Cell Alterations in the Development and Phenotype of Crohn's Disease. *Gastroenterology*. 2017;152(2):322-326. doi:10.1053/j.gastro.2016.10.003

195. Riba A, Olier M, Lacroix-Lamandé S, et al. Paneth Cell Defects Induce Microbiota Dysbiosis in Mice and Promote Visceral Hypersensitivity. *Gastroenterology*. 2017;153(6):1594-1606.e2. doi:10.1053/j.gastro.2017.08.044

196. Van Der Post S, Jabbar KS, Birchenough G, et al. Structural weakening of the colonic mucus barrier is an early event in ulcerative colitis pathogenesis. *Gut*. 2019;68(12):2142-2151. doi:10.1136/gutjnl-2018-317571

197. Vandussen KL, Liu TC, Li D, et al. Genetic variants synthesize to produce paneth cell phenotypes that define subtypes of crohn's disease. *Gastroenterology*. 2014;146(1):200-209. doi:10.1053/j.gastro.2013.09.048

198. Adolph TE, Tomczak MF, Niederreiter L, et al. Paneth cells as a site of origin for intestinal inflammation. *Nature*. 2013;503(7475):272-276. doi:10.1038/nature12599

199. Zhang Q, Pan Y, Yan R, et al. Commensal bacteria direct selective cargo sorting to promote symbiosis. *Nat Immunol*. 2015;16(9):918-926. doi:10.1038/ni.3233

200. Rocha JDB, Schlossmacher MG, Philpott DJ. LRRK2 and Nod2 promote lysozyme sorting in Paneth cells. *Nat Immunol*. 2015;16(9):898-900. doi:10.1038/ni.3255

201. Liu T-C, Gurram B, Baldridge MT, et al. Paneth cell defects in Crohn's disease patients promote dysbiosis. *JCI Insight*. 2016;1(8). doi:10.1172/jci.insight.86907

202. Satoh Y, Ishikawa K, Oomori Y, Takeda S, Ono K. Bethanechol and a G-protein activator, NaF/AlCl3, induce secretory response in Paneth cells of mouse intestine. *Cell Tissue Res*. 1992;269(2):213-220. doi:10.1007/BF00319611

203. Stahl M, Tremblay S, Montero M, et al. The Muc2 mucin coats murine Paneth cell granules and facilitates their content release and dispersion. *Am J Physiol Liver Physiol*. 2018;315(2):G195-G205. doi:10.1152/ajpgi.00264.2017

204. Dekaney CM, King S, Sheahan B, Cortes JE. Mist1 Expression Is Required for Paneth Cell Maturation. *CMGH*. 2019;8(4):549-560. doi:10.1016/j.jcmgh.2019.07.003

205. Pin CL, Michael Rukstalis J, Johnson C, Konieczny SF. The bHLH transcription factor Mist1 is required to maintain exocrine pancreas cell organization and acinar cell identity. *J Cell Biol*. 2001;155(3):519-530. doi:10.1083/jcb.200105060

206. Johnson CL, Kowalik AS, Rajakumar N, Pin CL. Mist1 is necessary for the establishment of granule organization in serous exocrine cells of the gastrointestinal tract. *Mech Dev*. 2004;121(3):261-272. doi:10.1016/j.mod.2004.01.003

207. Koslowski MJ, Kübler I, Chamaillard M, et al. Genetic variants of Wnt transcription factor TCF-4 (TCF7L2) putative promoter region are associated with small intestinal Crohn's disease. *PLoS One*. 2009;4(2). doi:10.1371/journal.pone.0004496

208. van Es JH, Jay P, Gregorieff A, et al. Wnt signalling induces maturation of Paneth cells in intestinal crypts. *Nat Cell Biol*. 2005;7(4):381-386. doi:10.1038/ncb1240

209. Ayabe T, Satchell DP, Wilson CL, Parks WC, Selsted ME, Ouellette AJ. Secretion of microbicidal α-defensins by intestinal Paneth cells in response to bacteria. *Nat Immunol*. 2000;1(2):113-118. doi:10.1038/77783

210. Bel S, Pendse M, Wang Y, et al. Paneth cells secrete lysozyme via secretory autophagy during bacterial infection of the intestine. *Science (80-)*. 2017;357(6355):1047-1052. doi:10.1126/science.aal4677

211. Holly MK, Smith JG. Paneth cells during viral infection and pathogenesis. *Viruses*. 2018;10(5):225. doi:10.3390/v10050225

212. Yokoi Y, Nakamura K, Yoneda T, et al. Paneth cell granule dynamics on secretory responses to bacterial stimuli in enteroids. *Sci Rep*. 2019;9(1). doi:10.1038/s41598-019-39610-7

213. Han J, Back SH, Hur J, et al. ER-stress-induced transcriptional regulation increases protein synthesis leading to cell death. *Nat Cell Biol*. 2013;15(5):481-490. doi:10.1038/ncb2738

214. Marciniak SJ, Yun CY, Oyadomari S, et al. CHOP induces death by promoting protein synthesis and oxidation in the stressed endoplasmic reticulum. *Genes Dev*. 2004;18(24):3066-3077. doi:10.1101/gad.1250704

215. Cray P, Sheahan BJ, Dekaney CM. Secretory Sorcery: Paneth Cell Control of Intestinal Repair and Homeostasis. *Cell Mol Gastroenterol Hepatol*. 2021;(July):1-12. doi:10.1016/j.jcmgh.2021.06.006

216. Brodrick B, Vidrich A, Porter E, Bradley L, Buzan JM, Cohn SM. Fibroblast growth factor receptor-3 (FGFR-3) regulates expression of paneth cell lineage-specific genes in intestinal epithelial cells through both TCF4/β-catenin-dependent and -independent signaling pathways. *J Biol Chem*. 2011;286(21):18515-18525. doi:10.1074/jbc.M111.229252

217. Vidrich A, Buzan JM, Brodrick B, et al. Fibroblast growth factor receptor-3 regulates Paneth cell lineage allocation and accrual of epithelial stem cells during murine intestinal development. *Am J Physiol - Gastrointest Liver Physiol*. 2009;297(1):G168-G178. doi:10.1152/ajpgi.90589.2008

218. Darfeuille-Michaud A, Boudeau J, Bulois P, et al. High prevalence of adherent-invasive Escherichia coli associated with ileal mucosa in Crohn's disease. *Gastroenterology*. 2004;127(2):412-421. doi:10.1053/j.gastro.2004.04.061

219. Salzman NH, Underwood MA, Bevins CL. Paneth cells, defensins, and the commensal microbiota: A hypothesis on intimate interplay at the intestinal mucosa. *Semin Immunol*. 2007;19(2):70-83. doi:10.1016/j.smim.2007.04.002

220. Ericksen B, Wu Z, Lu W, Lehrer RI. Antibacterial activity and specificity of the six human α-defensins. *Antimicrob Agents Chemother*. 2005;49(1):269-275. doi:10.1128/AAC.49.1.269-275.2005

221. Salzman NH, Ghosh D, Huttner KM, Paterson Y, Bevins CL. Protection against enteric salmonellosis in transgenic mice expressing a human intestinal defensin. *Nature*. 2003;422(6931):522-526. doi:10.1038/nature01520

222. Chu H, Pazgier M, Jung G, et al. Human α-defensin 6 promotes mucosal innate immunity through self-assembled peptide nanonets. *Science (80-)*. 2012;337(6093):477-481. doi:10.1126/science.1218831

223. Ouellette AJ, Darmoul D, Tran D, Huttner KM, Yuan J, Selsted ME. Peptide localization and gene structure of cryptdin 4, a differentially expressed mouse Paneth cell α-defensin. *Infect Immun*. 1999;67(12):6643-6651. doi:10.1128/iai.67.12.6643-6651.1999

224. Wehkamp J, Chu H, Shen B, et al. Paneth cell antimicrobial peptides: Topographical distribution and quantification in human gastrointestinal tissues. *FEBS Lett*. 2006;580(22):5344-5350. doi:10.1016/j.febslet.2006.08.083

225. Yu S, Balasubramanian I, Laubitz D, et al. Paneth Cell-Derived Lysozyme Defines the Composition of Mucolytic Microbiota and the Inflammatory Tone of the Intestine. *Immunity*. 2020;53(2):398-416.e8. doi:10.1016/j.immuni.2020.07.010

226. Liang SC, Tan XY, Luxenberg DP, et al. Interleukin (IL)-22 and IL-17 are coexpressed by Th17 cells and cooperatively enhance expression of antimicrobial peptides. *J Exp Med*. 2006;203(10):2271-2279. doi:10.1084/jem.20061308

227. Eyerich S, Eyerich K, Cavani A, Schmidt-Weber C. IL-17 and IL-22: siblings, not twins. *Trends Immunol*. 2010;31(9):354-361. doi:10.1016/j.it.2010.06.004

228. Kaser A, Lee A-H, Franke A, et al. XBP1 Links ER Stress to Intestinal Inflammation and Confers Genetic Risk for Human Inflammatory Bowel Disease. *Cell*. 2008;134(5):743-756. doi:10.1016/j.cell.2008.07.021

229. Eriguchi Y, Nakamura K, Yokoi Y, et al. Essential role of IFN-γ in T cell-associated intestinal inflammation. *JCI insight*. 2018;3(18). doi:10.1172/jci.insight.121886

230. Farin HF, Karthaus WR, Kujala P, et al. Paneth cell extrusion and release of antimicrobial products is directly controlled by immune cell-derived IFN-γ. *J Exp Med*. 2014;211(7):1393-1405. doi:10.1084/jem.20130753

231. Lemercier C, To RQ, Swanson BJ, Lyons GE, Konieczny SF. Mist1: A novel basic helix-loop-helix transcription factor exhibits a developmentally regulated expression pattern. *Dev Biol*. 1997;182(1):101-113. doi:10.1006/dbio.1996.8454

232. Acosta-Alvear D, Zhou Y, Blais A, et al. XBP1 Controls Diverse Cell Type- and Condition-Specific Transcriptional Regulatory Networks. *Mol Cell*. 2007;27(1):53-66. doi:10.1016/j.molcel.2007.06.011

233. Scharl M, Rogler G. The role for protein tyrosine phosphatase nonreceptor type 2 in regulating autophagosome formation. *Ann N Y Acad Sci*. 2012;1257(1):93-102. doi:10.1111/j.1749-6632.2012.06578.x

234. Scharl M, Wojtal KA, Becker HM, et al. Protein tyrosine phosphatase nonreceptor type 2 regulates autophagosome formation in human intestinal cells. *Inflamm Bowel Dis*. 2012;18(7):1287-1302. doi:10.1002/ibd.21891

235. Rashid HO, Yadav RK, Kim HR, Chae HJ. ER stress: Autophagy induction, inhibition and selection. *Autophagy*. 2015;11(11):1956-1977. doi:10.1080/15548627.2015.1091141

236. Gil J, Esteban M. Induction of apoptosis by the dsRNA-dependent protein kinase (PKR): Mechanism of action. *Apoptosis*. 2000;5(2):107-114. doi:10.1023/A:1009664109241

237. Kasper SH, Spalinger MR, Raselli T, Scharl M. A cell type-specific role of protein tyrosine phosphatase non-receptor type 2 in regulating ER stress signalling. *Digestion*. 2015;91(3):248-256. doi:10.1159/000375459

238. Zinszner H, Kuroda M, Wang XZ, et al. CHOP is implicated in programmed cell death in response to impaired function of the endoplasmic reticulum. *Genes Dev*. 1998;12(7):982-995. doi:10.1101/gad.12.7.982

239. Bettaieb A, Liu S, Xi Y, et al. Differential regulation of endoplasmic reticulum stress by protein tyrosine phosphatase 1B and T cell protein tyrosine phosphatase. *J Biol Chem*. 2011;286(11):9225-9235. doi:10.1074/jbc.M110.186148

240. Guan Y, Watson AJM, Marchiando AM, et al. Redistribution of the tight junction protein ZO-1 during physiological shedding of mouse intestinal epithelial cells. *Am J Physiol - Cell Physiol*. 2011;300(6):1404-1414. doi:10.1152/ajpcell.00270.2010

241. Bullen TF, Forrest S, Campbell F, et al. Characterization of epithelial cell shedding from human small intestine. *Lab Investig*. 2006;86(10):1052-1063. doi:10.1038/labinvest.3700464

242. Hu H, Tian M, Ding C, Yu S. The C/EBP homologous protein (CHOP) transcription factor functions in endoplasmic reticulum stress-induced apoptosis and microbial infection. *Front Immunol*. 2019;10(JAN):1-13. doi:10.3389/fimmu.2018.03083

243. Yu S, Tong K, Zhao Y, et al. Paneth Cell Multipotency Induced by Notch Activation following Injury. *Cell Stem Cell*. 2018;23(1):46-59.e5. doi:10.1016/j.stem.2018.05.002

244. Schmitt M, Schewe M, Sacchetti A, et al. Paneth Cells Respond to Inflammation and Contribute to Tissue Regeneration by Acquiring Stem-like Features through SCF/c-Kit Signaling. *Cell Rep*. 2018;24(9):2312-2328.e7. doi:10.1016/j.celrep.2018.07.085

245. Yan K, Chia L, Li X. The intestinal stem cell markers Bmi1 and Lgr5 identify two functionally distinct populations. *Pnas*. 2012;109(2):466-471. doi:10.1073/pnas.1118857109/-/DCSupplemental.www.pnas.org/cgi/doi/10.1073/pnas.1118857109

246. Borisova MA, Achasova KM, Morozova KN, et al. Mucin-2 knockout is a model of intercellular junction defects, mitochondrial damage and ATP depletion in the intestinal epithelium. *Sci Rep*. 2020;10(1):1-17. doi:10.1038/s41598-020-78141-4

247. Johansson MEV. Fast renewal of the distal colonic mucus layers by the surface goblet cells as measured by in vivo labeling of mucin glycoproteins. *PLoS One*. 2012;7(7):e41009. doi:10.1371/journal.pone.0041009

248. Oeser K, Schwartz C, Voehringer D. Conditional IL-4/IL-13-deficient mice reveal a critical role of innate immune cells for protective immunity against gastrointestinal helminths. *Mucosal Immunol*. 2015;8(3):672-682. doi:10.1038/mi.2014.101

249. Tawiah A, Cornick S, Moreau F, et al. High MUC2 Mucin Expression and Misfolding Induce Cellular Stress, Reactive Oxygen Production, and Apoptosis in Goblet Cells. *Am J Pathol*. 2018;188(6):1354-1373. doi:10.1016/j.ajpath.2018.02.007

250. Hasnain SZ, Tauro S, Das I, et al. IL-10 promotes production of intestinal mucus by suppressing protein misfolding and endoplasmic reticulum stress in goblet cells. *Gastroenterology*. 2013;144(2):357-368.e9. doi:10.1053/j.gastro.2012.10.043

251. Kühn R, Löhler J, Rennick D, Rajewsky K, Müller W. Interleukin-10-deficient mice develop chronic enterocolitis. *Cell*. 1993;75(2):263-274. doi:10.1016/0092-8674(93)80068-P

252. Kaser A, Blumberg RS. Endoplasmic reticulum stress and intestinal inflammation. *Mucosal Immunol*. 2010;3(1):11-16. doi:10.1038/mi.2009.122

253. Strugala V, Dettmar PW, Pearson JP. Thickness and continuity of the adherent colonic mucus barrier in active and quiescent ulcerative colitis and Crohn's disease. *Int J Clin Pract*. 2008;62(5):762-769. doi:10.1111/j.1742-1241.2007.01665.x

254. Itoh H, Beck PL, Inoue N, Xavier R, Podolsky DK. A paradoxical reduction in susceptibility to colonic injury upon targeted transgenic ablation of goblet cells. *J Clin Invest*. 1999;104(11):1539-1547. doi:10.1172/JCI6211

255. Singh V, Johnson K, Yin J, et al. Chronic Inflammation in Ulcerative Colitis Causes Long-Term Changes in Goblet Cell Function. *Cell Mol Gastroenterol Hepatol*. Published online August 18, 2021. doi:10.1016/j.jcmgh.2021.08.010

256. McCauley HA, Guasch G. Three cheers for the goblet cell: Maintaining homeostasis in mucosal epithelia. *Trends Mol Med*. 2015;21(8):492-503. doi:10.1016/j.molmed.2015.06.003

257. Asselin C, Gendron FP. Shuttling of information between the mucosal and luminal environment drives intestinal homeostasis. *FEBS Lett*. 2014;588(22):4148-4157. doi:10.1016/j.febslet.2014.02.049

258. Jarry A, Merlin D, Velcich A, Hopfer U, Augenlicht LH, Laboisse CL. Interferon-γ modulates cAMP-induced mucin exocytosis without affecting mucin gene expression in a human colonic goblet cell line. *Eur J Pharmacol Mol Pharmacol*. 1994;267(1):95-103. doi:10.1016/0922-4106(94)90229-1

259. Gerbe F, Jay P. Intestinal tuft cells: Epithelial sentinels linking luminal cues to the immune system. *Mucosal Immunol*. 2016;9(6):1353-1359. doi:10.1038/mi.2016.68

260. Van Der Sluis M, Bouma J, Vincent A, et al. Combined defects in epithelial and immunoregulatory factors exacerbate the pathogenesis of inflammation: Mucin 2-interleukin 10-deficient mice. *Lab Investig*. 2008;88(6):634-642. doi:10.1038/labinvest.2008.28

261. Robinson AM, Rahman AA, Carbone SE, et al. Alterations of colonic function in the Winnie mouse model of spontaneous chronic colitis. *Am J Physiol - Gastrointest Liver Physiol*. 2016;312(1):G85-G102. doi:10.1152/ajpgi.00210.2016